UNIVERSITY OF CALIFORNIA
RIVERSIDE

On Several Fundamental Problems of Optimization, Estimation, and Scheduling in Wireless Communications

A Dissertation submitted in partial satisfaction
of the requirements for the degree of

Doctor of Philosophy

in

Electrical Engineering

by

Qian Gao

March 2014

Dissertation Committee:
Dr. Yingbo Hua, Co-Chairperson
Dr. Gang Chen, Co-Chairperson
Dr. Ilya Dumer

The Dissertation of Qian Gao is approved:

Committee Co-Chairperson

Committee Co-Chairperson

University of California, Riverside

Acknowledgments

I would like to express my deepest gratitude to my advisor, Professor Yingbo Hua, for his continuous guidance, caring and support. From many invaluable interactions and insightful discussions with him, I have benefited academically and have grown up as a better person. Most importantly, I learnt how to identify the truly important problems and what it takes to find the best solution for both research and life.

I am also honored to have Professor Gang Chen as my co-advisor. Professor Chen illustrated me the richness of the new issues of optical wireless communications and gave me a lot of inspiring suggestions. I have been deeply encouraged by his diligence and earnestness with research.

I would also like to thank Prof. Ilya Dumer for serving on my committee. Professor Ilya Dumer and Professor Jay A. Farrell served on my oral qualifying exam committee and had provided many excellent advice about future of my research.

I would express my sincere appreciation to all the members in the Laboratory of Signals, Systems and Networks and the Center of Ubiquitous Communications by Light, past and present, from whom I got many helps and with whom I shared my laughs. Thanks to Dr. Shengyang Xu, Dr. Ting Kong, Dr. Yuan Yu, and Dr. Yi Huang for their helpful discussions. They were all extremely patient and efficient while explaining me many difficult problems. Thanks to Ali Cirik, Dr. Kaiyun Cui, Haitao Liu, Linchao Liao, Yiming Ma, Tian Lang, Zening Li, Arman Gholian, and Jie Liang for their help and friendship.

For my research on constellation design, Dr. Jonathan Manton, Dr. Rui Wang,

and Dr. Kaiyun Cui had given me many valuable suggestions and answered me plenty of questions.

Finally, I would like to thank my parents, my wife and my parents-in-law for their consistent support and encouragement, without which I could not have achieved much through my graduate study.

To my parents and my wife.

ABSTRACT OF THE DISSERTATION

On Several Fundamental Problems of Optimization, Estimation, and Scheduling in Wireless Communications

by

Qian Gao

Doctor of Philosophy, Graduate Program in Electrical Engineering
University of California, Riverside, March 2014
Dr. Yingbo Hua, Co-Chairperson
Dr. Gang Chen, Co-Chairperson

For both the conventional radio frequency and the comparably recent optical wireless communication systems, extensive effort from the academia had been made in improving the network spectrum efficiency and/or reducing the error rate. To achieve these goals, many fundamental challenges such as power efficient constellation design, nonlinear distortion mitigation, channel training design, network scheduling and etc. need to be properly addressed. In this dissertation, novel schemes are proposed accordingly to deal with specific problems falling in category of these challenges. Rigorous proofs and analyses are provided for each of our work to make a fair comparison with the corresponding peer works to clearly demonstrate the advantages.

The first part of this dissertation considers a multi-carrier optical wireless system employing intensity modulation (IM) and direct detection (DD). A block-wise constellation design is presented, which treats the DC-bias that conventionally used solely for biasing purpose as an information basis. Our scheme, we term it MSM-JDCM, takes advantage of the compactness of sphere packing in a higher dimensional

space, and in turn power efficient constellations are obtained by solving an advanced convex optimization problem. Besides the significant power gains, the MSM-JDCM has many other merits such as being capable of mitigating nonlinear distortion by including a peak-to-power ratio (PAPR) constraint, minimizing inter-symbol-interference (ISI) caused by frequency-selective fading with a novel precoder designed and embedded, and further reducing the bit-error-rate (BER) by combining with an optimized labeling scheme.

The second part addresses several optimization problems in a multi-color visible light communication system, including power efficient constellation design, joint pre-equalizer and constellation design, and modeling of different structured channels with cross-talks. Our novel constellation design scheme, termed CSK-Advanced, is compared with the conventional decoupled system with the same spectrum efficiency to demonstrate the power efficiency. Crucial lighting requirements are included as optimization constraints. To control non-linear distortion, the optical peak-to-average-power ratio (PAPR) of LEDs can be individually constrained. With a SVD-based pre-equalizer designed and employed, our scheme can achieve lower BER than counterparts applying zero-forcing (ZF) or linear minimum-mean-squared-error (LMMSE) based post-equalizers. Besides, a binary switching algorithm (BSA) is applied to improve BER performance.

The third part looks into a problem of two-phase channel estimation in a relayed wireless network. The channel estimates in every phase are obtained by the linear minimum mean squared error (LMMSE) method. Inaccurate estimate of the relay to

destination (RtD) channel in phase 1 could affect estimate of the source to relay (StR) channel in phase 2, which is made erroneous. We first derive a close-form expression for the averaged Bayesian mean-square estimation error (ABMSE) for both phase estimates in terms of the length of source and relay training slots, based on which an iterative searching algorithm is then proposed that optimally allocates training slots to the two phases such that estimation errors are balanced. Analysis shows how the ABMSE of the StD channel estimation varies with the lengths of relay training and source training slots, the relay amplification gain, and the channel prior information respectively.

The last part deals with a transmission scheduling problem in a uplink multiple-input-multiple-output (MIMO) wireless network. Code division multiple access (CDMA) is assumed as a multiple access scheme and pseudo-random codes are employed for different users. We consider a heavy traffic scenario, in which each user always has packets to transmit in the scheduled time slots. If the relay is scheduled for transmission together with users, then it operates in a full-duplex mode, where the packets previously collected from users are transmitted to the destination while new packets are being collected from users. A novel expression of throughput is first derived and then used to develop a scheduling algorithm to maximize the throughput. Our full-duplex scheduling is compared with a half-duplex scheduling, random access, and time division multiple access (TDMA), and simulation results illustrate its superiority. Throughput gains due to employment of both MIMO and CDMA are observed.

Contents

List of Figures

List of Tables

Chapter 1

Introduction

In recent decades, there has been an increasing level of interests in optical wireless communications, including infrared, visible light, and ultraviolet communications [2, 37, 58, 76]. Optical wireless communications offer a potential of high-speed transmissions in unregulated bands. Analogous to the multicarrier modulation employed in the RF systems [6], multiple-subcarrier modulation (MSM) has been proposed for the optical systems [18, 10, 1, 25], where a transmitter modulates multiple electrical subcarriers onto the optical carrier through intensity modulation (IM), and a receiver captures the intensity modulated signals by a way of direct detection (DD). This is a non-coherent system and much cheaper to implement than its counterparts known as the all-optical systems [29]. MSM along with IM/DD is a widely considered scheme for use in scattering environments [74, 46, 28]. For flat-fading environment, MSM is known to yield a higher spectral efficiency than traditional binary modulation techniques such as on-off keying (OOK) and pulse position modulation (PPM) [57, Chapter 5].

As a IM/DD system in particular, indoor visible light communication (VLC) by light-emitting-diodes (LEDs) has attracted extensive academic attention [75, 12] (and references therein), driven by advancements in designing and manufacturing of LEDs [40]. Adoption of LEDs as lighting source can significantly reduce energy consumption and at the same time offering high speed wireless communication, which is the primary focus of VLC research [21, 72, 74]. Most of the existing schemes employ blue LEDs with a yellow phosphor coating, while with RGB LEDs higher data rate is possible because of wavelength division multiplexing.

A point-to-point system as above may suffer from limited coverage, and wireless relays can be rapidly deployed to enlarge coverage as well as increasing capacity and spectrum efficiency. In recent years, the deployment of relay nodes to assist wireless communications has been investigated intensively [42]-[43]. The relay nodes may have limited signal processing capability, making the non-regenerative relays preferable [24] and [41]. A simply two-hop relaying system contains one source-to-relay (StR) and one relay-to-destination (RtD) link. To enjoy all benefits the relaying system could provide, accurate StR and RtD channel state information (CSI) is required at the destination.

With multiple spatially dispersed source nodes in wireless relaying networks, cooperative relaying has been shown as an effective technique to increase overall capacity by exploiting diversity in fading channels [52, 53, 54, 33]. The network capacity can be further improved by deployment of MIMO antennas at source/relay/destination nodes, a relay with full-duplex mode, or if efficient multiple access schemes such as code division

multiple access (CDMA) is exploited.

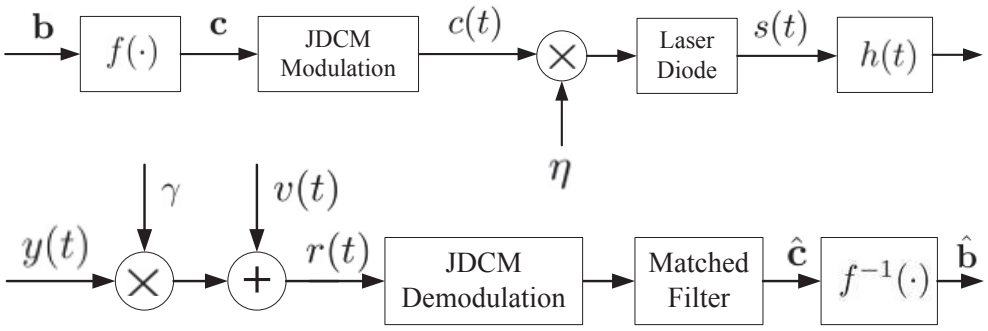

Figure 1.1: The system block diagram with the MSM-JDCM.

1.1 Multi-subcarrier Modulated Optical Wireless Systems

Constellation design is important for MSM IM/DD systems [77, 66, 67]. A good constellation design should be power efficient, including electrical, optical and peak-power efficiencies. A stream-wise scheme termed MSM-Normal is proposed in [77], and a block-wise one termed MSM-SSPS (subcarrier signal point sequence) is in [66] and [67]. With the MSM-Normal, bit sequences are independently modulated onto individual subcarriers using BPSK/QPSK (binary phase shift keying and quadrature phase shift keying). But the sum of the subcarrier waveforms likely contains a large negative peak which needs to be compensated by a DC (direct current) power, which compromises the power efficiency. With the MSM-SSPS, a more general constellation for multiple subcarriers with both I and Q channels is designed, which requires a less DC power for negative peak compensation. However, none of these two schemes treats the DC-bias as part of the information basis. In [38], a sphere packing problem is formulated for constellation design of a single-carrier

system, which treats the DC-bias as an information carrying basis.

For this topic, we will consider the constellation design for the MSM IM/DD system with either flat fading or frequency-selective fading channels. We propose a joint DC and multicarrier constellation design scheme, termed MSM-JDCM. The system diagram is shown by Figure 1.1. This scheme provides an optimized constellation in a connected region in high dimensional space with the DC-bias as an information basis. Convex optimization problems are formulated in later and solved by CVX [17] to provide optimized constellations. A good constellation design should not only be power efficient but also robust to the HPA and/or LD's nonlinearities. To deal with these nonlinearities, traditional schemes include selective mapping [13], partial transmit sequence [50], clipping [73], tone reservation [14], vector precoding [7], companding transform [36], and others [27]. We show that our constellation design scheme MSM-JDCM, along with short-term PAPR (peak to average power ratio) or long-term PAPR constraints, provides a robustness against the nonlinearities. We also consider a labeling problem (i.e., bits-to-symbols mapping) after a constellation is given to minimize the bit error rate (BER). In the literature, the labeling schemes include the Gray Code mapping [26], set-partitioning mapping [70], [71], maximum squared Euclidean weight mapping [65], the binary switching algorithm (BSA) [60]. Among them, the Binary Switching Algorithm (BSA) is able to accommodate labeling in a high dimensional space, and our simulation results show that the labeling using BSA noticeably reduces the BER for a fixed SER (symbol error rate).

1.2 Multi-color Modulated Optical Wireless Systems

With RGB LEDs, color-shift keying (CSK) was recommended by the IEEE 802.15.7 Visible Light Communication Task Group [32]. A few authors have promoted this idea by designing constellations using signal processing tools. Drost et al. had a efficient constellation designed for CSK based on billiard algorithm [19]. Monteiro et al. designed constellation for CSK using an Interior Point Method, operating with peak and color cross-talk constraints [49]. Bai et al. considered the constellation design for CSK to minimize the bit error rate (BER) subject to some lighting constraints [3].

Despite the fact that the three-dimensional constellation design problems have been formulated nicely in [19, 49, 3], a few important questions have not been addressed. First, how do we fairly compare a system with CSK employed and a conventional system with the same number of colored LEDs modulated separately, e.g. by OOK or M-PAM? Second, how will system performance be impacted if the color for illumination is not white? Third, can peak-to-average power ratio (PAPR) be controlled with constellation designs?

For this topic, we propose a novel constellation design scheme, termed CSK-Advanced, in arbitrary dimensional space, and attempt to answer the above questions while comparing with schemes based on ideas from other paper on related context. By arbitrary dimensional space, it is meant that any non-equal number of red, blue, and green LEDs can be selected for the design. With fixed average optical intensity and targeted average color, we formulate an optimization problem seeking to minimize the system symbol error rate (SER) by maximizing the minimum Euclidean distance (MED) among transmitted symbol

pairs. For practical concerns, the color rendering index (CRI) and luminous efficacy rate (LER) are also taken into account. Further, optical PAPR is included as an additional constraint.

For systems having channel with cross-talks (CwC), an SVD-based pre-equalizer is applied and the constellations are redesigned subject to a transformed set of constraints. Systems employing such optimized constellations could achieve significantly lower BER than those applying ZF or LMMSE based post-equalizers. Besides constellation design, a binary switching algorithm (BSA) originally proposed in [78] is applied to further reduce the BER when symbol error rate is fixed through searching for the best bits-to-symbol mapping.

1.3 Channel Estimation for a Two-hop Non-Regenerative Wireless Relay System

There are plenty of channel estimation scheme for a two-hop non-regenerative wireless relay system as shown by Figure 1.2 in the literature, including so-termed one phase and two phase schemes. To estimation CSI in a one phase scheme, the destination only requires the source to transmit training sequences which is amplified by the relay. In particular, the authors of [45] have developed an one-phase expectation-maximization (EM) based maximum a posteriori (MAP) estimation scheme for a Rician-Rayleigh channel model originally proposed by [64]. Despite of the advantage of avoiding sending pilots from the relay, the applicability of the one-phase scheme in [45] relies on the non-zero

mean assumption of the Rician StR channel. To avoid such assumption and obtain separable estimates of StR and RtD channels, two-phase estimation schemes are alternatives. In Phase 1 of a two-phase scheme, the relay first transmits pilots to the destination, where RtD channel is estimated. In Phase 2, the source transmits pilots to destination through the relay, and the destination can estimate the StR channel based on the estimate of the RtD channel obtained in Phase 1. In particular, the authors in [44] proposed a least-square (LS) based channel estimation algorithm, which estimates both StR and RtD channels up to a scalar ambiguity. In [48], an interim channel estimation method was proposed, which does not have the scalar ambiguity. In [68]-[35], a prior knowledge of the channel statistics was exploited for more accurate estimate of CSI.

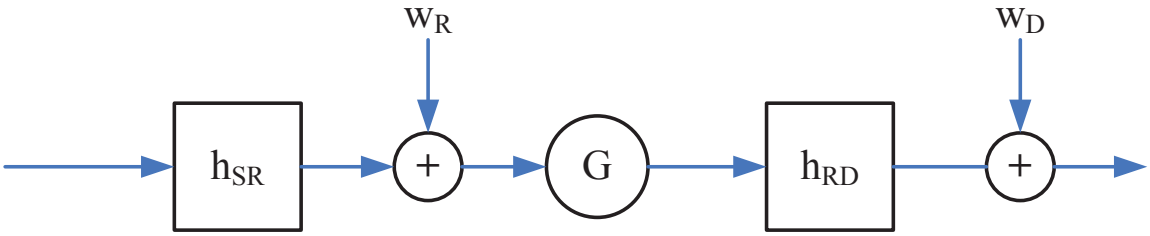

Figure 1.2: A two-hop AF relaying system

The RtD channel estimated in Phase 2 is based on the StR channel estimate obtained in Phase 1, which can be inaccurate. Therefore, the noise is not the only factor that affects the Phase 2 channel estimation. With equal resources for both phases, the estimate from the second phase tends to be less reliable than that from the first phase due to the error propagation. To the best of our knowledge, analysis of such estimation error propagates is not available in the literature. For this new topic, we will first derive a closed-form ex-

pression of the averaged Baycian mean square estimation error (ABMSE) of the StR and RtD channel estimates. Then such expression is used to develop an iterative algorithm to optimally allocate the training slots for both phases. To simplify the problem, we consider a single-input and single-output (SISO) relay system instead of a MIMO relay system. However, we believe that the insight shown in this paper will be useful for MIMO relay systems.

1.4 Transmission Scheduling for Wireless Relay Systems

For this topic, we consider a network as illustrated in Figure 1.3, where there are multiple MIMO users, a single MIMO relay and a single MIMO destination. Packets sent from the users can be recovered by the destination as long as the signal to interference and noise ratio (SINR) exceeds a pre-chosen threshold β. The relay collects the packets lost from the direct link from the users to the destination and then sends them later to the destination to improve throughput.

The authors in [53] considered a similar network structure, where they derived a throughput expression with fast-fading Rayleigh channels. They also considered using a relay to assist the transmissions by collecting and retransmitting lost packets. An efficient algorithm was proposed to optimize the averaged throughput, which was shown to outperform the time division multiple access (TDMA). The scheduled access, although increasing the overhead of transmission, can be useful in many practical scenarios. However, the work [53] is based on a half-duplex relay and SISO nodes each with a single antenna.

We consider MIMO nodes and a full-duplex relay. Although all currently practical radios for wireless communications are half-duplex, the feasibility of full-duplex radios is high, e.g., see [34]-[31].

We compare four different access schemes, which are the proposed full-duplex cooperative scheduling scheme, the half-duplex cooperative scheduling scheme proposed in [53], the TDMA scheme which allows users to sequentially access the channel, and the random access scheme which randomly picks a set of users to access the channel. Through simulations it is observed that our scheme achieves the highest throughput. An application of our work is the wireless sensor network composed of K sensors transmitting data to the collection center.

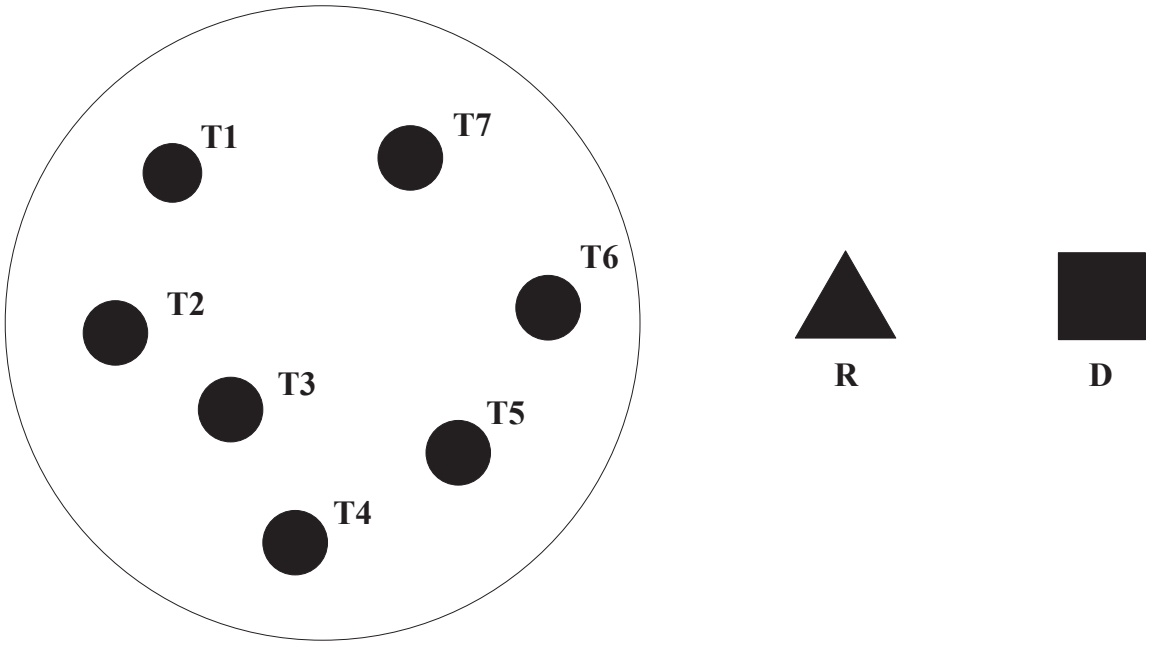

Figure 1.3: A cooperative network with multiple transmitters (T_i), a single relay (R), and a destination (D).

1.5 Dissertation Scope and Outline

The rest of this dissertation is organized as follows: in Chapter 2, a constellation design scheme for a multi-subcarrier modulated optical channel is considered. A convex optimization problem is establish to iteratively find electrical/optical/peak power efficient constellations, which could be robust to channel selective-fading and nonlinear distortions. A binary switching algorithm is applied to find the optimized bits-to-symbols mapping to further increase the power efficiency. In Chapter 3, another convex optimization problem is built to search for optimized constellations for indoor visible light communications with multi-colored LEDs. We also design a SVD-based pre-equalizer, and discusses the robustness of our scheme against channel cross-talks. Many crucial lighting constraints are included in our optimizations. In Chapter 4, we consider the problem of channel estimation error propagation in a two-hop wireless relayed network. The close-form expression of the estimation errors for both phases are derived, based on which an iterative searching algorithm is provided to optimally allocate training resources to both phases in order that the estimation errors are balanced. In Chapter 5, a multiple-access scheduling problem in a full-duplex MIMO fast-fading relaying wireless network is addressed. We derive a novel expression of the MIMO throughput is first derived, based on which a scheduling algorithm is developed to maximize the throughput. By simulation, we show that our full-duplex scheduling outperforms half-duplex scheduling, random access, and TDMA. Some conclusions are drawn in Chapter 6.

Shown below is a list of my papers related to this dissertation.

- Q. Gao, J. Manton, G. Chen, and Y. Hua, "*Constellation Design for a Multicarrier Optical Wireless Communication Channel,*" IEEE Trans. on Communi., vol. 62, no. 1, pp. 214 - 225, 2014.
- Y. Hua, P. Liang, Y. Ma, A Cirik, and Q. Gao, "*A Method for Broadband Full-Duplex MIMO Radio,*" IEEE Signal Processing Letters, vol.19, no.12 , Dec. 2012.
- Q. Gao, G. Chen, and Y. Hua, "*Constellation Design for Multicolor Visible Light Communications Robust Against Interference,*" submitted, Optics Express, 2014.
- Q. Gao, J.H. Manton, G. Chen, and Y. Hua, "*Power-efficient Constellation Design for a Multicarrier Optical Wireless System,*" IEEE Milcom, pp. 1645-1650, Nov. 2013.
- Q. Gao, T. Lang, Feng B., G. Chen, and Y. Hua, "*Precoder Design for Indoor Visible Light Communications with Multiple RGB LEDs,*" Procs. of SPIE, 8574-33, San Diego, Aug. 2013.
- Q. Gao, G. Chen, L. Liao, and Y. Hua, "*Full-duplex Cooperative Transmission Scheduling in Fast-fading MIMO Relaying Wireless Networks,*" in press, IEEE ICNC Workshops - CNC, 2014.
- Q. Gao, G. Chen, and Y. Hua, "*Training Slot Allocation for Mitigating Estimation Error Propagation in a Two-Hop Relaying System,*" in press, IEEE Asilomar, Jan. 2014.
- Q. Gao, L. Liao, G. Chen, and Y. Hua, "*Free-space Optical Multisubcarrier Communications Employing Power-efficient Constellations,*" submitted, IEEE SPAWC, 2014.

Chapter 2

Constellation Design for a Multi-carrier Wireless Communication Channel

2.1 MSM IM/DD Optical Channel Model

2.1.1 The Flat-fading Channel Model

Figure 1.1 shows the system block diagram of an IM/DD optical wireless network. The received signal $y(t)$ can be written as [37]

$$y(t) = \gamma\eta s(t) * h(t) + v(t) \tag{2.1}$$

where t is continuous time index, $s(t)$ denotes the intensity signal sent by the laser diode (LD), $y(t)$ the received photocurrent by the photodetector (PD), $h(t)$ the channel impulse response, η the electro-optical conversion factor in watts per ampere (W/A), and γ the

photodetector responsivity. Signal intensity has to be non-negative, i.e.,

$$s(t) \geq 0 \tag{2.2}$$

which is the fundamental constraint differentiating IM/DD from many coherent modulated systems and an important basis of the schemes mentioned later in this article.

The proposed methods for constellation design and labeling require the channel state information which is typically static and easy to obtain for practical indoor optical wireless communications. We consider flat-fading channel model first. With a constant channel $h = 1$ assumed for multiple symbol intervals, the model is simplified to

$$r(t) = \gamma\eta s(t) + n(t) \tag{2.3}$$

where $\gamma\eta = 1$ can be further assumed without loss of generality. In our design, $s(t)$ is chosen from a signal set $\mathcal{S} = \{s_1(t), s_2(t), \ldots, s_{N_c}(t)\}$, where each signal in the set is to be designed and N_c is the constellation size. The discrete vector channel model can be written as:

$$\mathbf{r}[p] = \mathbf{s}[p] + \mathbf{n}[p] \qquad p \in [1, N_c] \tag{2.4}$$

where we assume the noise vector $\mathbf{n}[p]$ has independent random Gaussian elements with zero mean and variance $N_0/2$ per dimension. We refer the readers to [38] for details about the relationship between the discrete and continuous channel models. It should be noted that $[p]$ is to index the "discrete" signal space and (t_n) will be used to index the "discrete" time samples of the continuous signal waveforms.

Power metrics are thus defined: 1. the average electrical power $\Psi_e(t) = \frac{1}{T_s}\mathcal{E}_i[s_i^2(t)]$

(the average is taken over i); 2. the average optical power $\Psi_o(t) = \frac{\eta}{\sqrt{T_s}}\mathcal{E}_i[s_i(t)]$, 3. the peak optical power $\Psi_{po}(t) = \eta \max_{i,t} s_i(t)$. The index i is uniformly taking value from set $\mathcal{I} = \{1, 2, \ldots, N_c\}$ and T_s is the symbol interval.

2.1.2 The Information Basis

Denote $\boldsymbol{\phi}(t) = [\phi_1(t), \phi_2(t), \ldots, \phi_M(t)]^T$ as a sequence of orthonormal information basis modulated by $\mathbf{c}_i$, the i-th symbol vector. $\phi_1(t)$ is associated with the DC-bias, which is as well used by MSM-Normal and MSM-SSPS, but only for biasing purpose (not an information basis and is dropped by the receiver). The transmitted signal $s_i(t)$ by the LD is given by $s_i(t) = \eta\boldsymbol{\phi}^T(t)\mathbf{c}_i$.

If both I and Q channels are used by each subcarrier for MSM-JDCM, we term it MSM-JDCM-IQ, thus $M = 2K + 1$. If only the I channels are used, we term it MSM-JDCM-I, thus $M = K + 1$. The information basis is typically chosen as follows.

$$\phi_1(t) = \sqrt{\frac{1}{T_s}}\Pi(\frac{t}{T_s}) \tag{2.5}$$

$$\phi_{2k}(t) = \sqrt{\frac{2}{T_s}}\cos(2\pi f_k t)\Pi(\frac{t}{T_s}) \qquad k = 1, 2, \ldots, K \tag{2.6}$$

$$\phi_{2k+1}(t) = \sqrt{\frac{2}{T_s}}\sin(2\pi f_k t)\Pi(\frac{t}{T_s}) \qquad k = 1, 2, \ldots, K \tag{2.7}$$

where

$$\Pi(t) = \begin{cases} 1, & \text{if } 0 \leq t < 1 \\ 0, & \text{otherwise.} \end{cases} \tag{2.8}$$

where $f_k = \frac{k}{T_s}$ is the frequency of k-th subcarrier. The rectangular window defined in (2.8) is not a practical signal to use in a real-world IM/DD channel due to its infinite band-

width requirement, thus in this paper we propose to employ a "time-domain raised cosine (TDRC)" window defined as follows

$$\tilde{\Pi}(t) = \begin{cases} 0.5\big(1+\cos[\frac{\pi}{\beta}(t-\beta)]\big) & \text{if } \ 0 < t < \beta, \\ 1 & \text{if } \ \beta \le t \le 1-\beta, \\ 0.5\big(1+\cos[\frac{\pi}{\beta}(t-1+\beta)]\big) & \text{if } \ 1-\beta < t \le 1. \end{cases} \tag{2.9}$$

We will choose a small β in this dissertation.

2.1.3 The Waveform Distances

The basis waveforms are typically normalized, i.e., the following holds

$$< \phi_n(t), \phi_m(t) >= \begin{cases} 1 & m = n, \\ 0 & \text{otherwise.} \end{cases} \tag{2.10}$$

Straightforwardly, the inner product and Euclidean distance relationships between two waveforms hold as follows

$$< c_i(t), c_j(t) >=< \mathbf{c}_i, \mathbf{c}_j > \tag{2.11}$$

$$||c_i(t) - c_j(t))|| = ||\mathbf{c}_i - \mathbf{c}_j|| \tag{2.12}$$

The detection performance at the receiver, especially at high signal-to-noise ratio (SNR), is governed by the minimum distance among all waveform pairs.

2.1.4 MSM-JDCM vs MSM-SSPS

The advantage of the MSM-JDCM over the MSM-SSPS is threefold: 1. the dimension of information basis of the MSM-JDCM is always higher than the MSM-SSPS by

one, which is due to the use of DC-bias as information basis; 2. the MSM-JDCM searches constellation points in a continuous space, while MSM-SSPS restricts the searching space to a "discrete lattice" of size 9^K. Each subcarrier picks symbols from a (8+1)-APSK constellation [67]; 3. MSM-SPSS has to use both I and Q channels for each subcarrier.

2.2 ISI-Robust Constellation Design

While multiple non-line-of-sight optical links exist, we choose the geometric series model for analysis in the paper, i.e.,

$$h'(t) = \gamma \sum_i \beta_i \delta(t - \tau_i) \tag{2.13}$$

where $\delta(\cdot)$ is a dirac-delta function, $0 < \beta_i < 1$ and $\tau_i \ll T_s$ are real numbers denoting the gain and delay of the i-th channel tap respectively. γ is a very small value denoting the common path-loss which can be lumped into noise variance, and therefore we only consider the simplified channel

$$h(t) = \sum_i \beta_i \delta(t - \tau_i) \tag{2.14}$$

There are other choices for modeling the selective-fading channel, e.g., the exponential decay model, ceiling bounce model, and etc.. Comparisons among different channel models can be found in [11]. With the chosen $h(t)$, we propose to design a set of pre-equalizers before $\mathbf{c}_i$ comes into the JDCM modulator.

Proposition 1 () The pre-equalizers that mitigate the effect of frequency-selective channel

(2.14) *are linear, and have the following form:*

$$\mathbf{P}_k = \frac{1}{|z_k|^2}\begin{bmatrix} Re(z_k) & -Im(z_k) \\ Im(z_k) & Re(z_k) \end{bmatrix}, \qquad \textit{for k-th subcarrier}$$

$$p_o = \frac{1}{\sum_i \beta_i}, \qquad \textit{for DC-bias}$$

where $z_k = \sum_i \beta_i e^{-k2\pi f_k \tau_i}$. *Thus the modulating vector* $\tilde{\mathbf{c}}_i = \mathbf{P}\mathbf{c}_i$, *where the symbol vector* $\mathbf{c}_i$ *is pre-equalized by the block-diagonal matrix* $\mathbf{P} = \textbf{\textit{bdiag}}\{p_0, \mathbf{P}_1, \ldots, \mathbf{P}_K\}$.

2.3 The Optimization Problem

2.3.1 The Objective Functions

The MSM-JDCM is targeted at optimizing the joint symbol vector $\mathbf{c_T} = [\mathbf{c}_1^T, \mathbf{c}_2^T, \ldots, \mathbf{c}_{N_c}^T]^T \in \mathcal{R}^{(2K+1)N_c}$ (for the IQ channels case). When the optimization goal is to minimize the average electrical power, the objective function is given by

$$\Psi_e(\mathbf{c_T}) = \frac{1}{N_c T_s}\sum_{i=1}^{N_c} ||\mathbf{c}_i||^2 = \frac{1}{N_c T_s}\mathbf{c_T}^{\boldsymbol{T}}\mathbf{c_T} \tag{2.15}$$

where i is uniformly distributed over $\mathcal{I}$. While for minimizing the optical average power, the objective function is written as

$$\Psi_o(\mathbf{c_T}) = \frac{\eta}{N_c\sqrt{T_s}}\sum_{i=1}^{N_c} c_{i,1} = \frac{\eta}{N_c\sqrt{T_s}}\sum_{i=1}^{N_c}\mathbf{j}_{(i-1)M+1}^T\mathbf{c_T} \tag{2.16}$$

where $\mathbf{j}_{(i-1)M+1} = [0, \ldots, 1, \ldots, 0]^T$ is a $(2K+1)N_c \times 1$ column vector with all zeros at except the $(i-1)M+1$'s element, and therefore only the DC-bias part of each candidate waveform is averaged. The exact form of optical peak power constraint is hard to get and

we aim at the upper bound of it as in the following. For a an arbitrary packet, the optical peak power is

$$\begin{aligned}
\Psi_{po}(\mathbf{c_T}) &= \eta \max_{t,i} c_i(t - jT_s) = \eta \max_{t,i} c_i(t) \\
&\leq \frac{\eta}{\sqrt{T_s}} \max_i \{\sum_{k=1}^{K} \sqrt{2(c_{i,2k}^2 + c_{i,2k+1}^2)} + c_{i,1}\} \\
&= \frac{\eta}{\sqrt{T_s}} \max_i \{\sum_{k=1}^{K} ||\mathbf{A}_k \mathbf{c}_i|| + \mathbf{a}_0^T \mathbf{c}_i\} \\
&= \frac{\eta}{\sqrt{T_s}} \max_i \{\sum_{k=1}^{K} ||\mathbf{A}_k \mathbf{J}_i \mathbf{c_T}|| + \mathbf{a}_0^T \mathbf{J}_i \mathbf{c_T}\} \\
&= \frac{\eta}{\sqrt{T_s}} \max_i \{\sum_{k=1}^{K} ||\mathbf{W}_{i,k} \mathbf{c_T}|| + \mathbf{w}_{i,0}^T \mathbf{c_T}\} \qquad (2.17)
\end{aligned}$$

$$\Psi_{pe}(\mathbf{c_T}) = \frac{\Psi_{po}^2(\mathbf{c_T})}{\eta^2} \qquad (2.18)$$

(5.28) can be straightforwardly derived to upper bound the peak power, and we later show in 2.3.4 that this bound can be replaced by a set of point-wise constraints. By introducing the following notations: $\mathbf{A}_k = \sqrt{2}\,\mathrm{diag}(0, \ldots, 0, 1, 1, 0, \ldots, 0)$ with the $2k$-th and $2k+1$-th elements as 1's, $\mathbf{a}_0 = [1, 0, \ldots, 0]^T$ of dimension $(2K+1) \times 1$, $\mathbf{J}_i = [\mathbf{O}_{2K+1}, \ldots, I_{2K+1}, \mathbf{O}_{2K+1}, \ldots, \mathbf{O}_{2K+1}]$ of dimension $2K+1 \times N_c(2K+1)$, $\mathbf{W}_{i,k} \triangleq \mathbf{A}_k \mathbf{J}_i$, and $\mathbf{w}_{i,0}^T \triangleq -\mathbf{a}_0^T \mathbf{J}_i$. The optical peak power $\Psi_{po}(\boldsymbol{c})$ and electrical peak $\Psi_{pe}(\boldsymbol{c})$ power has a relationship of (5.29) such that optimizing one automatically guarantees the optimality of the other.

Besides the performance metrics mentioned above, one can choose to use linear combination of a number of objectives, or by running the optimization solver multiple times with more and more severe constraints. In other words, because there are competing per-

formance metrics, there could be a range of different answers depending on which metrics are more important. This is important in practice and one can formulate different problems with combining or modifying the problems we address in this paper.

2.3.2 The Constraints

With IQ channels, The symbol vector $\mathbf{c}_i \in \mathcal{R}^{2K+1}$ can take values from a connected region as long as the nonnegative constraint is satisfied as follows.

$$\min_t c_i(t) = \min_{i,t} \boldsymbol{\phi}(t)^T \mathbf{c}_i = \min_t \sum_{m=1}^{2K+1} c_{i,m}\phi_m(t) \geq 0 \tag{2.19}$$

With derivations in the equation at the bottom of the page, a sufficient but not necessary set of constraints can be used to guarantee the nonnegativeness of the transmitted signals as follows

$$\begin{aligned} G_i(\mathbf{c_T}) &\triangleq c_{i,1} - \sum_{k=1}^{K} \sqrt{2(c_{i,2k}^2 + c_{i,2k+1}^2)} \\ &= \mathbf{w}_{i,0}^T \mathbf{c_T} + \sum_{k=1}^{K} ||\mathbf{W}_{i,k}\mathbf{c_T}|| \geq 0 \qquad \forall i \end{aligned} \tag{2.20}$$

These are convex constraints in $\mathbf{c_T}$. Later we show in 2.3.4 that a set of point-wise constraints serves as a replacement of this bound, with very little computational redundancy.

Besides the non-negativeness of signal, constraint has to be put also on the minimum distance among all constellation point pairs.

$$h_l(\mathbf{c_T}) \triangleq \mathbf{c_T}^T \mathbf{F}_l \mathbf{c_T} \geq d_{min}, \qquad l = 1, 2, \ldots \frac{(N_c - 1)N_c}{2} \tag{2.21}$$

where $\mathbf{F}_{l(p,q)} = \mathbf{E}_{pq}$, $\mathbf{E}_p = \mathbf{e}_p^T \otimes \mathbf{I}_{N_c}$, $\mathbf{e}_p$ has a dimension of $(2K+1) \times 1$, and $\mathbf{E}_{pq} =$

$\mathbf{E}_p^T\mathbf{E}_p - \mathbf{E}_p^T\mathbf{E}_q - \mathbf{E}_q^T\mathbf{E}_p + \mathbf{E}_q^T\mathbf{E}_q$. The following relation holds.

$$l(p,q) = (p-1)N_c - \frac{p(p+1)}{2} + q, \qquad p,q \in 1,2,\ldots,N_c,\ p<q \tag{2.22}$$

For short, replace $l(p,q)$ with l. $d_{min} = 1$ is assumed throughout this paper without loss of generality.

The distance constraints are nonconvex in $\mathbf{c_T}$ and we firstly approximate the exteriors of the ellipses (high order cylinders) $h_l(\boldsymbol{c}) < 1$ with the first order Taylor series at $\mathbf{c_T}^{(0)}$, i.e.

$$\begin{aligned} h_l(\mathbf{c_T}) &\cong H_l^{(0)}(\mathbf{c_T}) \\ &= h_l(\mathbf{c_T}^{(0)}) + \nabla h^T(\mathbf{c_T}^{(0)})(\mathbf{c_T} - \mathbf{c_T}^{(0)}) \\ &= \mathbf{c_T}^{(0)T}\mathbf{F}_l\mathbf{c_T}^{(0)} + 2\mathbf{c_T}^{(0)T}\mathbf{F}_l(\mathbf{c_T} - \mathbf{c_T}^{(0)}) \\ &= 2\mathbf{c_T}^{(0)T}\mathbf{F}_l\mathbf{c_T} - \mathbf{c_T}^{(0)T}\mathbf{F}_l\mathbf{c_T}^{(0)} \geq 1, \qquad \forall l \end{aligned} \tag{2.23}$$

This approximation restricts the feasible region into a half space defined by $H_l^{(0)}(\mathbf{c_T}) \geq 1$. By running the algorithm with the above approximation once a new point $\mathbf{c_T}^{(1)}$ is found, which is guaranteed to maintain $1 \leq \mathbf{c_T}^{(1)T}\mathbf{F}_l\mathbf{c_T}^{(1)} \leq \mathbf{c_T}^{(0)T}\mathbf{F}_l\mathbf{c_T}^{(0)}$ [4]. Then using Taylor series again at $\mathbf{c_T}^{(1)}$, the feasible region is now approximated by a new halfspace $H_l^{(1)}(\mathbf{c_T}) \geq 1$, which has $H_l^{(0)}(\mathbf{c_T}) \geq 1$ as a subspace. We call this process as the "iterative Taylor series approximation", which iteratively finds the supporting hyperplane of $h_l(\mathbf{c_T}) < 1$ as the feasible region containing a local optimum. With multiple runs at a set of wide spread initial points, we expect to find the global optimum.

For simplicity, we drop the iteration index and write the minimum distance con-

straint as:

$$1 - H_l(\mathbf{c_T}) \leq 0, \qquad \forall l \tag{2.24}$$

2.3.3 The Optimization Problems

We explicitly write out the formulation with peak power minimization objective:

$$\begin{aligned} \min_{\mathbf{c_T}, v} \quad & v \\ \text{s.t.} \quad & \mathbf{w}_{i,0}^T \mathbf{c_T} + ||\mathbf{W}_{i,k}\mathbf{c_T}|| \geq 0, \qquad \forall i \\ & -\mathbf{w}_{i,0}^T \mathbf{c_T} + ||\mathbf{W}_{i,k}\mathbf{c_T}|| \leq v, \qquad \forall i \\ & 1 - 2\mathbf{c_T}^{(0)T}\mathbf{F}_l\mathbf{c_T} + \mathbf{c_T}^{(0)T}\mathbf{F}_l\mathbf{c_T}^{(0)} \leq 0, \qquad \forall l \end{aligned} \tag{2.25}$$

The optimization is done iteratively, and the initial point $\mathbf{c_T}^{(0)}$ has to be a feasible point, i.e., satisfying the constraints $\mathbf{c_T}^{(0)T}\mathbf{F}_l\mathbf{c_T}^{(0)} \geq d_{min}$ and $\mathbf{w}_{i,0}^T\mathbf{c_T}^{(0)} + ||W_{i,k}\mathbf{c_T}^{(0)}|| \leq 0$ for all i. It is straight forward to show after each iteration, the new solution $\mathbf{c_T}^{(1)}$ will also be a feasible point and $p_1 \leq p_0$ accordingly [4]. The stopping criterion is chosen as $||p_k - p_{k+1}|| < \epsilon$, where ϵ is a small real value such as 10^{-4} (we choose different ϵ values for different goals in our simulation). Similar remarks can be made for those with criterion $\Psi_e(\mathbf{c_T})$ and $\Psi_o(\mathbf{c_T})$.

When the number of subcarriers is large, the computation of the MSM-JDCM and the MSM-SSPS grow so that regular PCs typically cannot handle the designs. We could turn to super computers with larger memory and higher processing capability, since this is just a "once-off" process.

2.3.4 The point-wise constraints

As mentioned, the upper bound of peak power and lower bound of non-negative constraint can be replaced by a set of point-wise constraints respectively. The reason for such replacement is that these bounds are not tight enough and a tighter bound is hard to find. By point-wise constraint, it is meant that all possible waveforms $c_i(t)$ defined in $[0, T_s]$ are sampled at a set of discrete points t_n and instead of $c_i(t)$, $c_i(t_n)$ $\forall n$ are constrained, where

$$t_n = \frac{nT_s}{N} = \frac{nT_s}{2KN_O}, \qquad n = 0, 1, \ldots, N \tag{2.26}$$

where N_O denotes the oversampling rate for the subcarrier with highest frequency. It is observed in our simulations that with $N_O \geq 4$, the MSM-JDCM with point-wise constraints is able to outperform its counterpart with bounds. With flat-fading channel, the peak power minimization with point-wise constraints can be written as:

$$\begin{aligned} \min_{\mathbf{c_T}, v} \quad & v \\ \text{s.t.} \quad & \mathbf{u}_n^T \mathbf{J}_i \mathbf{c_T} \geq 0, \qquad \forall (i, n) \\ & \mathbf{u}_n^T \mathbf{J}_i \mathbf{c_T} \leq v, \qquad \forall (i, n) \\ & 1 - 2\mathbf{c_T}^{(0)T} \mathbf{F}_l \mathbf{c_T} + \mathbf{c_T}^{(0)T} \mathbf{F}_l \mathbf{c_T}^{(0)} \leq 0, \qquad \forall l \end{aligned} \tag{2.27}$$

where $\mathbf{u}_n = [u_{n,0}, u^c_{n,1}, u^s_{n,1}, \ldots, u^c_{n,K}, u^s_{n,K}]^T$, $u_{n,0} = \sqrt{1/T_s}$, $u^c_{n,k} = \sqrt{2/T_s}\cos(2\pi f_k t_n)$, and $u^s_{n,k} = \sqrt{2/T_s}\sin(2\pi f_k t_n)$. We use MSM-JDCMP as an abbreviation for MSM-JDCM with point-wise constraints to distinguish from MSM-JDCMB, which denotes the MSM-JDCM with upper or lower bounds as constraints. With selective-fading channel, $\mathbf{c_T}$ is replaced with $\mathbf{P}\mathbf{c_T}$ in the first two constraints.

With point-wise non-negative constraints, the waveforms are guaranteed to take non-negative values at the sample points, while they might take slightly negative values at the points in the middle. We thus propose to add an additional small DC bias term after obtaining waveforms designed with the MSM-JDCMP. Simulation results later on show that with $N_O \geq 8$, the negative peak of the designed waveforms is much smaller than the primary DC. Therefore, adding a additional DC does not noticeably cause severe performance loss. With more time samples, the complexity increases while a smaller additional DC is necessary for nonnegative waveforms. There is a tradeoff between the amount of the additional DC and the complexity.

2.4 HPA Nonlinear Distortion Mitigation by MSM-JDCMP

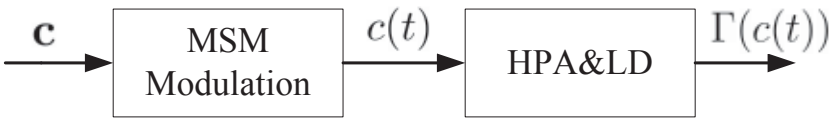

Figure 2.1: System impaired by the HPA and LD.

In practice, the system encompasses a HPA as in Figure 2.1, which may cause nonlinear distortion. Next to HPA, nonlinear distortion is caused by saturation of the output power of the LD. In this paper for illustrative purpose, we only consider the combined effect of these two blocked by studying the associated transfer function $\Gamma(\cdot)$ of the HPA and LD, which can be approximately seen as a linear function for input amplitude smaller than a

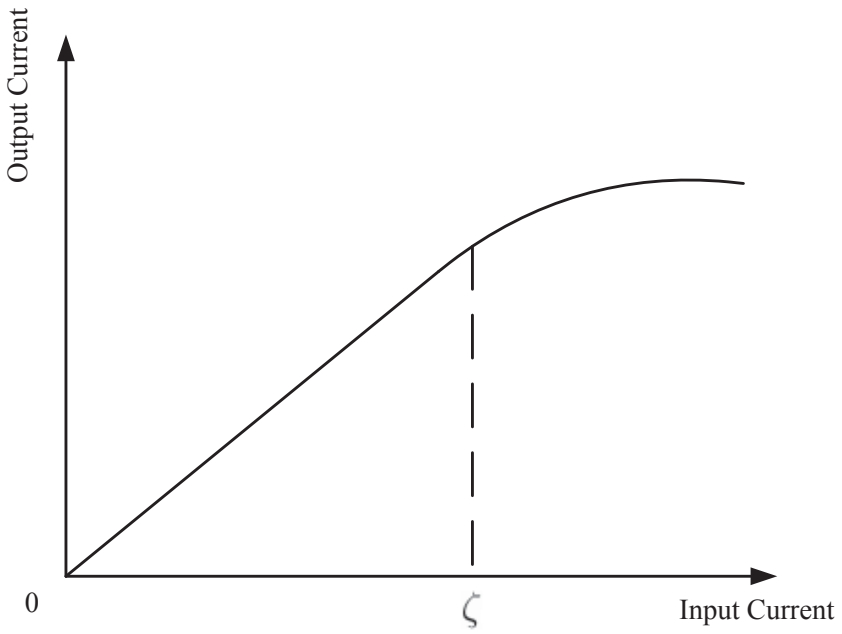

Figure 2.2: System impaired by the HPA and LD.

certain threshold ζ. After the input reaches ζ, $\Gamma(\cdot)$ becomes a nonlinear function as shown by Figure 2.2. All sequences $s_i(t)$ contributes to the nonlinear distortion if it falls out of the region $[0, \zeta]$.

We propose to mitigate the nonlinear distortion by our MSM-JDCMP with minimizing the dynamic range, instantaneous PAPR, and long-term PAPR of all possible waveforms as the objective function. With the nonnegative constraint, it is straightforward to observe that the dynamic range is optimized though peak power limitation, i.e, is formulated by (2.25) or (2.27). No single objective is always the best. Depending on particular interests and specific HPA transfer functions, one can choose the most appropriate metric among all, which is beyond the scope of this paper. We only formulate the optimization problems with the constraints and give simulation results later.

2.4.1 The Short-term PAPR Minimization

- Short-term PAPR: is the ratio of the peak of an individual waveform over its average power. Each individually waveform is constrained under certain PAPR α_i.

The short-term PAPR while symbol $\mathbf{c}_i$ is transmitted is:

$$\begin{aligned}\check{\Psi}_{e,i}(\mathbf{c_T}) &= \frac{(\sum_{k=1}^{K} ||\mathbf{W}_{i,k}\mathbf{c_T}|| + \mathbf{w}_{i,0}^T\mathbf{c_T})^2}{\mathbf{c}_i^T\mathbf{c}_i} \\ &= \frac{(\sum_{k=1}^{K} ||\mathbf{W}_{i,k}\mathbf{c_T}|| + \mathbf{w}_{i,0}^T\mathbf{c_T})^2}{\mathbf{c_T}^T\mathbf{J}_i^T\mathbf{J}_i\mathbf{c_T}}\end{aligned} \tag{2.28}$$

$\check{\Psi}_{e,i}(\mathbf{c_T})$ is a convex function of $\mathbf{c_T}$. We seek to minimize the total electrical power under with the short-term PAPR constraint $\check{\Psi}_{e,i}(\mathbf{c_T}) \leq \alpha_i$ ($10\log_{10}\alpha_i$ in dB), we formulate the optimization problem as:

$$\begin{aligned}\min_{\mathbf{c_T}} \quad & \mathbf{c_T}^T\mathbf{c_T} \\ \text{s.t.} \quad & \mathbf{u}_n^T\mathbf{J}_i\mathbf{c_T} \geq 0, \qquad \forall(i,n) \\ & -\mathbf{w}_{i,0}^T\mathbf{c_T} + ||\mathbf{W}_{i,k}\mathbf{c_T}|| - \sqrt{\alpha_i\mathbf{c_T}^T\mathbf{J}_i^T\mathbf{J}_i\mathbf{c_T}} \leq 0, \forall i \\ & 1 - 2\mathbf{c_T}^{(0)T}\mathbf{F}_l\mathbf{c_T} + \mathbf{c_T}^{(0)T}\mathbf{F}_l\mathbf{c_T}^{(0)} \leq 0, \forall l\end{aligned} \tag{2.29}$$

Linearization is initially done at the point $\mathbf{c_T}^{(0)}$ to yield a convex approximation of the nonconvex PAPR constraint. $\mathbf{c_T}^{(0)}$ is also the starting point of the iterations, which satisfies the nonnegative and minimum distance constraints such that the linearization updates with the iterations.

$$
\begin{aligned}
\min_{\mathbf{c_T}} \quad & {\mathbf{c_T}}^T \mathbf{c_T} \\
\text{s.t.} \quad & \mathbf{u}_n^T \mathbf{J}_i \mathbf{c_T} \geq 0, \qquad \forall (i,n) \\
& -\mathbf{w}_{i,0}^T \mathbf{c_T} + ||\mathbf{W}_{i,k}\mathbf{c_T}|| - \sqrt{\alpha_i}[({\mathbf{c_T}}^{(0)T} \mathbf{J}_i^T \mathbf{J}_i {\mathbf{c_T}}^{(0)})^{\frac{1}{2}} - \\
& ({\mathbf{c_T}}^{(0)T} \mathbf{J}_i^T \mathbf{J}_i {\mathbf{c_T}}^{(0)})^{-\frac{1}{2}} {\mathbf{c_T}}^{(0)T} \mathbf{J}_i^T (\mathbf{J}_i \mathbf{c_T} - \mathbf{J}_i {\mathbf{c_T}}^{(0)})] \leq 0, \forall i \\
& 1 - 2{\mathbf{c_T}}^{(0)T} \mathbf{F}_l \mathbf{c_T} + {\mathbf{c_T}}^{(0)T} \mathbf{F}_l {\mathbf{c_T}}^{(0)} \leq 0, \forall l
\end{aligned}
\tag{2.30}
$$

2.4.2 The Long-term PAPR Minimization

- Long-term PAPR: is the ratio of the peak of all waveforms over their averaged power, which is assumed to be less than α.

For our scheme, the long-term PAPR is given by:

$$
\begin{aligned}
\tilde{\Psi}_e(\mathbf{c_T}) &= \frac{\{\max_i(\sum_{k=1}^K ||\mathbf{W}_{i,k}\mathbf{c_T}|| + \mathbf{w}_{i,0}^T \mathbf{c_T})\}^2}{{\mathbf{c_T}}^T \mathbf{c_T}/N_c} \\
&= \frac{N_c\{\max_i(\sum_{k=1}^K ||\mathbf{W}_{i,k}\mathbf{c_T}|| + \mathbf{w}_{i,0}^T \mathbf{c_T})\}^2}{{\mathbf{c_T}}^T \mathbf{c_T}}
\end{aligned}
\tag{2.31}
$$

With the long-term PAPR constraint $\tilde{\Psi}_e(\mathbf{c_T}) \leq \alpha$ linearized similarly with the short-term PAPR, the optimization problem can be formulated as:

$$
\begin{aligned}
\min_{\mathbf{c_T}} \quad & {\mathbf{c_T}}^T \mathbf{c_T} \\
\text{s.t.} \quad & \mathbf{u}_n^T \mathbf{J}_i \mathbf{c_T} \geq 0, \qquad \forall (i,n) \\
& -\mathbf{w}_{i,0}^T \mathbf{c_T} + ||\mathbf{W}_{i,k}\mathbf{c_T}|| - \sqrt{\frac{\alpha}{N_c}}[({\mathbf{c_T}}^{(0)T} {\mathbf{c_T}}^{(0)})^{\frac{1}{2}} \\
& - ({\mathbf{c_T}}^{(0)T} {\mathbf{c_T}}^{(0)})^{-\frac{1}{2}} {\mathbf{c_T}}^{(0)T} (\mathbf{c_T} - {\mathbf{c_T}}^{(0)})] \leq 0, \quad \forall i \\
& 1 - 2{\mathbf{c_T}}^{(0)T} \mathbf{F}_l \mathbf{c_T} + {\mathbf{c_T}}^{(0)T} \mathbf{F}_l {\mathbf{c_T}}^{(0)} \leq 0, \qquad \forall l
\end{aligned}
\tag{2.32}
$$

2.5 Constellation Labeling

2.5.1 The Bit-to-symbol Mapping

For the MSM-JDCM and MSM-SPSS, the bit sequence $\mathbf{b}_i$ is mapped onto a symbol vector $\mathbf{c}_i$ jointly, i.e.,

$$\mathbf{c}_i = f(\mathbf{b}_i) \tag{2.33}$$

where $\mathbf{b}_i \in \{\mathbf{b}_1, \mathbf{b}_2, \ldots, \mathbf{b}_{N_c}\} \in \mathcal{R}^{N_b}$, $\mathbf{c}_i \in \{\mathbf{c}_1, \mathbf{c}_2, \ldots, \mathbf{c}_{N_c}\} \in \mathcal{R}^{M}$, and $N_c = 2^{N_b}$. $f(\cdot)$ is called the "block-wise (BLW)" mapping function.

For the MSM-Normal, "subcarrier-wise (SCW)" mapping is employed, which maps bits onto subcarriers individually, i.e.

$$(c_{I,k}, c_{Q,k}) = \tilde{f}(b_{I,k}, b_{Q,k}) \qquad k = 1, \ldots, K \tag{2.34}$$

where I and Q stand for real and imaginary part respectively. $(c_{I,k}, c_{Q,k})$ can take values from only $(\pm a, \pm a)$. The summation of all subcarriers pulses is then biased. The designing of the mapping functions is referred to as "constellation labeling" problem.

2.5.2 The Binary Switching Algorithm

After the optimization problem is solved, we obtain $N_c = 2^{N_b}$ constellation points in a $2K + 1$ dimensional space with the minimum Euclidean distance d_{min}. The SER is thus governed by d_{min}. Good constellation labeling scheme, i.e., bit-to-symbol mapping $\mathbf{c}_i = f(\mathbf{b}_i)$, serves to reduce the number of bits in error while the SER is fixed. For smaller constellation sizes, brute force method can be applied to find a global optimal, while for

larger constellations the complexity of exhaustive search soon becomes prohibitive. For constellations in high dimensional space as we design, there is no well recognized way of labeling. One heuristic algorithm, termed binary switching algorithm (BSA) by [78] was applied by [60] to output Gray or quasi-Gray mappings for two-dimensional constellations. The BSA can also be applied for labeling constellations in high dimensional space and we show that it significantly outperforms the random mapping.

Denote ξ_d^n as the subset of symbols $\mathbf{c}_i \in \xi$, whose label $\mathbf{b}_i$ has value $d \in \{0,1\}$ in position n, i.e., $\xi_d^n = \{\mathbf{c}_i = f(\mathbf{b}_i),\ \forall \mathbf{b}_i \in \{0,1\}^{N_b} | b_{i,n} = d\}$, $\xi = \{\xi_d^n,\ \forall d \in \{0,1\}, n \in \{1, \cdots, N_b\} \in \mathbb{Z}\}$ (we refer readers to [60, section 2] for details on the definitions), and the cost function to minimize for AWGN channel without prior knowledge can be written as [60, Eq.6]:

$$D^a = \frac{1}{N_b 2^{N_b}} \sum_{n=1}^{N_b} \sum_{d=0}^{1} \sum_{\mathbf{c}_i \in \xi_d^n} \sum_{\hat{\mathbf{c}}_i \in \xi_{\bar{d}}^n} \exp\left(- \frac{|\mathbf{c}_i - \hat{\mathbf{c}}_i|^2}{4N_0} \right) \tag{2.35}$$

where $\bar{d}$ is the complement of d, i.e., if $d = 0$ then $\bar{d} = 1$. The BSA iteratively finds a local optimum for a random initial mapping, and several runs are executed to reach the global optimum (details can be found in [60] and references therein).

2.6 Performance Evaluation

In this section, we assess the power efficiencies and error performances of the MSM-JDCM, MSM-SSPS, and MSM-Normal. Flat-fading channel and rectangular pulse shaping function are assumed through Section VI-A to VI-D and VI-F for illustrative purpose. A practical design example assuming selective-fading channel and TDRC pulse shap-

ing function is also included. Comparison between MSM and single carrier schemes such as on-off keying (OOK) can be found in [77] and is not included in this paper.

2.6.1 SER and BER

For the MSM-JDCM and MSM-SPSS, we assume that each symbol is transmitted with equal probability. The union bound of SER is derived as [38, Eq.25]

$$E_{s,1} \approx \frac{2N_n}{N_c} Q\left(\sqrt{\frac{d_{min,1}^2}{2N_0}}\right) \triangleq p_1 Q\left(\sqrt{\frac{d_{min,1}^2}{2N_0}}\right) \tag{2.36}$$

where $Q(x) = \frac{1}{\sqrt{2\pi}} \int_x^\infty \exp(-t^2/2)dt$ is the Gaussian Q-function, $d_{min,1}$ is the minimum Euclidean distance, and N_n is the number of neighbor pairs (which is defined in later sections). The corresponding BER is

$$E_{b,1} = \frac{\lambda_1}{N_b} E_{s,1} = \frac{\lambda_1}{N_b} p_1 Q\left(\sqrt{\frac{d_{min,1}^2}{2N_0}}\right) \tag{2.37}$$

where λ_1 denotes the average number of bits in error when one symbol is in error.

For the MSM-Normal, we regard that one symbol is in error if any subcarrier is not correctly detected. The SER can then be derived as

$$\begin{aligned} E_{s,2} &= \tilde{p}_2 \left[1 - \left(1 - Q\left(\sqrt{\frac{d_{min,2}^2}{2N_0}}\right)\right)^K\right] \\ &\approx \tilde{p}_2 K Q\left(\sqrt{\frac{d_{min,2}^2}{2N_0}}\right) \triangleq p_2 Q\left(\sqrt{\frac{d_{min,2}^2}{2N_0}}\right) \end{aligned} \tag{2.38}$$

where $0 < \tilde{p}_2 < 1$ and $p_2 < p_1$ typically. The approximate equation is valid for medium-to-high SNR case, where the Q-function dominate the SER. The corresponding BER is

$$E_{b,2} = \lambda_2 p_2 Q\left(\sqrt{\frac{d_{min,2}^2}{2N_0}}\right), \qquad \text{for small } N_0 \tag{2.39}$$

where λ_2 is the average number of bits in error when one symbol is in error.

2.6.2 The Symbol Waveforms and Power Gains

For the MSM-JDCMP, define the constellations optimized for electrical power, optical power, and peak power with size N_c and K subcarriers as $\Theta_{E,N_c}^{0,K}$, $\Theta_{O,N_c}^{0,K}$, and $\Theta_{P,N_c}^{0,K}$. For the MSM-JDCMB, define the corresponding constellations as $\Theta_{E,N_c}^{1,K}$, $\Theta_{O,N_c}^{1,K}$, and $\Theta_{P,N_c}^{1,K}$. The coordinates of selected optimized constellations are given in Appendix A. Though the MSM-SSPS in [67] is design specifically for reducing the dc-bias, we generalize it to accommodate the electrical power, optical power, and peak power reduction and the corresponding optimized constellations with size N_c are denoted as $\Theta_{E,N_c}^{2,K}$, $\Theta_{O,N_c}^{2,K}$, and $\Theta_{P,N_c}^{2,K}$. For the MSM-Normal, no optimization is associated. $\Theta_{N_c}^{3,K}$ stands for the corresponding constellation with adaptive bias and $\Theta_{N_c}^{4,K}$ for enough-biased[1]. We assume $T_s = 1$ without loss of generality. The oversampling rate $N_O = 8$ without severely adding to computational cost. 300 random initializations are chosen in order to obtain the best constellation. Due to space limit, only the corresponding waveforms with $N_b = 4$ for the three schemes are shown for illustrative purpose.

We compare the power efficiencies of the three schemes when *the same target SER and the same spectrum efficiency (bit/s/Hz) are achieved*. The power gains are defined as

$$g_{Z,N_c}^{xy,k_xk_y} = 10\log_{10}\frac{P_{Z,N_c}^{y,k_y}}{P_{Z,N_c}^{x,k_x}}\ [\text{dB}] \tag{2.40}$$

where N_c is the constellation size, $Z \in \{E, O, P\}$, $x, y \in \{0, 1, 2, 3, 4\}$, k_x and k_y are the number of subcarriers scheme x and y use respectively. Since the Q-function part dominate

[1] Enough-biased means the DC bias added to each unbiased waveform equals the absolute value of the largest negative peak of all signal waveforms.

the SERs with medium-to-high SNR, we can neglect the multiplicative factor p_1 and p_2 in this case with only negligible over-estimation of the power gains[2], as in Table I at the bottom of this page.

Figure 2.3−Figure 2.9 include the designed symbol waveforms for the MSM-Normal, MSM-SPSS, and MSM-JDCMP with $N_b = 4$ and $K = 2$, and Figure 2.10−Figure 2.15 has accordingly waveforms while $N_b = 6$ and $K = 3$. Different waveforms are associated with different colors. We observe that the waveforms associated with the MSM-Normal and MSM-SPSS are less "irregular" while the one with MSM-JDCMP seems more random. Intuitively, the MSM-JDCMP is expected to take better usage of the design space. The Monte-Carlo simulation comparing the symbol error rate performance of the three schemes is shown by Figure 2.16, where the testing symbol sequence is of length 2×10^6.

[2]In other words, with medium-to-high SNR, we only need to slightly increase $d_{min,1}$ to obtain a large decrease of SER without significantly increase the overall power.

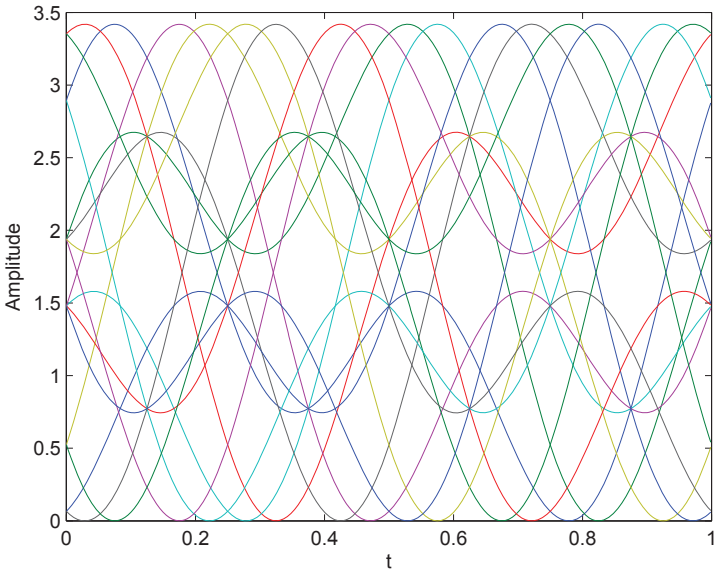

Figure 2.3: MSM-Normal symbol waveforms with adaptive bias ($N_b = 4$).

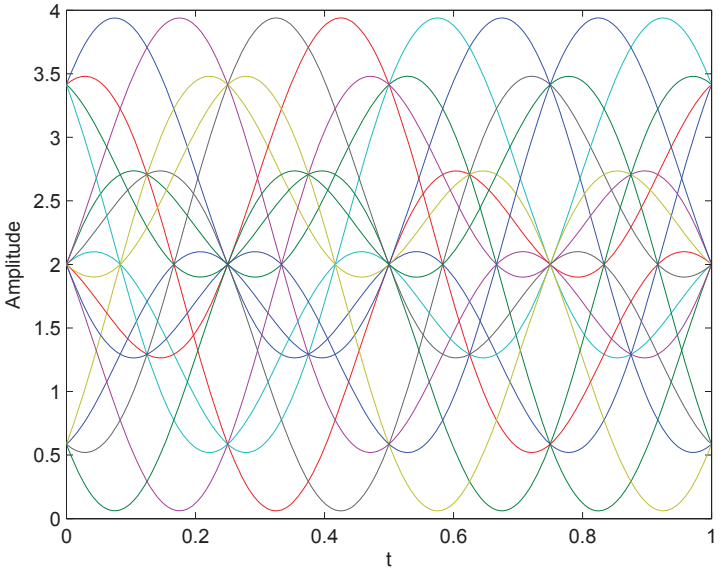

Figure 2.4: MSM-Normal symbol waveforms with enough bias ($N_b = 4$).

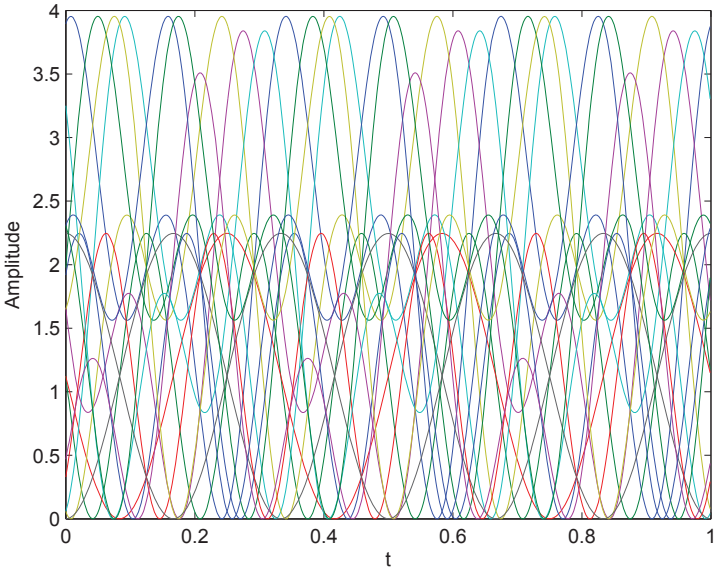

Figure 2.5: MSM-SSPS symbol waveforms minimizing the electrical power ($N_b = 4$).

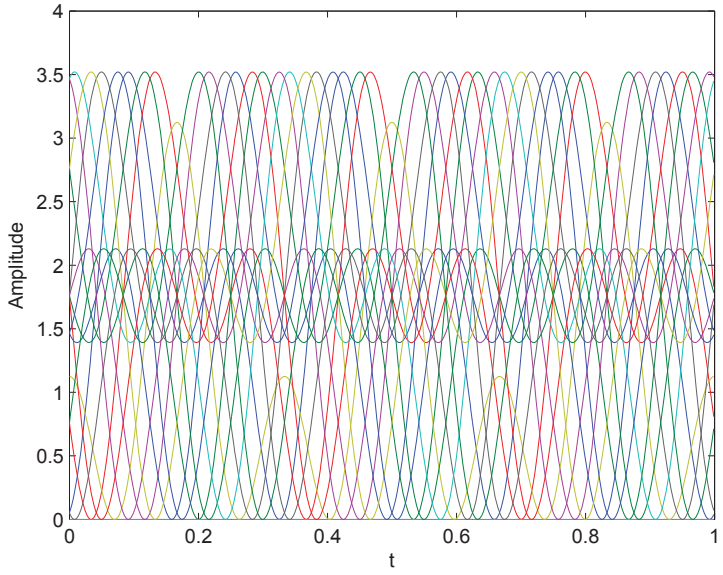

Figure 2.6: MSM-SPSS symbol waveforms minimizing the optical power ($N_b = 4$).

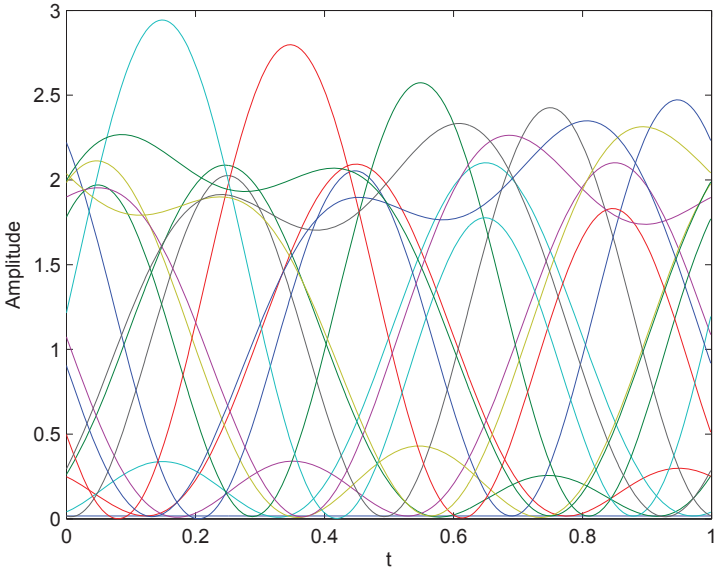

Figure 2.7: MSM-JDCMP symbol waveforms minimizing the electrical power ($N_b = 4$).

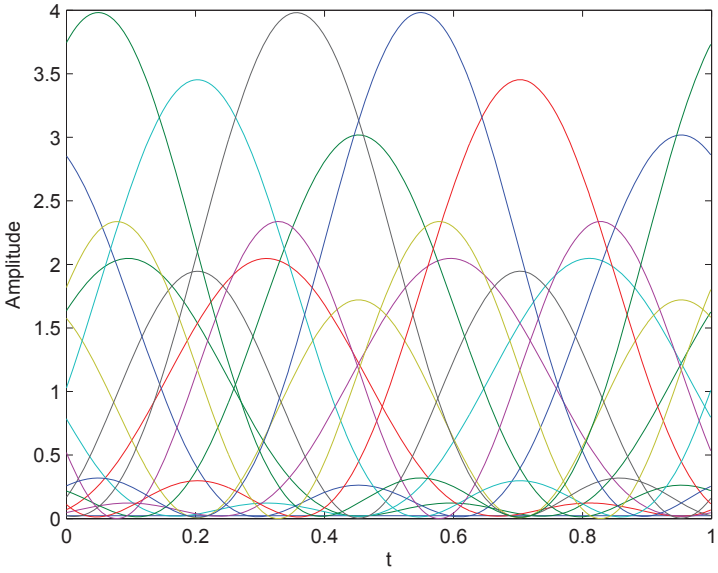

Figure 2.8: MSM-JDCMP symbol waveforms minimizing the optical power ($N_b = 4$).

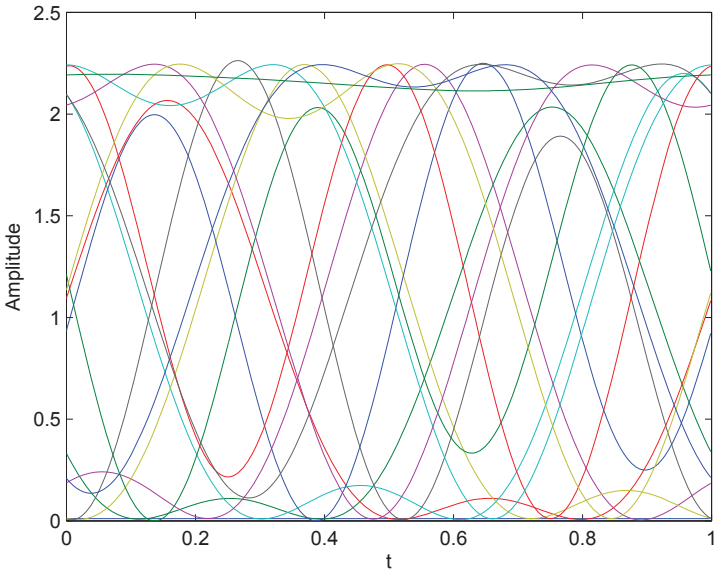

Figure 2.9: MSM-JDCMP symbol waveforms minimizing the peak power ($K = 2, N_b = 4$).

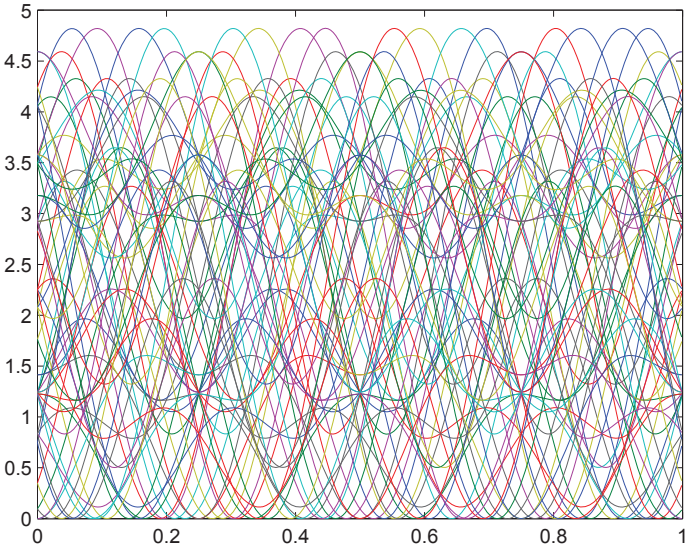

Figure 2.10: MSM-Normal symbol waveforms with adaptive bias ($N_b = 6$).

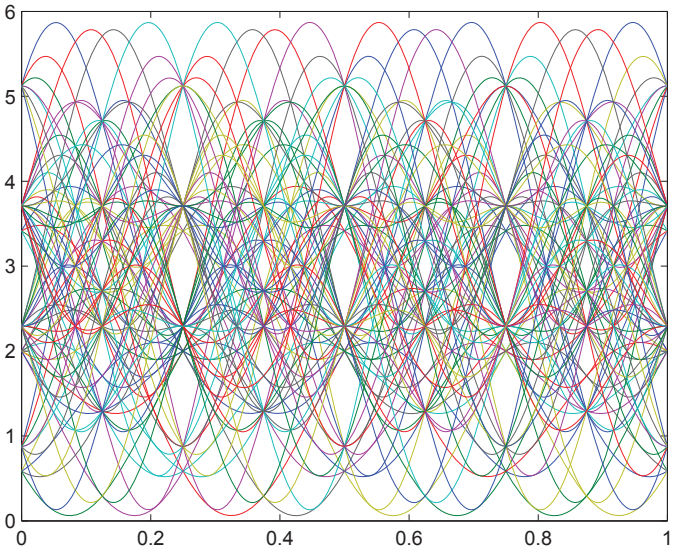

Figure 2.11: MSM-Normal symbol waveforms with enough bias ($N_b = 6$).

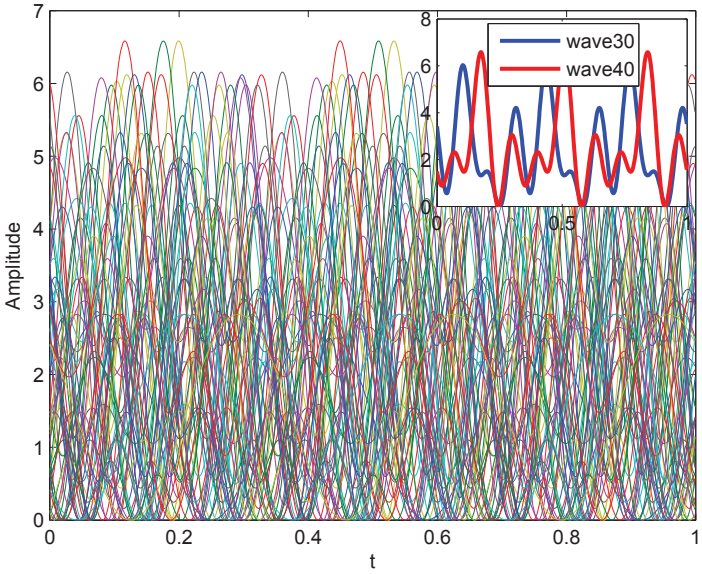

Figure 2.12: MSM-SSPS symbol waveforms minimizing the electrical power ($N_b = 6$).

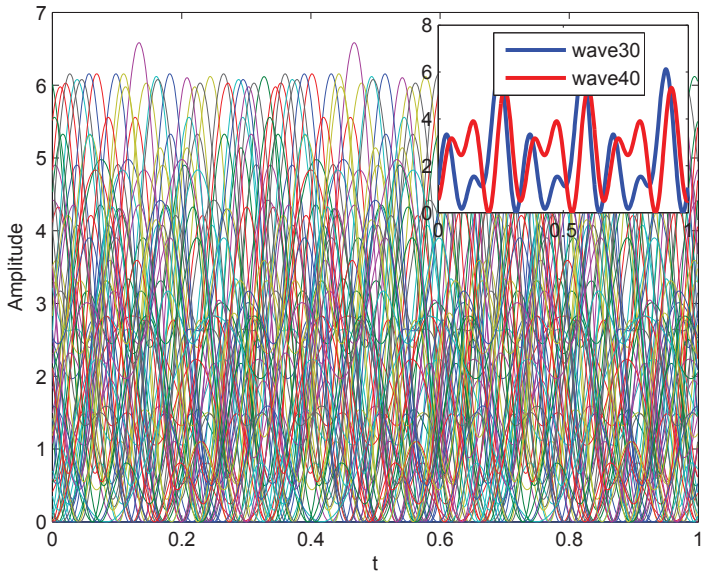

Figure 2.13: MSM-SPSS symbol waveforms minimizing the optical power ($N_b = 6$).

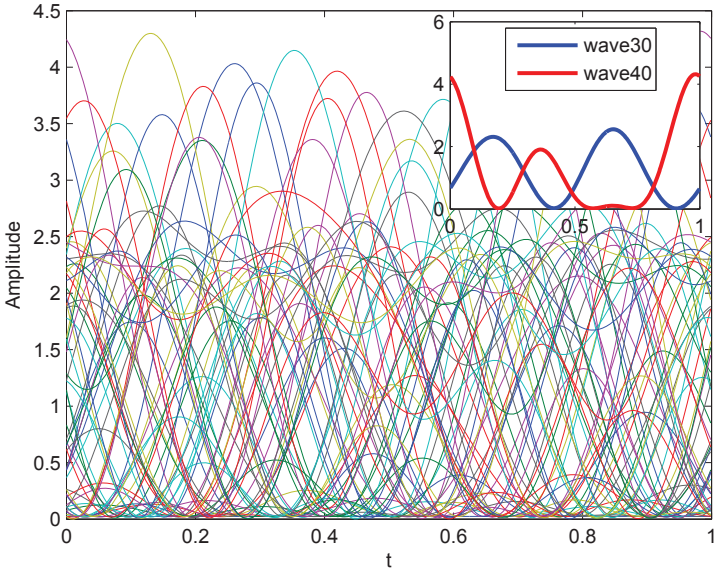

Figure 2.14: MSM-JDCMP symbol waveforms minimizing the electrical power ($N_b = 6$).

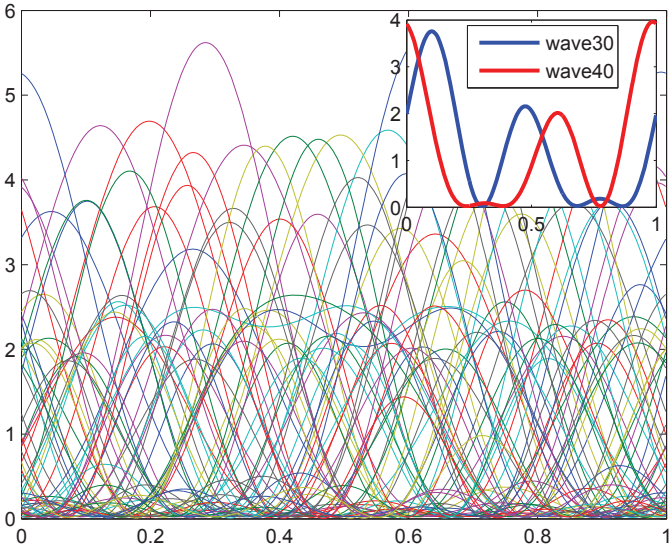

Figure 2.15: MSM-JDCMP symbol waveforms minimizing the optical power ($N_b = 6$).

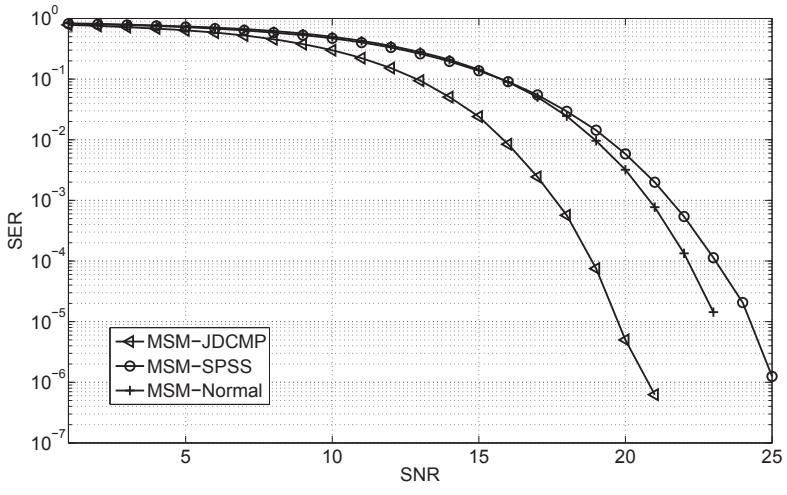

Figure 2.16: SER performance of the three schemes when $K = 2$, $N_b = 4$, with the same E_a.

2.6.3 Spectral Efficiency and Power Efficiency Tradeoff

Increasing K for a fixed N_b, i.e., sacrificing a portion of the spectrum efficiency, could serve to increase the power efficiency. $\Theta_{E,16}^{0,4}$ offers 2.31dB electrical power gain over $\Theta_{E,16}^{0,2}$. Corresponding waveforms are shown in Figure 2.17. It should be noted that no further gain is guaranteed to be achieved with further increasing K, e.g. $\Theta_{E,16}^{0,6}$ is no better than $\Theta_{E,16}^{0,4}$.

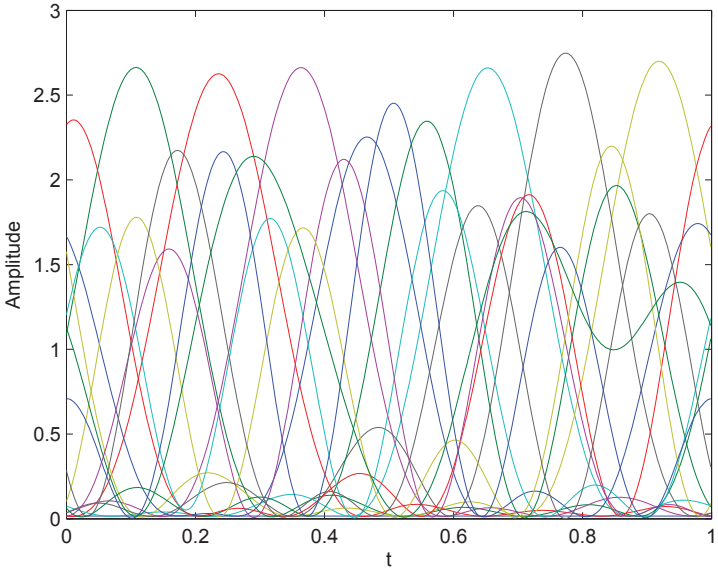

Figure 2.17: MSM-JDCMP symbol waveforms minimizing the electrical power ($K = 4, N_b = 4$).

2.6.4 Nonlinear Distortion Mitigation with MSM-JDCMP

Figure 2.18 - Figure 2.21 show the waveforms designed to constraint the short-term PAPR to be 3dB with $K = 2$ and $N_b = 4$ by choosing $\alpha_i = \alpha \; \forall i$. Figure 2.22- Figure 2.25 show the waveforms designed to constraint the long-term PAPR to be 3dB. Whether

one criterion is better than the others depends on the exact form of the transfer function of HPA and the probabilities of symbol occurrence. If a certain sequence has a nontrivially higher chance of transmission, it is better to force its amplitude into the linear region and in the mean time control the dynamic range of all sequences.

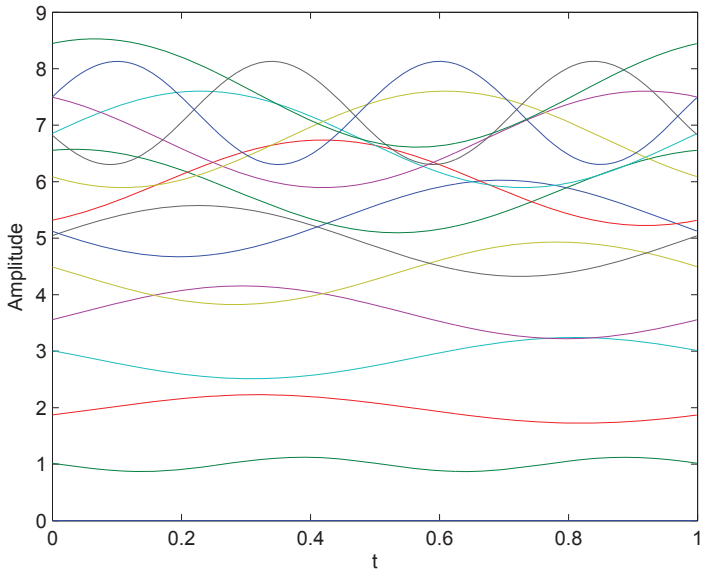

Figure 2.18: MSM-JDCMP symbol waveforms with short-term PAPR $\leq$ 1dB.

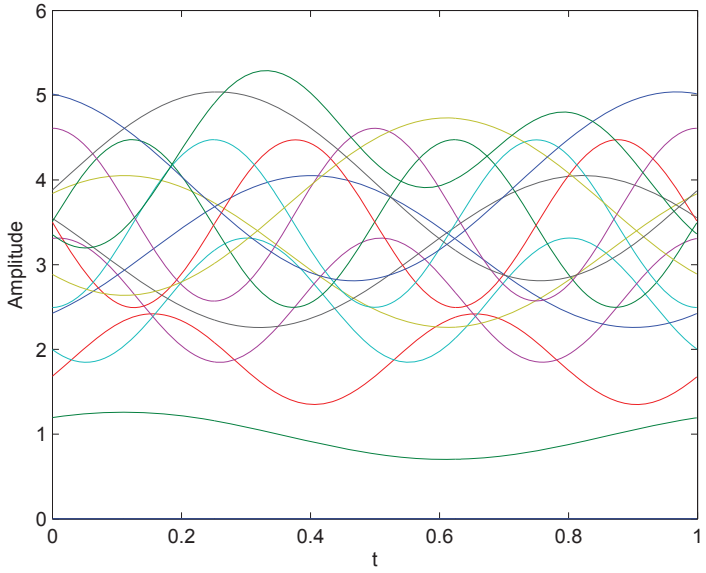

Figure 2.19: MSM-JDCMP symbol waveforms with short-term PAPR $\leq$ 2dB.

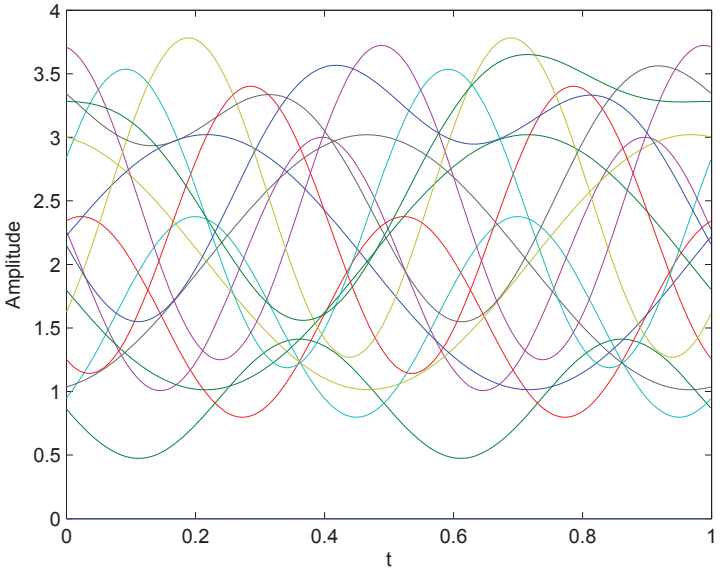

Figure 2.20: MSM-JDCMP symbol waveforms with short-term PAPR $\leq$ 3dB.

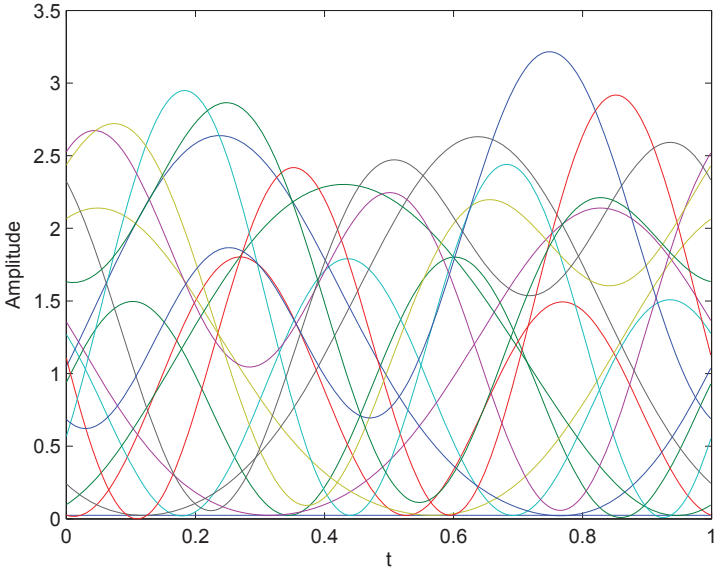

Figure 2.21: MSM-JDCMP symbol waveforms with short-term PAPR $\leq$ 5dB.

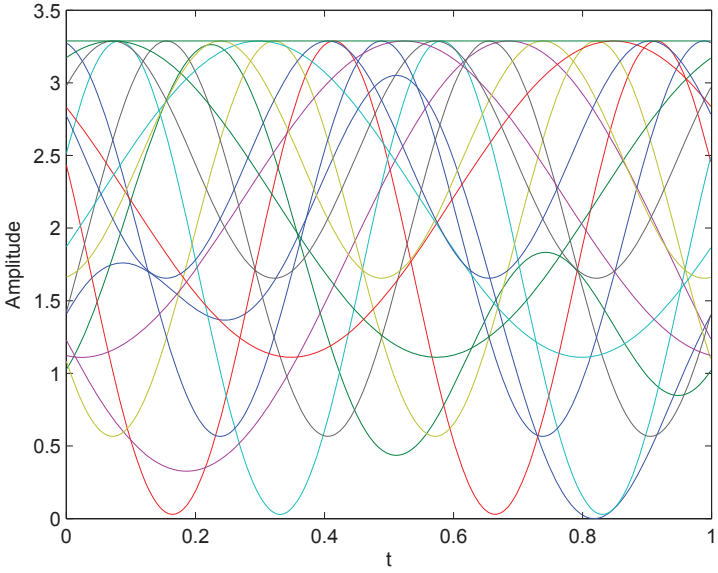

Figure 2.22: MSM-JDCMP symbol waveforms with long-term PAPR $\leq$ 1dB.

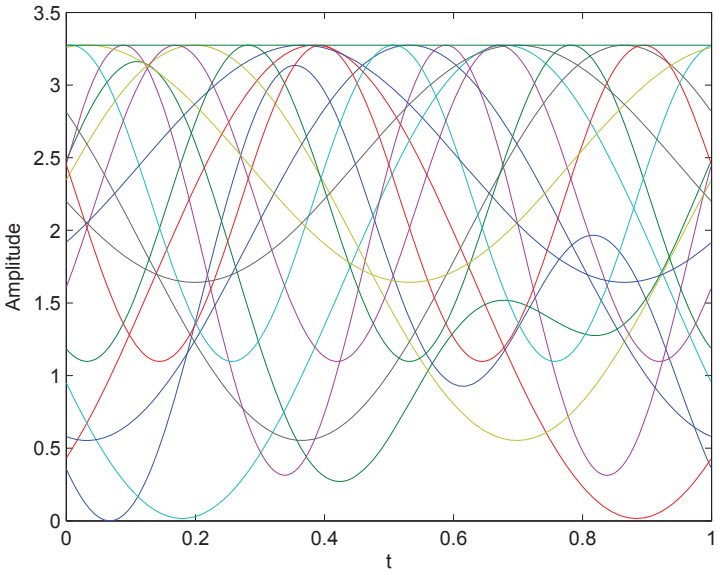

Figure 2.23: MSM-JDCMP symbol waveforms with long-term PAPR $\leq$ 2dB.

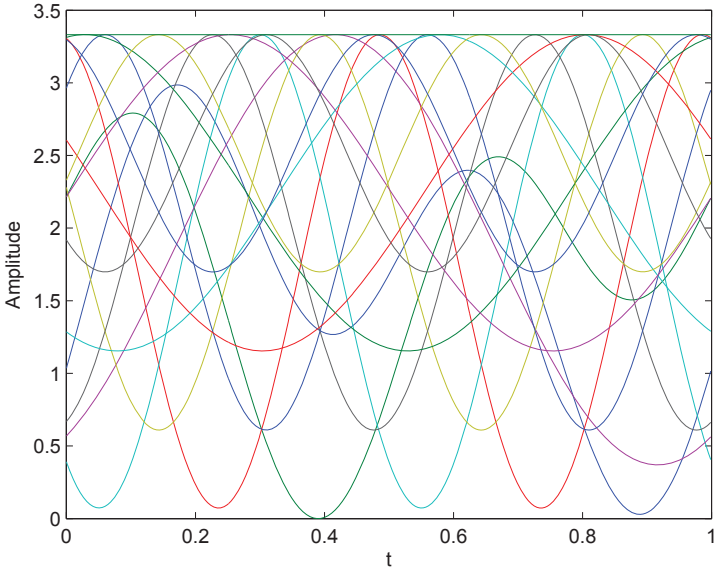

Figure 2.24: MSM-JDCMP symbol waveforms with long-term PAPR $\leq$ 3dB.

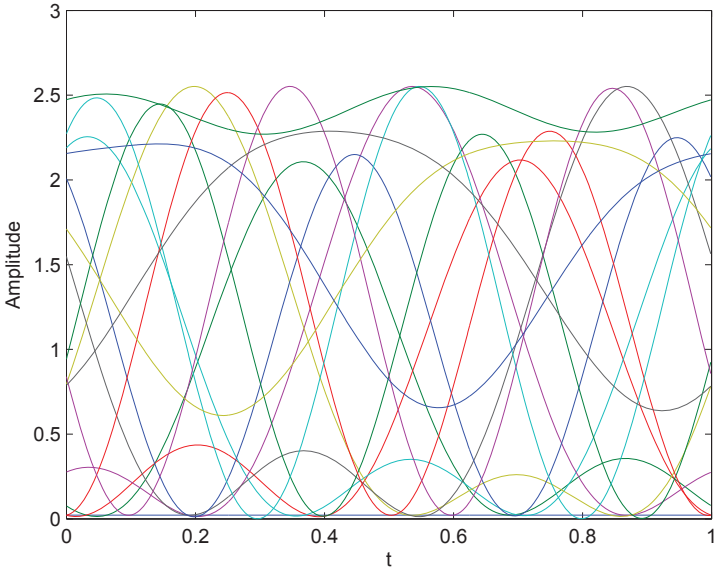

Figure 2.25: MSM-JDCMP symbol waveforms with long-term PAPR $\leq$ 3dB.

2.6.5 Selective-fading Channel with TDRC Pulse Shaper: A Design Example

We consider a chosen selective-fading channel

$$h(t) = \frac{1}{2}\delta(t) + \frac{1}{4}\delta(t - \frac{1}{18}) + \frac{1}{10}\delta(t - \frac{1}{9}) + \frac{1}{20}\delta(t - \frac{1}{6}) \tag{2.41}$$

And we use the window function as defined in (2.9) as pulse shaper, with the roll-off factor $\beta = 0.1$. When $K = 2$ and $N_b = 4$, we can obtain the pre-equalizer by using Proposition

1 calculated as follows

$$\mathbf{P} = \begin{bmatrix} 1.1111 & 0 & 0 & 0 & 0 \\ 0 & 1.1350 & 0.2620 & 0 & 0 \\ 0 & -0.2620 & 1.1350 & 0 & 0 \\ 0 & 0 & 0 & 1.2230 & 0.5409 \\ 0 & 0 & 0 & -0.5409 & 1.2230 \end{bmatrix} \tag{2.42}$$

With MSM-JDCMP, the designed waveforms are shown by Figure 2.26.

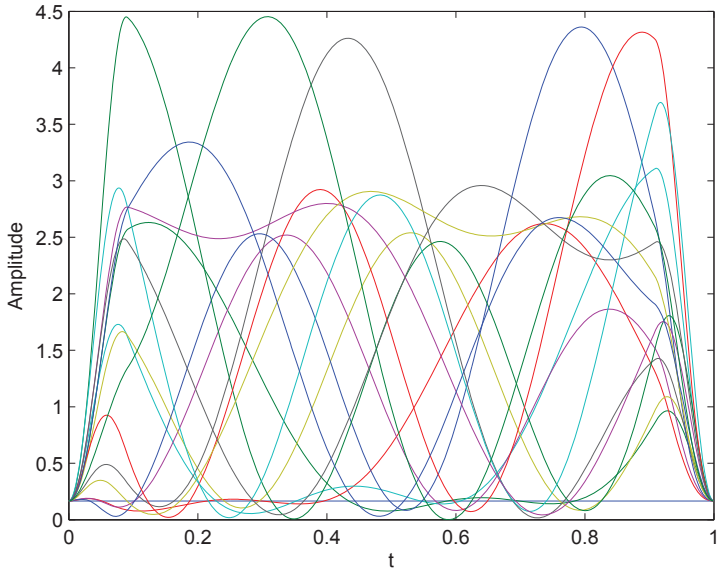

Figure 2.26: MSM-JDCMP symbol waveforms minimizing the electrical power with selective-fading channel ($K = 2, N_b = 4$).

2.6.6 The improved labelings

Recall the BER in (2.37)

$$P_b = \frac{2\lambda_1 N_n}{N_b N_c} Q\left(\sqrt{\frac{1}{2N_0}}\right) \tag{2.43}$$

where the erroneous number of bits λ needs to be minimized. In the previous sections we only calculated the Q function part, while this assumption is only accurate with medium to high SNRs. The constant multiplicative part should also be taken into account with lower SNR.

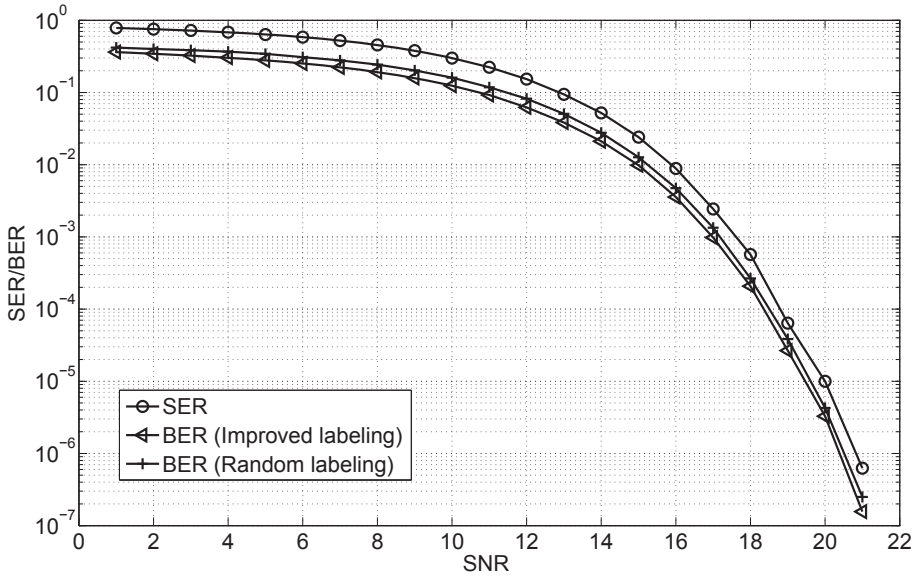

Figure 2.27: SER and BER performance with/without improved labeling using MSM-JDCMP to minimize electrical power.

Two points are treated as neighbors if the following holds

$$1 \leq ||\mathbf{c}_i - \mathbf{c}_j|| \leq 1 + \delta \tag{2.44}$$

where δ is chosen such that

$$\frac{Q(\sqrt{E_a/2N_0})}{Q(\sqrt{(1+\delta)^2 E_a/2N_0})} \geq \mu \tag{2.45}$$

$$\text{SNR} = 10 \log_{10} \frac{E_a}{N_0} \text{ [dB]} \tag{2.46}$$

where SNR stands for the signal-to-noise ratio, E_a is the average electrical energy over all waveforms, μ is a large number so that only pairs with distances smaller than $1 + \delta$ are treated as neighbors, i.e., The pairwise error associated with non-neighbor pairs is neglected. $\mu = 100$ is chosen in this section. It can be observed by simulations that further increasing μ does not change the results much. For $\Theta_{E,16}^{0,2}$, the best corresponding constellation labeling is found for each SNR value by BSA. The exhaustive search method, if applied, needs to compare $64!$ different labeling such that it is too costly to be useful. It can be observed from Figure 2.27 that improved labeling offers a marginal BER gain (0.1dB at 10^{-6} BER) over the random average (over 100 arbitrary trials) labeling ($K = 2, N_b = 4$).

2.7 Chapter Conclusion

In this chapter, we have proposed a novel and efficient constellation design scheme, termed MSM-JDCM for the optical IM/DD systems. It offers significant power gains over the traditional methods. With the MSM-JDCMP, highly compact sphere packings in higher dimensional space that minimize the electrical/optical/peak powers are found in both flat-fading and selective-fading scenarios. Besides, the MSM-JDCM with PAPR constraints mitigates the system nonlinear distortion. It could potentially be a supplement to many other existing anti-distortion algorithms. In addition, we applied the binary switching algorithm to search for the best labeling. The obtained labeling greatly reduces the BER of the system.

Chapter 3

Constellation Design for Multi-color Visible Light Communications

3.1 Constellation Design with Ideal Channel

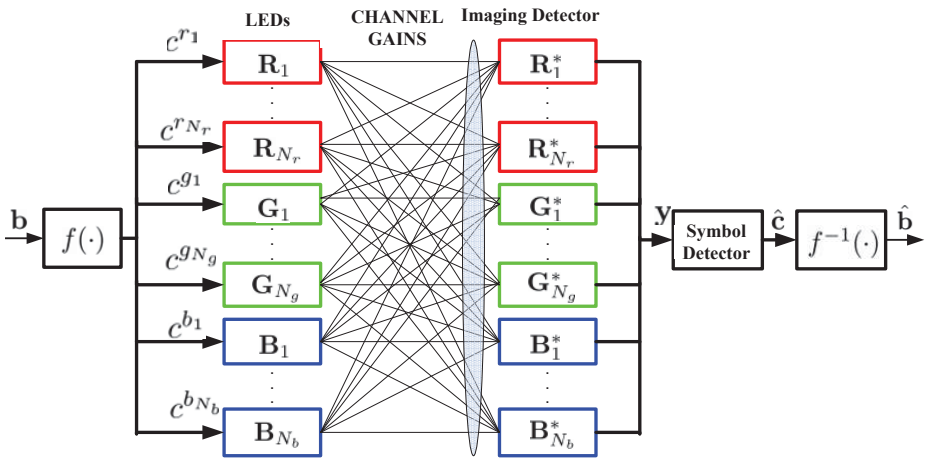

Figure 3.1: System diagram of the proposed CSK-Advanced System.

The system diagram is shown by Fig. 1, where N_r red LEDs, N_g green LEDs, and N_b blue LEDs are applied. In one symbol interval of length T_s, a random bit sequence $\mathbf{b}$ of size $N_b \times 1$ is first mapped by a BSA mapper $f(\cdot)$ to a symbol vector $\mathbf{c}$ of size $N_T \times 1$, where $N_T = N_r + N_g + N_b$. The symbol $\mathbf{c}$ is chosen from a constellation

$$\mathcal{C} = (\mathbf{c}_1, \mathbf{c}_2, \ldots, \mathbf{c}_{N_c}). \tag{3.1}$$

where $N_c = 2^{N_b}$ denotes the constellation size. Intensity modulation (IM) is applied by each LED light such that $\mathbf{c} \geq 0$. The symbol $\mathbf{c}$ is then passed through the optical channel $\mathbf{H}$ of size $N_T \times N_T$. The output of the color filters can be written as

$$\mathbf{y} = \gamma\eta\mathbf{H}\mathbf{c} + \mathbf{n}. \tag{3.2}$$

where η is the electro-optical conversion factor, γ is the photodetector responsivity, and $\gamma\eta = 1$ is assumed without loss of generality (w.l.o.g.). Each dimension of $\mathbf{n}$ is assumed as a zero mean Gaussian random variable with variance $N_0/2$ [79]. Such noise assumption is valid for both ideal channel and channel with cross-talks case [49, 19]. The received intensity vector $\mathbf{y}$ is passed through an imaging detector to obtain estimate of the transmitter symbol, which is then de-mapped by $f^{-1}(\cdot)$ to recover the bit sequence.

We first formulate the optimization problem with ideal channel, i.e. $\mathbf{H} = \mathbf{I}_{N_T}$. Define a joint constellation vector $\mathbf{c_T} = [\mathbf{c}_1^T\ \mathbf{c}_2^T\ \ldots \mathbf{c}_{N_c}^T]^T$, and the i-th symbol is written as

$$\mathbf{c}_i = [c_i^{r_1} \ldots c_i^{r_{N_r}}\ c_i^{g_1} \ldots c_i^{g_{N_g}}\ c_i^{b_1} \ldots c_i^{b_{N_b}}] = \mathbf{J}_i\mathbf{c_T}. \tag{3.3}$$

where $\mathbf{J}_i = [\mathbf{O}_{N_T} \ldots \mathbf{I}_{N_T} \ldots \mathbf{O}_{N_T}]$ is a selection matrix with all zeros except for an identity matrix at the i-th block.

3.1.1 The objective function

The SER performance of the system is governed by the MED among all pairs of constellation points when the signal-to-noise-ratio (SNR) is sufficient, which is typically true for VLC. Therefore, we seek to minimize the SER by maximizing the MED. In order that the MED is larger than t, the following conditions must hold [4]

$$\mathbf{c}_T^T \mathbf{F}_l \mathbf{c_T} \geq t. \tag{3.4}$$

where $\mathbf{F}_{l(p,q)} = \mathbf{E}_{pq}$, $\mathbf{E}_p = \mathbf{e}_p^T \otimes \mathbf{I}_{N_c}$ (Kronecker product), $\mathbf{e}_p$ of size $N_T \times 1$ has all zeros except the p-th element being one, $\mathbf{E}_{pq} = \mathbf{E}_p^T\mathbf{E}_p - \mathbf{E}_p^T\mathbf{E}_q - \mathbf{E}_q^T\mathbf{E}_p + \mathbf{E}_q^T\mathbf{E}_q$, and

$$l \cong (p-1)N_c - \frac{p(p+1)}{2} + q,\ p, q \in 1, 2, \ldots, N_c,\ p < q. \tag{3.5}$$

The distance constraints (5.16) are nonconvex in $\mathbf{c_T}$. We approximate (5.16) by a first order Taylor series approximation around $\mathbf{c_T}^{(0)}$, i.e.

$$\mathbf{c}_T^T \mathbf{F}_l \mathbf{c_T} \cong 2\mathbf{c_T}^{(0)T} \mathbf{F}_l \mathbf{c_T} - \mathbf{c_T}^{(0)T} \mathbf{F}_l \mathbf{c_T}^{(0)} \triangleq h_l^{(0)}(\mathbf{c_T}) \geq t. \tag{3.6}$$

where $\mathbf{c_T}^{(0)}$ is either a random initialization point or a previously attained estimate.

3.1.2 The average color and average power constraint

The average of all LEDs' intensities can be written as a $N_T \times 1$ vector

$$\bar{\mathbf{c}} = \big(\frac{1}{N_c}\sum_{i=1}^{N_c} \mathbf{J}_i\big)\mathbf{c_T} = \bar{\mathbf{J}}\mathbf{c_T} = [\bar{c}^{r_1} \ldots \bar{c}^{r_{N_r}}\ \bar{c}^{g_1} \ldots \bar{c}^{g_{N_g}}\ \bar{c}^{b_1} \ldots \bar{c}^{b_{N_b}}]^T. \tag{3.7}$$

If only the average of r/g/b intensities are specified instead of average of all streams, the following 3×1 vector is used

$$\mathbf{c}_3 = P_o \cdot [\bar{c}^r\ \bar{c}^g\ \bar{c}^b]^T = \mathbf{K}\bar{\mathbf{c}} = \mathbf{K}\bar{\mathbf{J}}\mathbf{c_T}. \tag{3.8}$$

which is the average color and power constraint, where $\mathbf{K}$ is a selection matrix summing up r/g/b intensities accordingly, P_o is the average optical power, and

$$\bar{c}^r + \bar{c}^g + \bar{c}^b = 1. \tag{3.9}$$

$$P_o \bar{c}^x = \bar{c}^{x_1} + \ldots + \bar{c}^{x_{N_x}}. \tag{3.10}$$

where $x \in \{r, g, b\}$. By properly selecting $\mathbf{c}_3$, the CRI and LER constraints can be met [9].

3.1.3 The optical PAPR constraint

For each LED, the optical PAPR is defined as the ratio of the highest power over the average power. Mathematically, the PAPR of the j-th LED can be written as

$$\Phi_j = \frac{\max(\mathbf{K}_j \mathbf{c_T})}{1/N_c \cdot \text{sum}(\mathbf{K}_j \mathbf{c_T})}, \ \ \forall j \in [1, N_T] \tag{3.11}$$

where by $\text{sum}(\mathbf{a})$ the elements in vector $\mathbf{a}$ are added up, $\mathbf{K}_j$ is a selection matrix of size $N_c \times N_c N_T$ and by $\max(\mathbf{K}_j \mathbf{c_T})$ the largest intensity from the N_c values for the j-th LED is selected.

The PAPR of an individual LED can be constrained as

$$\Phi_j \leq \alpha_j, \ \ \forall j \in [1, N_T] \tag{3.12}$$

3.1.4 CRI and LER constraints

The color rendering index (CRI), sometimes called color rendition index, is a quantitative measure of the ability of a light source to reproduce the colors of various objects faithfully in comparison with an ideal or natural light source. Light sources with a

high CRI are desirable in color-critical applications such as photography and cinematography [15]. Luminous efficacy is a measure of how well a light source produces visible light. It is the ratio of luminous flux to power. Depending on context, the power can be either the radiant flux of the source's output, or it can be the total power (electric power, chemical energy, or others) consumed by the source [63]. The CRI and LER are important practical lighting constraints. By properly selecting $\mathbf{c}_3$, specific CRI and LER constraints can be met.

3.1.5 The optimization problem

When $\mathbf{H} = \mathbf{I}_{N_T}$ the problem can be formulated as

$$\begin{aligned} \underset{\mathbf{c_T},t}{\text{Maximize}} \quad & t \\ \text{subject to} \quad & \mathbf{K}\bar{\mathbf{J}}\mathbf{c_T} = \mathbf{c}_3, \\ & \mathbf{c_T} \geq 0, \\ & h_l^{(0)}(\mathbf{c_T}) \geq t \qquad \forall l, \\ & N_c \max(\mathbf{K}_j\mathbf{c_T}) - \alpha_j \text{sum}(\mathbf{K}_j\mathbf{c_T}) \leq 0 \qquad \forall j. \end{aligned} \tag{3.13}$$

which can be straightforwardly proven as a convex optimization problem. With the first three constraints, it is termed a regular optimization problem and with all constraints a PAPR-constrained problem. By iteratively solving (3.13), a local optimal constellation $\mathbf{c_T}^1$ can be obtained [1]. With multiple runs starting from different initial point $\mathbf{c_T}^{(0)}$, the best of solutions, $\mathbf{c_T}^*$ is selected.

[1] One can refer to a similar problem in [4] for convergence, complexity and performance analysis.

3.2 Constellation Design with CwC

The channel cross-talks are caused by the mismatch between the emission spectra of the transmitter LEDs and the transmission spectra of the receiver filters. The CwC has the following structure assuming single RGB LED is employed based on [19, 49] and experiments.

$$\mathbf{H}_c = \begin{bmatrix} 1-\epsilon & \epsilon & 0 \\ \epsilon & 1-2\epsilon & \epsilon \\ 0 & \epsilon & 1-\epsilon \end{bmatrix}$$

where the parameter $\epsilon \in [0, 0.5)$ characterizes both attenuation and interference effects.

By SVD (singular value decomposition), $\mathbf{H}_c = \mathbf{USV}^H$, where $\mathbf{U}$ and $\mathbf{V}$ are unitary matrices of size $N_T \times r$, $\mathbf{S}$ is a diagonal matrix of size $r \times r$, and r is the rank of $\mathbf{H}_c$. In this case, r is the dimension of space for constellation design instead of N_T, and the more severe are the images overlap the small value r takes. We apply a pre-equalizer $\mathbf{P} = \mathbf{VS}^{-1}$ at the transmitter-side and a post-equalizer $\mathbf{U}^H$ at the receiver-side to equalize

the channel[2]. Define $\mathbf{P_T} = \mathbf{I}_{N_c} \otimes \mathbf{P}$, and the optimization in (3.13) can be transformed as

$$\begin{aligned} \underset{\mathbf{c_T},t}{\text{Maximize}} \quad & t \\ \text{subject to} \quad & \mathbf{K}\bar{\mathbf{J}}\mathbf{P_T}\mathbf{c_T} = \mathbf{c}_3, \\ & \mathbf{P_T}\mathbf{c_T} \geq 0, \\ & h_l^{(0)}(\mathbf{c_T}) \geq t \qquad \forall l, \\ & N_c \max(\mathbf{K}_j\mathbf{P_T}\mathbf{c_T}) - \alpha_j \text{sum}(\mathbf{K}_j\mathbf{P_T}\mathbf{c_T}) \leq 0 \; \forall j. \end{aligned} \tag{3.14}$$

It should be noted that $\mathbf{c_T}$ now is of dimension $N_c r \times 1$, i.e., the constellation is designed in a r-dimensional space. With a decreased r, performance loss is expected.

As has been discussed, with $\mathbf{c_T}^*$ the lowest system SER is achieved with a fixed optical power (thus we call it a power-efficient constellation). To further minimize the system BER with a fixed SER, a good bit-to-symbol mapping function $f(\cdot)$ as shown in Fig. 1 need to be found. In this paper, we apply the binary switching (BSA) algorithm to find an optimized mapping. Since it is not the main focus of this paper, the details of BSA are omitted (we refer the readers interested to [60]).

3.3 Performance Evaluation

In this section, we provide numerical illustration of advantages of the CSK-Advanced with one RGB LED, i.e. $N_r = N_g = N_b = 1$. Both the CSK-Advanced and the conventional decoupled scheme can work with arbitrary color illumination. With one RGB LED, c_i $(i \in [1, 3])$ for the decoupled scheme takes value from OOK (2-PAM) constellations. To

[2] $\mathbf{n}$ and $\mathbf{U}^H\mathbf{n}$ have the same distribution, since $\mathbf{U}^H$ is unitary.

make a fair comparison, an 8-CSK-Advanced constellation should be designed. It needs to be noted that the spectrum efficiency (bits/sec/Hz) of both systems are chosen to be the same, the average optical powers are equal, and the average colors are identical.

3.3.1 Constellation design with ideal channel

Balanced lighting system

If the average intensity of each color is similar, we call the corresponding system "Balanced lighting system". For example, we choose average color as $\mathbf{c}_3^B = 10 \cdot [1/3,\ 1/3,\ 1/3]^T$ and the average power $P_o = 10$. For the conventional scheme, each LED can simply take value independently from binary constellations

$$\mathcal{C}_{B,r} = \mathcal{C}_{B,g} = \mathcal{C}_{B,b} = [0, 6.67].$$

The MED for each branch is $d_{min} \approxeq 6.67$. For our scheme, the optimized constellation is

$$\mathcal{C}_B^8 = \begin{bmatrix} 0 & 0 & 0 & 4.8485 & 0 & 0 & 14.5455 & 7.2727 \\ 14.5455 & 0 & 7.2727 & 4.8485 & 0 & 0 & 0 & 0 \\ 0 & 14.5455 & 0 & 4.8485 & 0 & 7.2727 & 0 & 0 \end{bmatrix}$$

The MED equals 7.27, such that we could expect a lower SER with sufficient SNR. The asymptotic power gain is approximately 0.86dB (=$10 \times \log(7.27/6.67)$).

Unbalanced lighting system

We choose the average color as $\mathbf{c}_3^U = 10 \cdot [0.44,\ 0.33,\ 0.22]^T$. With the conventional scheme, the LEDs take value from constellations

$$\mathcal{C}_{U,r} = [0, 8.88]\ \ \mathcal{C}_{U,g} = [0, 6.66]\ \ \mathcal{C}_{U,b} = [0, 4.44].$$

With our scheme, the optimized constellation

$$\mathcal{C}_u^8 = \begin{bmatrix} 0 & 7.2590 & 14.5550 & 0 & 6.4454 & 0 & 7.2960 & 0 \\ 6.4859 & 0 & 0 & 12.9718 & 7.2090 & 0 & 0 & 0 \\ 3.2598 & 7.2589 & 0 & 0 & 0 & 7.2590 & 0 & 0 \end{bmatrix}$$

The MED is approximately 7.26, which is smaller than MED of one branch but larger than MEDs of two branches of the conventional scheme.

Extremely Unbalanced lighting system

We choose the average color as $\mathbf{c}_3^E = 10 \cdot [0.7,\ 0.15,\ 0.15]^T$. With the conventional scheme, the LEDs take value from constellations

$$\mathcal{C}_{E,r} = [0, 14]\ \ \mathcal{C}_{E,g} = [0, 3]\ \ \mathcal{C}_{E,b} = [0, 3].$$

With our scheme, the optimized constellation is

$$\mathcal{C}_8^E = \begin{bmatrix} 12.6277 & 0 & 0 & 6.3139 & 9.0584 & 0 & 9.0584 & 18.9416 \\ 0 & 0 & 6.3139 & 0 & 0 & 0 & 5.6861 & 0 \\ 0 & 0 & 0 & 0 & 5.6861 & 6.3139 & 0 & 0 \end{bmatrix}$$

The MED is approximately 6.31, which is smaller than MED of one branch but larger than MEDs of two branches of the conventional scheme.

PAPR-constrained system

If *identical individual PAPR constraints* are added, i.e. $\alpha_j = \alpha$ into the optimization. The corresponding MEDs with varying PAPR are summarized in Table 1. It can be observed from that there is a tradeoff between power efficiency and PAPR for the three cases. With extremely low PAPR, e.g. $\alpha = 1.5$, the system suffers from severe power loss. With a PAPR increase of 3dB, e.g. from $\alpha = 2$ to $\alpha = 4$ which is typically tolerable, the power gain of unbalance systems are larger than balanced system.

We then simulate using bit sequence of length $N = 9 * 10^6$ for selected cases above to compare the BER performance among different systems versus different optical SNR, defined as [38, Eq.27]

$$\gamma_o = 10 \log_{10} \frac{P_o}{\sqrt{N_b N_0}} \tag{3.15}$$

where w.l.o.g. $T_s = 1$ is assumed.

Selected BER curves versus optical SNR are included in Fig. 2 and Fig. 3. In Fig. 2, CSK-Advanced system applies constellation $\mathcal{C}_8(\mathbf{c}_3^B)$ and in Fig. 3 constellation $\mathcal{C}_8(\mathbf{c}_3^E)$ is used. It can be observed that the with CSK-Advanced scheme non-trivial power gain is obtained over the conventional system, especially when the average color is not balanced.

Table 3.1: MED with varying PAPR and average color.

d_{min}	$\mathcal{C}_B^8$	$\mathcal{C}_U^8$	$\mathcal{C}_E^8$
$\alpha = 1.5$	3.54	3.40	2.84
$\alpha = 2$	6.67	5.58	4.38
$\alpha = 4$	7.07	7.26	6.31
$\alpha = 6$	7.27	7.26	6.31

The optimized mapping by BSA offers additional power gain for all OSNR range.

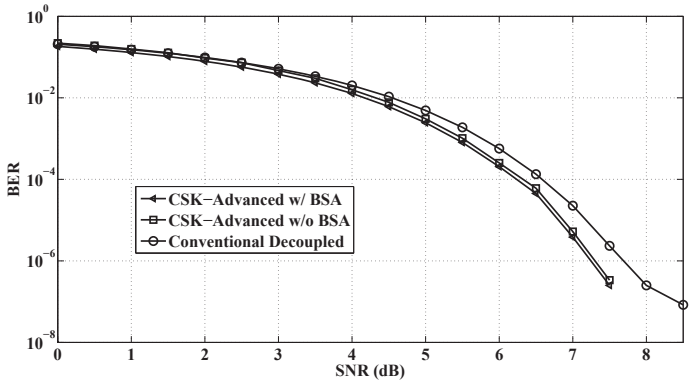

Figure 3.2: Balanced conventional system vs CSK-Advanced systems.

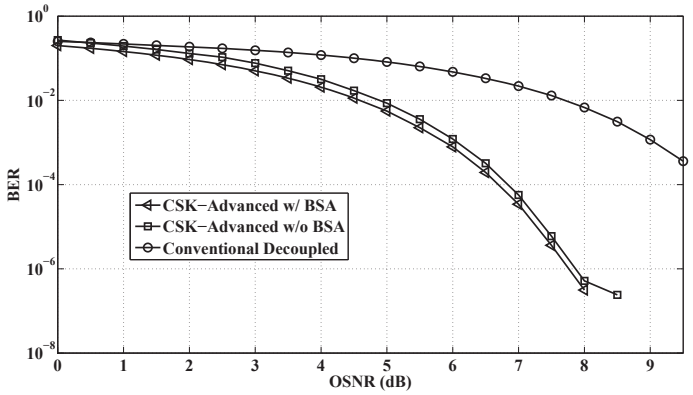

Figure 3.3: Extremely Unbalanced conventional system vs CSK-Advanced systems.

Histogram of MEDs of 1000 local optimal constellations for the balanced system is shown by Fig. 4. It can be seen that approximately $1/4$ of the runs will converge to satisfactory MEDs. Therefore, we would suggest only $20-30$ runs in practice to reduce complexity.

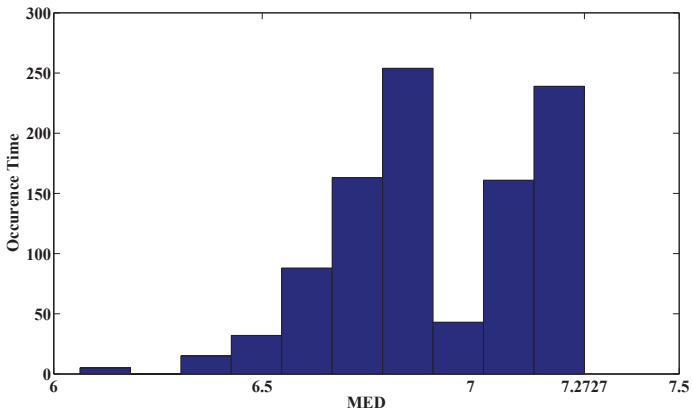

Figure 3.4: Histogram of MEDs of 1000 local optimal constellations.

Constellation labeling

The optimized bit-to-symbol mapping obtained by the binary switching algorithm when $\gamma_o = 5$dB is included in Table 2. With optimized mapping, only 1.33 out of 3 bits on average are in error when a symbol error occurs. Without BSA based mapping how average, 1.73 out of 3 bits on average (over results observed from 100 random labelings) are mis-interpreted instead. The optimized mapping tables can be computed offline.

Table 3.2: Optimized Bit-to-symbol mapping with OSNR=5dB.

Constellation Point	Optimized Labeling
(0, 0, 7.27)	000
(0, 0, 0)	001
(0, 14.55, 0)	010
(0, 7.27, 0)	011
(0, 0, 14.55)	100
(7.27, 0, 0)	101
(14.55, 0, 0)	110
(4.85, 4.85, 4.85)	111

3.3.2 Constellation design with CwC

SVD-based pre-equalizer

Consider the following 3×3 channel with moderate cross-talks, e.g. $\epsilon_1 = 0.1$,

$$\mathbf{H}_{\epsilon_1} = \begin{bmatrix} 0.9 & 0.1 & 0 \\ 0.1 & 0.8 & 0.1 \\ 0 & 0.1 & 0.9 \end{bmatrix}$$

By SVD we have $\mathbf{H}_{\epsilon_1} = \mathbf{U}_{\epsilon_1}\mathbf{S}_{\epsilon_1}\mathbf{V}_{\epsilon_1}^H$. The pre-equalizer $\mathbf{P}_{\epsilon_1,pr} = \mathbf{V}_{\epsilon_1}\mathbf{S}_{\epsilon_1}^{-1}$ and post-equalizer $\mathbf{P}_{\epsilon_1,po} = \mathbf{U}_{\epsilon_1}^H$. The corresponding optimized constellation for balanced system is

$$\mathcal{C}_{\epsilon_1}^8 = \begin{bmatrix} -7.8376 & -5.7208 & -4.6893 & -0.0000 & -8.4386 & -3.9188 & -7.8123 & -7.7708 \\ 8.6391 & -0.9559 & -5.1688 & -0.0000 & 4.5539 & 4.3196 & 0.0000 & -0.0742 \\ 3.8794 & -2.0338 & 2.3211 & 0.0000 & -2.2190 & 1.9397 & -7.7338 & 3.8463 \end{bmatrix}$$

The MED with varying area of overlap for balance, unbalanced, and extremely unbalanced systems are summarized in Table 3. In practice, the mismatch between the emission spectra of the transmitter LEDs and the transmission spectra of the receiver filters is restricted, and cases with $\epsilon \geq 0.2$ are too rare to be included.

Comparison with post-equalized systems

Instead of redesign the constellations subject to a transformed set of constraints due to employment of a pre-equalizer $\mathbf{P}$, zero-forcing (ZF) $\mathbf{G}_Z$ or linear minimum-mean-squared-error (LMMSE) based post-equalizer $\mathbf{G}_L$ can be employed at the receiver [**?**] to

Table 3.3: MED with varying area of overlap.

d_{min}	$\mathcal{C}^8_{B,D}$	$\mathcal{C}^8_{U,D}$	$\mathcal{C}^8_{E,D}$
$\epsilon = 0$	7.2727	7.2590	6.3139
$\epsilon = 0.05$	6.7621	6.6748	5.9275
$\epsilon = 0.1$	6.3275	6.1464	5.5657
$\epsilon = 0.15$	5.9462	5.7769	5.1635
$\epsilon = 0.2$	5.5670	5.3692	4.7727

mitigate the cross-talks.

Fig. 5 shows the corresponding BERs against increased crosstalks for a balanced system employing different schemes when OSNR is fixed to 5dB. It is seen that our SVD-based scheme significantly outperforms systems employing either ZF or LMMSE post-equalizers. Fig. 6 shows the BERs against OSNR for a balanced system when ϵ is fixed to 0.1. With this particular parameters chosen, there is no significant difference between ZF and LMMSE based system performance and therefore we only included the LMMSE based results.

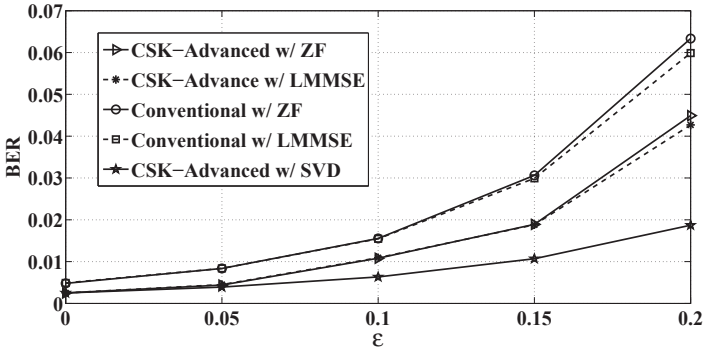

Figure 3.5: BER against ϵ with OSNR=5dB for a balanced system.

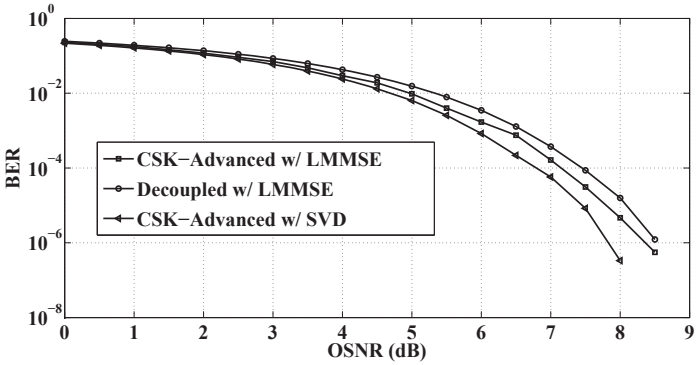

Figure 3.6: BER against OSNR with $\epsilon = 0.1$ for a balanced system.

3.4 Conclusion

A novel constellation design scheme, CSK-Advanced, for visible light communications with arbitrary number of RGB LEDs is proposed in this paper. With both optimized constellation and bits-to-symbols mapping, non-trivial power gains are observed comparing with conventional decoupled systems. The more unbalanced color illumination the system works with, the larger power gains are expected. To avoid excessive nonlinear distortion, individuals optical PAPR constraints can be included with the optimization. Further, to deal with CwC, an SVD-based pre-equalizer is introduced, and the constellations are re-designed subject to a transformed set of constraints. It is shown by simulations that such SVD-based approach greatly outperforms counterparts employing ZF or LMMSE-based post-equalizers.

Chapter 4

Training Resource Allocation for Mitigating Estimation Error Propagation in a Wireless Relaying System

4.1 Channel Model

As in Figure 1.2, we consider a three-node AF relaying system without direct link from source to destination. Each node is equipped with a singular antenna (a single transceiver on the relay works well in half-duplex mode). The channel h_{XY} from X to Y adopts Rayleigh fading, i.e., is a circular symmetric complex Gaussian (CSCG) random

variable (RV) with prior statistics $h_{XY} \sim CN(0, \sigma_{XY}^2)$. The source-to-relay channel h_{SR} and relay-to-destination channel h_{RD} are independent but not identical (i.n.i.d.). To avoid analytical redundancy, all noise elements in both phases are assumed to be CSCG RVs with zero mean and identical variance σ_w^2.

4.2 Channel Estimation for Phase-1

In phase 1, the relay transmits to the destination a training sequence $\mathbf{s}_R \in C^{N_R \times 1}$, across N_R time slots (during which h_{RD} is assumed to be constant). Each of the N_R symbols is assumed to have equal power P_R such that $\mathbf{s}_R \mathbf{s}_R^H = N_R P_R$ (any non-identical column drawn from a $N_R \times N_R$ DFT matrix scale by $\sqrt{N_R P_R}$ can be a good candidate).

The received signal at the destination node is:

$$\mathbf{y}_D^{(1)} = h_{RD}\mathbf{s}_R + \mathbf{w}_D^{(1)} \tag{4.1}$$

This is a well-known linear Gaussian model. The LMMSE estimator of h_{RD} is just the MMSE estimator [39], which can be found by:

$$\begin{aligned} \hat{h}_{RD} &= R_{h_{RD},\mathbf{y}_D^{(1)H}} R^{-1}_{\mathbf{y}_{RD}^{(1)},\mathbf{y}_{RD}^{(1)H}} \mathbf{y}_D^{(1)} \\ &= \sigma_{RD}^2 \mathbf{s}_R^H (\sigma_{RD}^2 \mathbf{s}_R \mathbf{s}_R^H + \sigma_w^2 I_{N_R})^{-1} \mathbf{y}_D^{(1)} \end{aligned} \tag{4.2}$$

Applying the matrix inversion lemma $(A + UCV)^{-1} = A^{-1} - A^{-1}U(C^{-1} + VA^{-1}U)^{-1}VA^{-1}$ to the covariance matrix $R^{-1}_{\mathbf{y}_{RD}^{(1)},\mathbf{y}_{RD}^{(1)H}}$, the mean squared error MSE_{RD},

which is the covariance of the estimation error $\delta h_{RD} = h_{RD} - \hat{h}_{RD}$ can be calculated as:

$$MSE_{RD} = \sigma^2_{\delta h_{RD}} = tr(E((h_{RD} - \hat{h}_{RD})(h_{RD} - \hat{h}_{RD})^*))$$

$$= R_{h_{RD},h^*_{RD}} - R_{h_{RD},\mathbf{y}^{(1)H}_D} R^{-1}_{\mathbf{y}^{(1)}_{RD},\mathbf{y}^{(1)H}_{RD}} R^H_{h_{RD},\mathbf{y}^{(1)H}_D}$$

$$= \frac{\sigma^2_{RD}}{N_R P_R \frac{\sigma^2_{RD}}{\sigma^2_w} + 1} \tag{4.3}$$

The estimator $\hat{h}_{RD}$ is unbiased with variance:

$$\sigma^2_{\hat{h}_{RD}} = E(\hat{h}_{RD}\hat{h}^*_{RD}) = \frac{N_R P_R \sigma^2_{RD}}{N_R P_R + \frac{\sigma^2_w}{\sigma^2_{RD}}} \tag{4.4}$$

Both δh and $\hat{h}$ are CSCG RVs (independent of each other and $\sigma^2_{\hat{h}_{RD}} = \sigma^2_{RD} - \sigma^2_{\delta h_{RD}}$). Hence, $\delta h_{RD} \sim CN(0, \sigma^2_{\delta h_{RD}})$ and $\hat{h}_{RD} \sim CN(0, \sigma^2_{\hat{h}_{RD}})$.

4.3 Channel Estimation for Phase-2

In phase 2, the source transmits to the relay a training sequence $\mathbf{s}_S \in C^{N_s \times 1}$, across N_S time slots. $\mathbf{s}_S$ is, similar with $\mathbf{s}_R$, chosen from a scaled DFT matrix to guarantee identical per symbol power and $\mathbf{s}^H\mathbf{s} = N_S P_S$. The relay receives

$$\mathbf{y}^{(2)}_R = h_{SR}\mathbf{s}_S + \mathbf{w}^{(2)}_R \tag{4.5}$$

and multiplies $\mathbf{y}^{(2)}_R$ with an amplification gain g as in (5.13), which is assumed to be non-adaptive with different symbols for the slot allocation problem, and in turn the long term average transmitting powers from the relay are equal for both phases. While g can be any positive real number in practice varying with different symbols.

$$g = \sqrt{\frac{P_R}{P_S \sigma^2_{SR} + \sigma^2_w}} \tag{4.6}$$

The relay forwards:

$$\mathbf{x}_R^{(2)} = gh_{SR}\mathbf{s}_S + g\mathbf{w}_R^{(2)} \tag{4.7}$$

The destination receives:

$$\begin{aligned}\mathbf{y}_D^{(2)} &= h_{RD}\mathbf{x}_R^{(2)} + \mathbf{w}_D^{(2)} \\ &= h_{RD}gh_{SR}\mathbf{s}_S + h_{RD}g\mathbf{w}_R^{(2)} + \mathbf{w}_D^{(2)}\end{aligned} \tag{4.8}$$

which can be treated as a Gaussian linear model for estimating h_{SR} based on a known source-to-relay channel. The LMMSE estimator of h_{SR}, which coincides with the MMSE estimator, can be derived as in (5.16):

$$\begin{aligned}\hat{h}_{SR} &= R_{h_{SR},\mathbf{y}_D^{(2)H}} R^{-1}_{\mathbf{y}_D^{(2)H}\mathbf{y}_D^{(2)H}} \mathbf{y}_D^{(2)} \\ &= \frac{\sigma_{SR}^2 h_{RD}^* g^* \mathbf{s}_S^*}{\sigma_w^2 g^2 |h_{RD}|^2 + \sigma_w^2} (I_{N_S} + \frac{\sigma_{SR}^2 g^2 |h_{RD}|^2}{\sigma_w^2 g^2 |h_{RD}|^2 + \sigma_w^2} \mathbf{s}_S \mathbf{s}_S^H)^{-1} \mathbf{y}_D^{(2)}\end{aligned} \tag{4.9}$$

After the first phase training only estimated h_{RD} is obtain, so that h_{RD} in (5.16) need to be replaced with $\hat{h}_{RD}$, and we could obtain the Bayesian MSE:

$$\begin{aligned}MSE_{SR} &= tr(E((h_{SR} - \hat{h}_{SR})(h_{SR} - \hat{h}_{SR})^*)) \\ &= R_{h_{SR}h_{SR}^*} - R_{h_{SR}\mathbf{y}_D^{(2)H}} R^{-1}_{\mathbf{y}_D^{(2)}\mathbf{y}_D^{(2)H}} R^H_{h_{SR}\mathbf{y}_D^{(2)H}} \\ &= \frac{\sigma_{SR}^2 + \sigma_{SR}^2 g^2 |\hat{h}_{RD}|^2}{1 + g^2(1 + \frac{\sigma_{SR}^2}{\sigma_w^2} N_S P_S)|\hat{h}_{RD}|^2}\end{aligned} \tag{4.10}$$

where $|\hat{h}_{RD}|^2$ follows gamma distribution with shape $k = 1$ and scale $\theta = \sigma^2_{\hat{h}_{RD}}$, i.e., $|\hat{h}_{RD}|^2 \sim \text{Gamma}(1, \sigma^2_{\hat{h}_{RD}})$. The pdf of $|\hat{h}_{RD}|^2$ can be explicitly written as:

$$f_{|\hat{h}_{RD}|^2}(x) = \frac{1}{\sigma^2_{\hat{h}_{RD}}} Exp(-\frac{x}{\sigma^2_{\hat{h}_{RD}}}) \qquad x \geq 0 \tag{4.11}$$

Therefore, we have the averaged Bayesian MSE:

$$\begin{aligned}
&\overline{MSE_{SR}} = E_{|\hat{h}_1|^2}(MSE_{SR}) \\
&= \int_0^\infty (\sigma_{SR}^2 \cdot \frac{1}{1+\alpha x} + \sigma_{SR}^2 g^2 \cdot \frac{x}{1+\alpha x}) f_{|\hat{h}_{RD}|^2}(x)\,\mathrm{d}x \\
&= \frac{\sigma_{SR}^2 g^2}{\alpha} + \frac{\sigma_{SR}^2(g^2-\alpha)}{\sigma_{\hat{h}_{RD}}^2 \alpha^2} Exp(\frac{1}{\sigma_{\hat{h}_{RD}}^2 \alpha}) Ei(-\frac{1}{\sigma_{\hat{h}_{RD}}^2 \alpha})
\end{aligned} \tag{4.12}$$

where $Ei(x)$ is the exponential integral function defined in (4.13) and $\alpha \triangleq g^2(1+\frac{\sigma_{SR}^2}{\sigma_w^2} N_S P_S)$.

$$Ei(x) = \int_{-x}^{\infty} \frac{exp(-t)}{t} dt \tag{4.13}$$

$\overline{MSE_{SR}}$ can be verified to be a decreasing function of lengths of relay training and source training, N_R and N_S respectively. By increasing N_R we obtain a more accurate estimation of h_{RD}, which is in turn beneficial for the estimation of h_{SR} during the second phase.

4.4 An Iterative Searching Algorithm

Rewrite the MSEs in (4.3) and (5.22) as functions of lengths of relay and source training: $\overline{MSE_{RD}}(N_R)$ and $\overline{MSE_{SR}}(N_R, N_S)$ (Notice that $MSE_{RD}(N_R)$ equals $\overline{MSE_{RD}}(N_R)$ due to its non-randomness).

Our primary objective is to balance the MSEs as follows:

$$\begin{aligned}
\min_{N_R, N_S} \quad & \max(\overline{MSE_{RD}}(N_R), \overline{MSE_{SR}}(N_R, N_S)) \\
\text{subject to} \quad & (P_R + P_S)N_S + P_R N_R \leq E
\end{aligned} \tag{4.14}$$

where we assume that the total energy of both phases E is fixed, and the goal is to find appropriate slots pair (N_R^*, N_S^*) that minimizes the maximum estimation error results from two-phase, or say, to achieve balanced estimation errors. The relay amplification factor is chosen as in (5.13). As mentioned before, g can be chosen as other positive real numbers, leading to different average relay transmitting power for both phases, $P'_R \neq P_R$, which we don't consider for our slot allocation problem in this dissertation.

It can been easily proven that $\overline{MSE_{SR}}(N_R, 0) = \sigma_{SR}^2$, $\overline{MSE_{SR}}(N_R, \infty) = 0$, and $\overline{MSE_{RD}}(N_R)$ decreases with N_R towards zero (when we have infinity length). Therefore, a finite N'_R satisfying $\overline{MSE_{SR}}(N'_R, \infty) < \overline{MSE_{RD}}(N'_R) < \overline{MSE_{SR}}(N'_R, 0)$ is always available. $\overline{MSE_{SR}}(N_R, N_S)$ is a decreasing function of N_S. Hence, for any finite N'_R, a finite N'_S can be found to satisfy $\overline{MSE_{RD}}(N'_R) = \overline{MSE_{SR}}(N'_R, N'_S)$ by a bisection method [5], provided that enough energy available to allocate. Though in practice energy is limited, we still could find such pair by the iterative bisection algorithm at the end of this section.

Though scarcely possible in reality, it has to be pointed out that with limited energy, a pair (N'_R, N'_S) that satisfies $\overline{MSE_{RD}}(N'_R) = \overline{MSE_{SR}}(N'_R, N'_S)$ does not always exist, especially when we have much poorer prior knowledge of h_{RD} than of h_{SR}, i.e., σ_{RD}^2 is much larger than σ_{SR}^2. In this case, to balance the errors, we only save one symbol energy for the second phase training, i.e., $N_S = 1$, and allocate the rest of the energy for the first phase training, i.e., $N_R = N_{R,max}$. The functionality of this procedure, closing the gap of two MSEs, relies on the fact that $\overline{MSE_{RD}}(N_R)$ has a faster decreasing rate than $\overline{MSE_{SR}}(N_R, N_S)$ with respect to N_R, such that the initial large gap is being eliminated

while increasing N_R. This is clearly true due to the indirectness of the effect of increasing N_R on $\overline{MSE_{SR}}(N_R, N_S)$.

With the above discussions, we are able to propose the following iterative searching method to find the optimal slots allocation, instead of solving (4.14), which is a non-convex problem.

Algorithm Outline

S.1 Check whether or not $\overline{MSE_{RD}}(N_{R,max}) < \overline{MSE_{SR}}(N_{R,max}, 0)$ holds. If not, terminate program with default optimal setting $N_R = N_{R,max}$ and $N_S = 1$.

S.2 Pick a small relay training length $N_R^{(0)}$ ($0 < N_R^{(0)} < 1$) satisfying $\overline{MSE_{SR}}(N_R^{(0)}, \infty) < \overline{MSE_{RD}}(N_R^{(0)}) < \overline{MSE_{SR}}(N_R^{(0)}, 0)$. Use bisection search to find $N_S^{(0)}$ that satisfies $\overline{MSE_{RD}}(N_R^{(0)}) = \overline{MSE_{SR}}(N_R^{(0)}, N_S^{(0)})$. Check whether the energy constraint $(P_R + P_S)N_S^{(0)} + P_R^{(0)}N_R^{(0)} \leq E$ holds. If yes, set counter $i = 1$ and proceed with S.3. If not, terminate program with default optimal setting $N_R = 1$ and $N_S = N_{S,max}$.

S.3 With fixed N_R^i, use bisection search to find N_S^i satisfying $\overline{MSE_{RD}}(N_R^i) = \overline{MSE_{SR}}(N_R^i, N_S^i)$. (This is the inner bisection loop.)

S.4 Check whether all energy has been allocated, i.e., $(1 - \delta)E < (P_R + P_S)N_S^i + P_R^i N_R^i \leq E$ holds, where $\delta \ll 0$ (i.e., with a small portion of energy δE remaining since it is unlikely that optimal allocation consumes exactly all the energy). If so, terminate the program with converting the current pair into integers, $(N_R^*, N_S^*) = (\text{floor}(N_R^i), \text{floor}(N_S^i))$.

S.5 Check whether there is still more energy to allocate, i.e., $(P_R + P_S)N_S^i + P_R^i N_R^i < (1-\delta)E$ holds. Or by the current allocation the energy limit is already exceeded, i.e., $(P_R + P_S)N_S^i + P_R^i N_R^i > E$ holds. Then decide accordingly to which direction we adjust N_R^i (increase N_R^i when the former holds and decrease otherwise), then choose N_R^{i+1} to replace N_R^i. Set $i = i + 1$ and go to S.3 (This is the outer bisection loop).

Notice that except for the extreme cases, when the optimal pair is chosen as $(N_{R,max}, 1)$ or $(1, N_{S,max})$, we can always find a pair (N_R^i, N_S^i) (non-integers) that balances the errors and then round them to floor(N_R^*), floor(N_S^*). Also, the optimal pair for any given problem is unique. To prove this, consider if we have two optimal solutions: $(N_R^{*(1)}, N_S^{*(1)})$ and $(N_R^{*(2)}, N_S^{*(2)})$. Since $\overline{MSE_{RD}}(N_R)$ is only function of N_R and it monotonically decreases, $\overline{MSE_{RD}}(N_R^{*(1)}) = \overline{MSE_{RD}}(N_R^{*(2)})$ is not possible. Thus, the optimal solution is unique. Therefore, either solving the non-convex problem in (4.14) or applying this algorithm would result in the same optimal pair.

4.5 Performance Evaluation

In section A, analysis shows how the estimation errors of h_{SR} varies with different parameters: the length of relay training slots, the length of sources training slots, the relay amplification gain, and the prior information about source-to-relay and relay-to-destination channels. For the sake of simplicity, we assume that the powers $P_R = P_S = 1$, all noises have unit variance, and the prior variances of h_{SR} and h_{RD} are chosen to be $\sigma_{SR}^2 = 2$ and $\sigma_{RD}^2 = 3$ through Figure 4.2 to Figure 4.5. In section 4.5.2, an example of slot allocation is

illustrated.

4.5.1 Evaluation of the ABMSE

Figure 4.2 shows that for a better estimation of h_{SR}, an accurate $\hat{h}_{RD}$ is necessary by looking at the curve corresponding to a small N_R, while N_S and the noise level dominate when N_R is sufficiently large. Figure 4.3 and Figure 4.4 show that when N_R is insufficient, error floors exist no matter how we increase N_S or g. Figure 4.5 shows that the less prior knowledge is known about h_{SR} or h_{RD}, the larger the ABMSE.

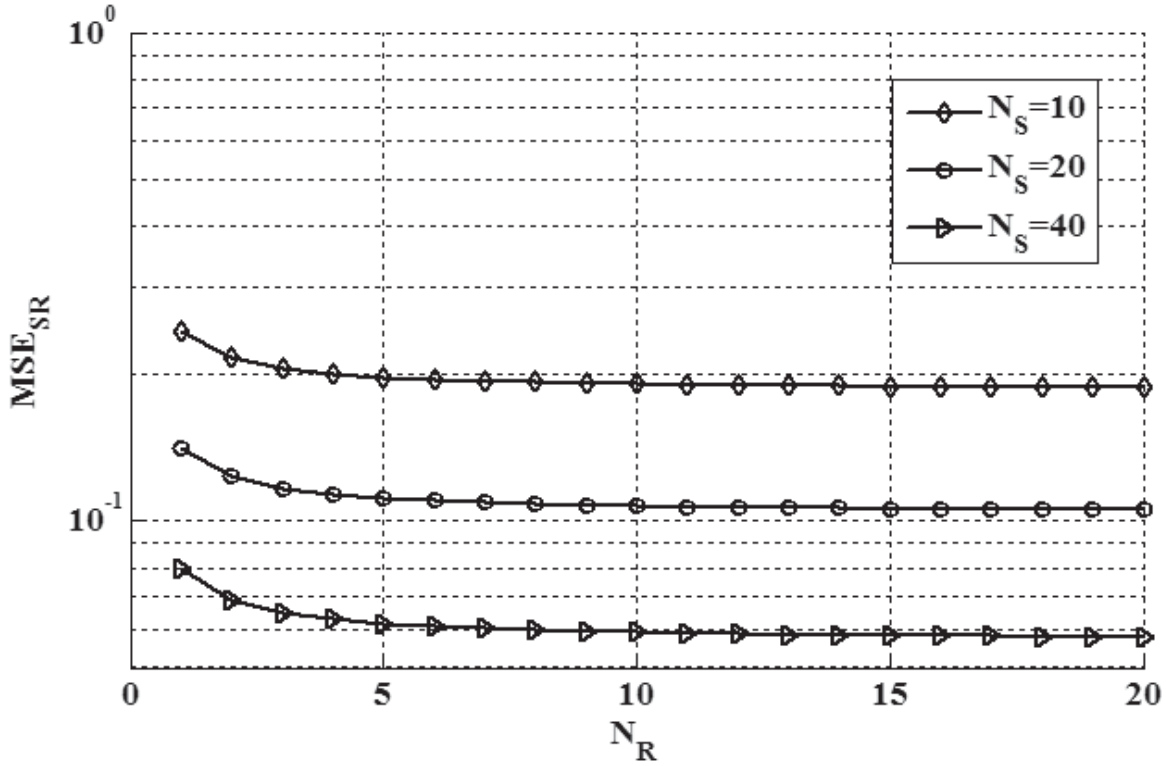

Figure 4.1: MSE in estimating h_{SR} as a function of the length of relay training slots N_R with $g = 2$.

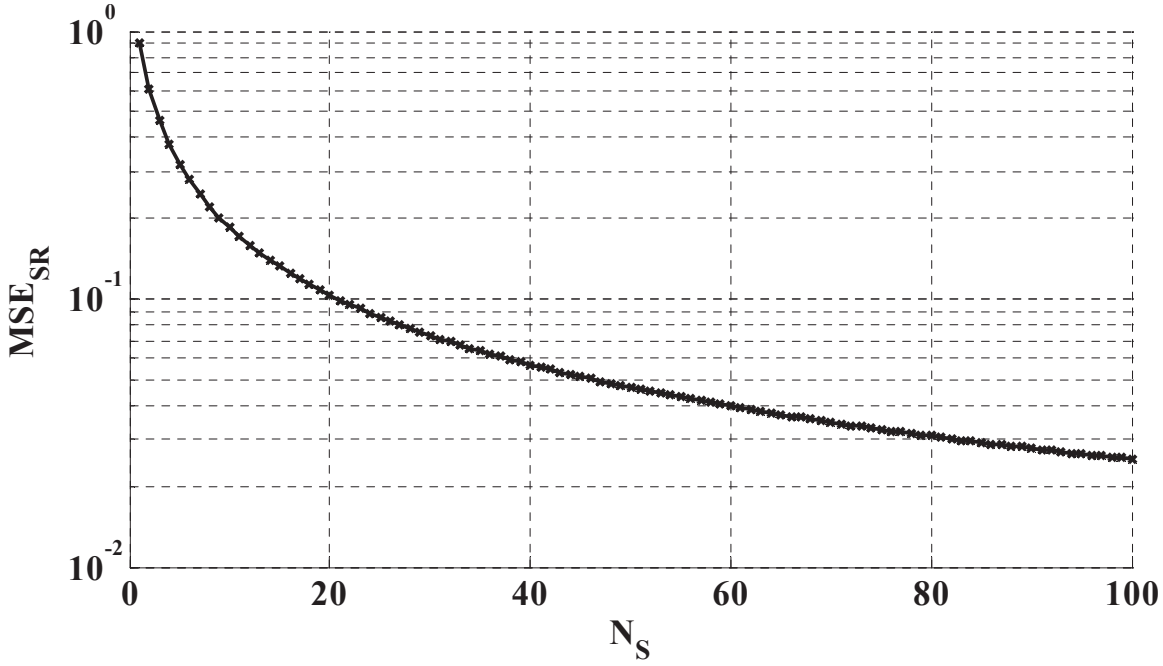

Figure 4.2: MSE in estimating h_{SR} as a function of the length of source training slots N_S with $g = 2$ and $N_R = 10$.

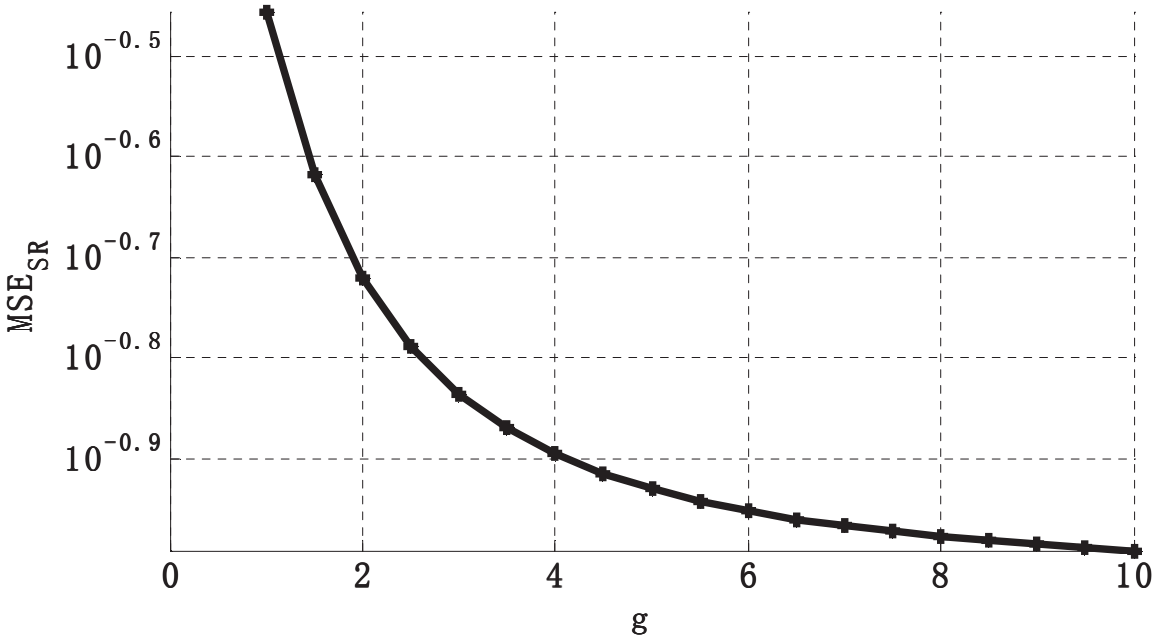

Figure 4.3: MSE in estimating h_{SR} as a function of the relay amplification gain g with $N_R = N_S = 10$.

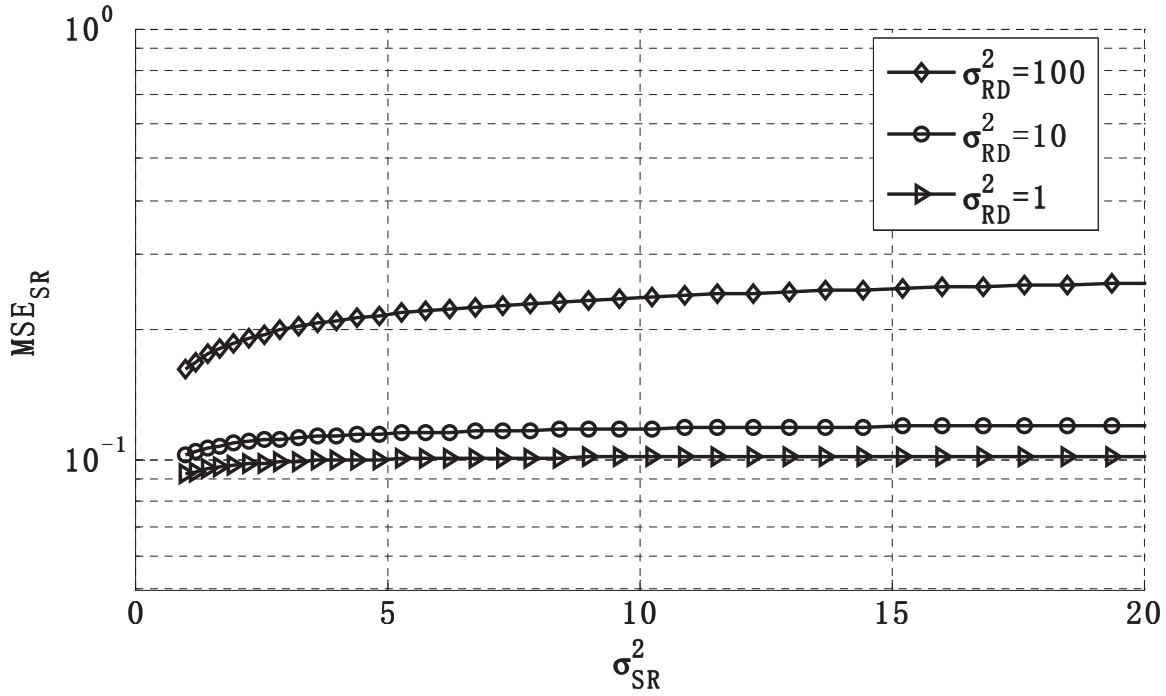

Figure 4.4: MSE in estimating h_{SR} as a function of prior information about source-to-relay and relay-to-destination channels with $g = 2$.

4.5.2 A Slot Allocation Example

We compare the performance of our proposed slot allocation scheme based on the iterative searching method in section III with allocations that choose the ratio $\frac{N_S}{N_R+N_S}$ randomly. The variances of channels and noises are chosen the same as in section IV.A. We assume the total energy for both phases $E = 1000$ with powers $P_R = P_S = 1$ (assuming a unit energy is consumed by transmitting one symbol with a unit power). The relay amplification factor g is chosen as in (5.13).

As shown in Table.1, the stared row denotes the optimal slots pair with $(N_R^*, N_S^*) =$

$(67, 467)$. If too less slots are allocated for the relay training, e.g. $(N_R, N_S) = (5, 497)$, the relay-to-destination channel estimation becomes too bad, which in turn affects the source-to-relay channel estimation, resulting in worse performances for both phases than with our scheme. If too many slots are allocated for the relaying training, e.g. $(N_R, N_S) = (980, 10)$, the energy left for source training is then not enough for combating inaccuracy brought by noise, which causes the $\overline{MSE_{SR}}$ to be 22 times higher than the stared counterpart. In practice, equal slot allocation is most used if without scheduled allocation, i.e., $(N_R, N_S) = (333, 334)$, the errors $(\overline{MSE_{RD}}, \overline{MSE_{SR}}) = (0.0030, 0.0220)$ resulting from both phases are severely unbalanced.

Table 4.1: Slot Allocation for Balanced Estimation Errors

N_R	N_S	$\frac{N_S}{N_S+N_R}$	$\overline{MSE}_{RD}$	$\overline{MSE}_{SR}$
5	497	0.99	0.1875	0.0168
53	474	0.90	0.0187	0.0154
*67	*467	*0.87	*0.0151	*0.0149
111	445	0.80	0.0090	0.0162
176	412	0.70	0.0057	0.0185
250	375	0.60	0.0040	0.0188
333	334	0.50	0.0030	0.0220
429	286	0.40	0.0023	0.0237
538	231	0.30	0.0019	0.0284
667	167	0.20	0.0015	0.0373
770	115	0.13	0.0013	0.0508
811	91	0.10	0.0012	0.0616
980	10	0.01	0.0010	0.3345

4.6 Conclusion

In this chapter, we have considered a fundamental problem of channel estimation error propagation for a two-hop amplify-and-forward relaying system. A close-form expression of ABMSE of channel estimation of both phases is derived as function of lengths of relay and/or source training slots. We have shown that the proposed iterative searching method finds the optimal allocation which balances the channel estimation errors. Analysis shows how the estimation errors of StR channel varies with different parameters: the length of relay training slots, the length of sources training slots, the relay amplification gain, and the prior information about StR and RtD channels. This allocation is done off-line before training.

Chapter 5

Full-duplex Cooperative Transmission Scheduling in a Fast-fading MIMO Relaying Wireless Network

5.1 Network Assumptions

A wireless network with K users, one relay node, and one destination node is considered as shown by Figure 1.3. The network is described as follows.

- Three time scales: period, frame and slot. One period contains multiple frames and one frame contains multiple time slots.
- The users: locations of users are fixed; they are able to transmit directly with the destination; each source transmits only one packet in one frame during its scheduled time slot and the schedule repeats from frame to frame.

- The relay: works with a full-duplex mode; it is able to collect packets lost from source-to-destination transmission (based on feedback from destination which is assumed to decrease throughput negligibly in this paper) and resend them later on; it can transmit multiple times in a frame if scheduled.
- The destination: has multiple reception capability, i.e., can receive multiple successful transmissions during one time slot; a packet is successfully received as long as the signal-to-noise-ratio (SINR) exceeds a threshold β.
- For ease of understanding, we only consider a single relay and single destination case, while it can be extended straightforwardly to include the multiple relays and destinations case.

A *baseline frame schedule* denotes a tuple

$$B = (H_1, H_2, \ldots, H_{M_1}). \tag{5.1}$$

where H_k is the set of users that transmit simultaneously in the k-th time slot. A *cooperative frame schedule* is a tuple

$$C = (\tilde{H}_1, \tilde{H}_2, \ldots, \tilde{H}_{M_2}). \tag{5.2}$$

where $\tilde{H}_k$ is either only some set of users or some users along with the relay node that transmit simultaneously in the k-th time slot. A *period schedule* is a tuple, for example

$$P = (B, B, \ldots, C, C, C, \ldots). \tag{5.3}$$

which contains multiple baseline frames and cooperative frames. During one period schedule, the number of packets entering into the relay equals the number of those leaving. Details about the above schedules are specified in Section IV.

User $T_i \in H_k$ can be successfully received by the destination if

$$\text{SINR}_{T_i,D}(k) = \frac{P^r_{T_i,D}}{\alpha \sum_{\bar{T} \in H_k \setminus \{T_i\}} P^r_{\bar{T},D} + P_n} \geq \beta. \tag{5.4}$$

where α is the correlation between different codes, $P^r_{T_i,D}$ is the signal power from T_i received at destination, P_n is the noise power at the destination, and $\bar{T}$ denotes other nodes transmitting at k-th time slot except T_i.

5.2 MIMO Throughput Calculation

Suppose that each user has N_T transmitting antennas, the relay has N_R receiving antennas and N_R transmitting antennas, and the destination has N_D receiving antennas. The channel matrix between the relay and destination is

$$\mathbf{H} = [\mathbf{h}_1^T \mathbf{h}_2^T \dots \mathbf{h}_{N_D}^T]^T. \tag{5.5}$$

The channel matrix between the i-th transmitter and destination is

$$\mathbf{G}^i = [\mathbf{g}_1^{iT} \mathbf{g}_2^{iT} \dots \mathbf{g}_{N_D}^{iT}]^T. \tag{5.6}$$

We assume that every antenna of all nodes has equal transmitting power, i.e.

$$\frac{P_R}{N_R} = \frac{P_T}{N_T} = p_a. \tag{5.7}$$

where P_R denote the total transmitting power of the relay, P_R denote the total transmitting power of the users, and p_a is the power per antenna.

We define d_R as the path-loss between relay and destination antenna pairs, since the spatial separation among antennas of a same node is much smaller than between that

between different nodes. With interference from the transmitters, a packet from the relay can be recovered by the destination if the $\gamma_{R,D}(k) = \text{SINR}_{R,D}$ satisfies the following relationship at the k-th time slot.

$$S = \Pr(\gamma_{R,D}(k) > \beta) = \Pr\big(\sum_{n=1}^{N_D} \frac{p_a \|\mathbf{h}_n\|^2 (1+r_R)^{-a}}{\alpha I_N(k) + \sigma_D^2} > \beta\big). \tag{5.8}$$

where r_R is the distance from relay to destination and S is defined as the throughput between relay and destination, $\gamma I_N(k)$ is the interference power at time slot k, σ_D^2 is the time-invariant noise power at the destination, and a is the path-loss exponent.

The interference $\alpha I_N(k)$ is calculated by

$$\alpha I_N(k) = \alpha \sum_{i \in H_k} \sum_{n=1}^{N_D} \sum_{m=1}^{N_T} |g_{n,m}^i|^2 p_a (1+r_i)^{-a}. \tag{5.9}$$

where $h_{n,m}$ and $g_{p,q}^i$ are assumed to be i.i.d. complex Gaussian random variables with zero means and unit variances. The SINR can be written as

$$\gamma_{R,D}(k) = \frac{p_a \sum_{n=1}^{N_D} \sum_{m=1}^{N_T} |h_{m,n}|^2 (1+r_R)^{-a}}{\alpha p_a \sum_{i \in H_k} \sum_{p=1}^{N_D} \sum_{q=1}^{N_T} |g_{p,q}^i|^2 (1+r_i)^{-a} + \sigma_D^2}. \tag{5.10}$$

Therefore, we only care about the path-loss between relay and destination

$$d_R = (1+r_R)^{-a}. \tag{5.11}$$

and the path-loss from transmitter i to destination

$$d_i = (1+r_i)^{-a}. \tag{5.12}$$

Then the SINR is thus simplified as

$$\gamma_{R,D}(k) = \frac{\sum_{n=1}^{N_D} \sum_{m=1}^{N_R} d_R |h_{n,m}|^2}{\alpha \sum_{i \in H_k} \sum_{p=1}^{N_D} \sum_{q=1}^{N_T} d_i |g_{p,q}^i|^2 + \theta}. \tag{5.13}$$

where $\theta = \sigma_D^2/p_a$. Define

$$h_{m,n}^{re} = \sqrt{2}\text{Re}\{h_{m,n}\}, \;\; h_{m,n}^{im} = \sqrt{2}\text{Im}\{h_{m,n}\},$$

$$g_{p,q}^{i,re} = \sqrt{2}\text{Re}\{g_{p,q}^{i}\}, \;\; g_{p,q}^{i,im} = \sqrt{2}\text{Im}\{g_{p,q}^{i}\}.$$

which all has zero mean and unit variance, the SINR is written as

$$\gamma_{R,D}(k) = \frac{\sum_{n=1}^{N_D}\sum_{m=1}^{N_R} d_R[(h_{m,n}^{re})^2 + (h_{m,n}^{im})^2]}{\sum_{i\in H_k}\sum_{p=1}^{N_D}\sum_{q=1}^{N_T}(\gamma d_i)|[(g_{p,q}^{i,re})^2 + (g_{p,q}^{i,im})^2] + 2\theta}. \tag{5.14}$$

Divide both the numerator and denominator by a common term

$$T = 2\gamma N_D N_T \sum_{i\in H_k} d_i \tag{5.15}$$

and the follows is obtained

$$\gamma_{R,D}(k) = \frac{\sum_{n=1}^{N_D}\sum_{m=1}^{N_R} \tilde{d}_R[(h_{m,n}^{re})^2 + (h_{m,n}^{im})^2]}{\sum_{i\in H_k}\sum_{p=1}^{N_D}\sum_{q=1}^{N_T} \tilde{d}_i|[(g_{p,q}^{i,re})^2 + (g_{p,q}^{i,im})^2] + 2\theta'}. \tag{5.16}$$

where

$$\sum_{i\in H_k}\sum_{p=1}^{N_D}\sum_{q=1}^{N_T} \tilde{d}_i = 1, \tag{5.17}$$

$$\tilde{d}_R = d_R/(2\gamma N_D N_T \sum_{i\in H_k} d_i), \tag{5.18}$$

$$\theta' = \theta/(2\gamma N_D N_T \sum_{i\in H_k} d_i). \tag{5.19}$$

Lemma 1 ***A quick and easy approximation to pdf of sum weighted chi-squares:***

$$X = \sum_{i=1}^{n} c_i x_i^2. \tag{5.20}$$

where the $x_1, \ldots, x_n$ are independent and identically distributed standard normal variables and c_i's are positive weights. Without loss of generalization we assume

$$\sum_{i=1}^{N} c_i = 1. \tag{5.21}$$

Let Y be the positive random variable with density function:

$$g_Y(y) = \frac{1}{2}\sum_{i=1}^{n}(\frac{y}{2c_i})^{\frac{1}{2c_i}-1}e^{-\frac{y}{2c_i}}/\Gamma(\frac{1}{2c_i}), \qquad y > 0 \tag{5.22}$$

It was proved that the first three moments of X and Y are identical, i.e.,

$$EY = EX, \;\; EY^2 = EX^2, \;\; EY^3 = EX^3. \tag{5.23}$$

Proof: See [22] (Gabler 1987).

Define random variable

$$Z = \sum_{m=1}^{N_D}\sum_{m=1}^{N_R}[(h_{m,n}^{re})^2 + (h_{m,n}^{im})^2], \tag{5.24}$$

$$Y = \sum_{i\in H_k}\sum_{p=1}^{N_D}\sum_{q=1}^{N_T}\tilde{d}_i[(g_{p,q}^{i,re})^2 + (g_{p,q}^{i,im})^2]. \tag{5.25}$$

We can find the pdf's of Z and Y as follows

$$f_Z(z) = \frac{1}{2^N\Gamma(N)}z^{N-1}e^{-z/2}, \qquad z > 0 \tag{5.26}$$

$$f_Y(y) = \frac{M}{2}\sum_{i=1}^{|H_k|}(\frac{y}{2\tilde{d}_i})^{\frac{1}{2\tilde{d}_i}-1}e^{-\frac{y}{2\tilde{d}_i}}/\Gamma(\frac{1}{2\tilde{d}_i}), \qquad y > 0 \tag{5.27}$$

where $N = 2N_DN_R$ and $M = 2N_DN_T$. The SINR can thus be denoted as a function of Z and Y

$$\gamma_{R,D}(k) = \frac{d_RZ}{Y + 2\theta'}. \tag{5.28}$$

The probability of detection can be calculated as follows

$$\begin{aligned}\Pr\big(\gamma_{R,D}(k) > \beta\big) &= 1 - \Pr\big(\gamma_{R,D}(k) \leq \beta\big) \\ &= 1 - \Pr\big(\frac{d_R Z}{Y + 2\theta'} \leq \beta\big) \\ &= 1 - \Pr\big(Z \leq \frac{\beta(Y + 2\theta')}{d_R}\big) \\ &= 1 - \int_0^\infty F_Z[\frac{\beta(y + 2\theta')}{d_R}] f_Y(y) dy. \end{aligned} \tag{5.29}$$

The cumulative distribution function

$$F_Z(z; N_R) = P(N_R, z/2) \tag{5.30}$$

where $P(s, z)$ is the regularized Gamma function defined as

$$P(s, z) = \frac{\gamma(s, z)}{\Gamma(s)} = \frac{1}{\Gamma(s)} \sum_{k=0}^{\infty} \frac{z^s e^{-z}}{s(s+1)\dots(s+k)}. \tag{5.31}$$

where $\Gamma(s)$ denotes the Gamma function. Plug in expression of $f_Y(y)$ we have

$$\begin{aligned}\Pr\big(\gamma_{R,D}(k) > \beta\big) &= 1 - \int_0^\infty F_X[\frac{\beta(y + 2\theta')}{d_R}] f_Y(y) dy \\ &= 1 - \frac{M}{2} \int_0^\infty P(N_R, \frac{\beta(y + 2\theta')}{2d_R}) \\ &\times \sum_{i=1}^{|H_k|} (\frac{y}{2\tilde{d}_i})^{\frac{1}{2\tilde{d}_i} - 1} e^{-\frac{y}{2\tilde{d}_i}} / \Gamma(\frac{1}{2\tilde{d}_i}) dy \\ &\cong 1 - \frac{M}{2} \int_0^c P(N_R, \frac{\beta(y + 2\theta')}{2d_R}) \\ &\times \sum_{i=1}^{|H_k|} (\frac{y}{2\tilde{d}_i})^{\frac{1}{2\tilde{d}_i} - 1} e^{-\frac{y}{2\tilde{d}_i}} / \Gamma(\frac{1}{2\tilde{d}_i}) dy. \end{aligned} \tag{5.32}$$

where by simulation we observe that by choosing $c \geq 30$ the the accuracy of the above approximation is guaranteed. The integration can easily be calculation by MATLAB.

5.3 Full-duplex Cooperation Framework

Figure 5.2 shows one transmission period under our full-duplex cooperation framework. One period contains N_b baseline frames (BF) and N_c cooperative frames (CF). Each BF is made up of M_1 time slots and each CF has M_2 time slots.

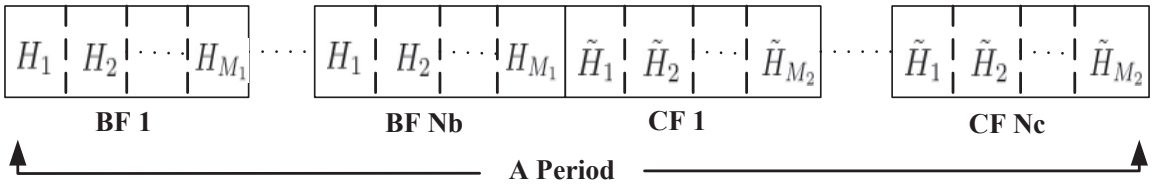

Figure 5.1: A transmission period.

In the BF's only users transmit, while relay can transmit during any time slot in the CF's, as long as it is scheduled. In one CF, we have $M_2 = Q_1 + Q_2$ slots in total, where Q_1 denotes the number of time slots that only users transmit and Q_2 denotes the number while users and relay transmit simultaneously. The full-duplex relay collects packets all the time in a period but only transmits during the Q_2 time slots. A packet enters a relay if it fails to be collected by the destination but is successfully detected by the relay. Denote the number of packets entering the relay during the BF as E_b and those during the CF as E_c as follows

$$E_b = \sum_{k=1}^{M_1} \sum_{T_i \in H_k} \Pr_{H_k}(T_i, R)[1 - \Pr_{H_k(T_i,D)}], \tag{5.33}$$

$$E_c = \sum_{k=1}^{M_2} \sum_{T_i \in \tilde{H}_k} \Pr_{\tilde{H}_k(T_i,R)}[1 - \Pr_{\tilde{H}_k}(T_i, D)]. \tag{5.34}$$

Since we assumed that the packets entering and leaving the relay are equal, the following

relation holds

$$N_b E_b + N_c E_c = N_c Q_2. \tag{5.35}$$

Then we obtain the ratio of CF's in one period

$$\begin{aligned} \eta &= \frac{N_c}{N_b + N_c} \triangleq \frac{N_c}{N_p} \\ &= \frac{E_b}{Q2 - E_c + E_b}. \end{aligned} \tag{5.36}$$

The overall throughput in one period is calculated by

$$\begin{aligned} S_p &= N_b S_b + N_c S_c \\ &= (1-\eta) N_p S_b + \eta N_p S_c. \end{aligned} \tag{5.37}$$

where S_b and S_c are the total throughput in one baseline and cooperative frame respectively. Once the scheduling is done, E_b, E_c, Q_2, S_b, S_c are known and η can be calculated. Then according to how long we want our period to be we choose $N_p = N_b + N_c$. Therefore, N_b and N_c can be calculated. In our simulations in Section VI, the average throughput in one time slot is compared for different schemes, which is calculated by

$$S_{avg} = \frac{S_p}{N_p}. \tag{5.38}$$

5.4 Scheduling Algorithm

An optimal schedule of the cooperative can be found by exhaustive search with complexity of $O(2^{K+1})$, which is prohibitive when K is large. Therefore, we instead schedule the cooperative frame by Algorithm 1, which has a complexity of $O((K+1)^2)$. We

refer the reader to [53] for details of the complexity analysis and the scheduling of the baseline frame.

Algorithm 1 Outline

S.1 Set $k = 1$ and mark all users and relay node as unscheduled.

S.2 Label both the unscheduled users and relay node according to decreasing values of the throughput when each node transmit alone. S_0 denoting the relay throughput is largest followed by throughput S_1, and the lowest throughput is S_K.

S.3 For each i, where $0 \leq i \leq K$, we form the set $\Theta_i = (S_i, S_{i+1}, \ldots, S_{i+n_i-1}, S_{i+n_i})$, where $i + n_i \leq K$. Add the sources $S_i, \ldots, S_{i+n_i}$ sequentially into the time slot until the throughput stops increasing. Calculate the corresponding throughput $T(\Theta_i)$.

S.4 Choose the optimal set $T(\Theta^{opt})$ among all $T(\Theta_i)$, i.e., $T(\Theta^{opt}) = \max\{T(\Theta_i), 0 \leq i \leq K\}$. $\tilde{H}_k = \Theta^{opt}$ and $k = k + 1$.

S.5 All users in Θ^{opt} is marked scheduled, while the relay node is still treated as unscheduled. Go to S.2 if the number of unscheduled node is larger than 1, while algorithm terminates otherwise.

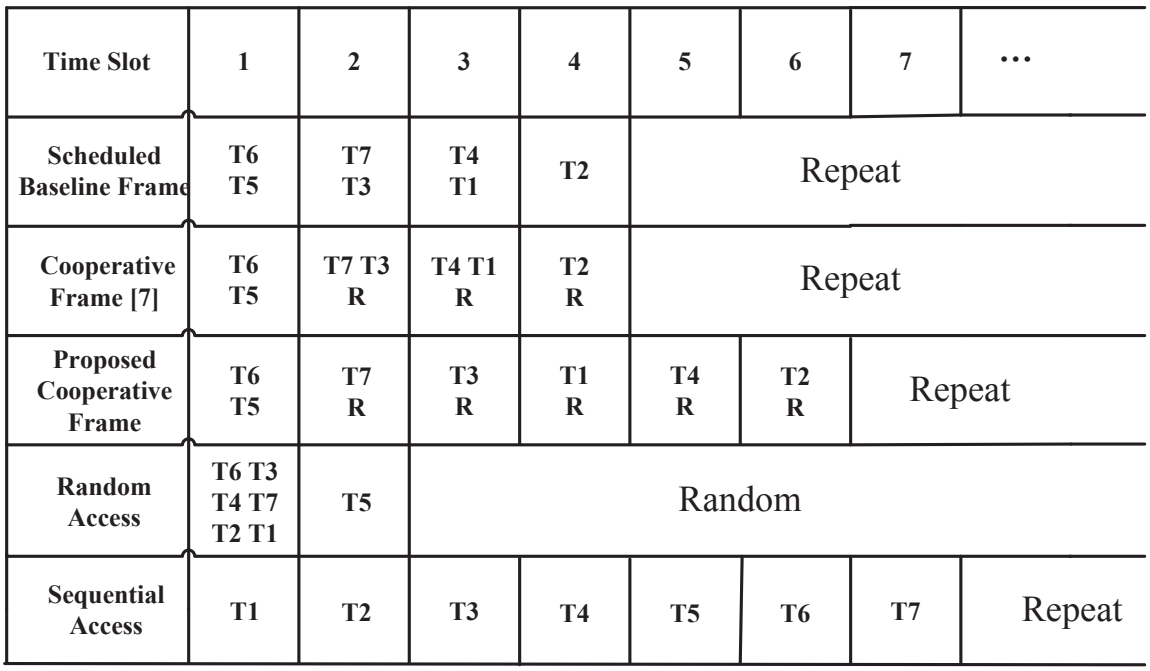

Figure 5.2: Proposed scheduling vs other schedulings.

5.5 Performance Evaluation

In this section, we compare the throughput obtained by using the half-duplex cooperative (HDC) scheme in [53], random access (RA) scheme, time division multiple access (TDMA) scheme, and our proposal full-duplex cooperative (FDC) scheme with varying the correlation parameter γ, the number of antennas equipped for each node, and the threshold β. For simplicity, we assume the same number of antennas are employed at transmitter, relay, and receiver, i.e., $N = N_T = N_R = N_D$.

In Figure 5.3 - Figure 5.5, we set the noise power $\sigma_D^2 = 10^{-3}$, the path-loss exponent $a = 3$, and γ ranges from 0 to 1. Each node is assumed to have unit trans-

mitting power, i.e., $P = 1$. The locations of the transmitters are randomly generated but fixed for all of our simulations. The distances between the users and the relay $\mathbf{d}_{TR} = [5.65\ 6.58\ 7.22\ 8.16\ 8.69\ 9.36\ 10.86]$, and the distances between the users and the destination $\mathbf{d}_{TD} = [7.55\ 8.69\ 9.36\ 9.77\ 10.86\ 10.86\ 12.57]$. Once the locations of users are changed, we should reschedule our transmission.

In Figure 5.3, assuming $\beta = 1$, $N = 2$, we compare the average throughput S_{avg} of the four schemes. It is observed that cooperative schemes significantly outperform noncooperative schemes and among cooperative schemes FDC outperforms HDC scheme. When γ is very small, one can schedule all the node to transmit at the same time slot and expect to reach the maximum throughput so that we can just apply the TDMA scheme.

In Figure 5.4, assuming $\beta = 1$, we compare the throughput by applying FDC scheme with vary the number of antennas N at all nodes and γ. It is observed that using multiple antennas significantly increases throughput as expected.

In Figure 5.5, assuming $\gamma = 0.5$, $N = 2$, we compare the throughput by applying FDC and HDC schemes with varying the threshold β. It again shows the superiority of FDC over HDC scheme.

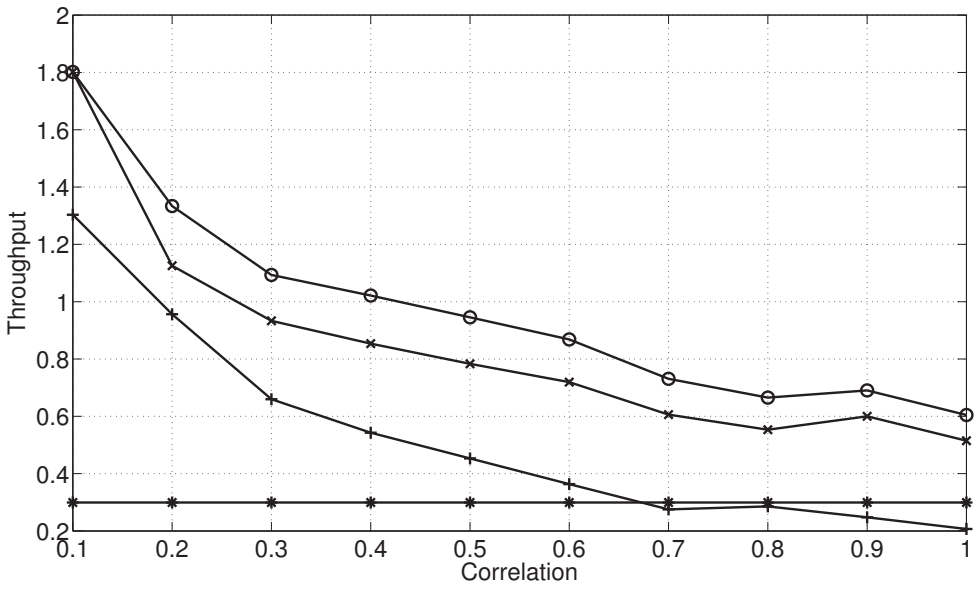

Figure 5.3: Throughput comparison among FDC, HDC, RA, and TDMA with varying correlation γ.

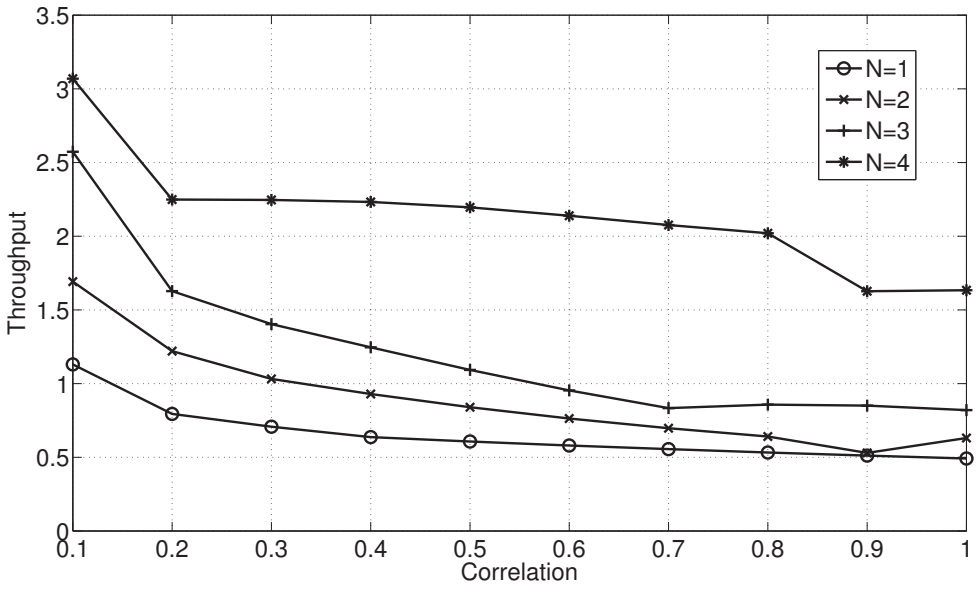

Figure 5.4: Throughput by using FDC with varying number of antennas N with varying correlation γ.

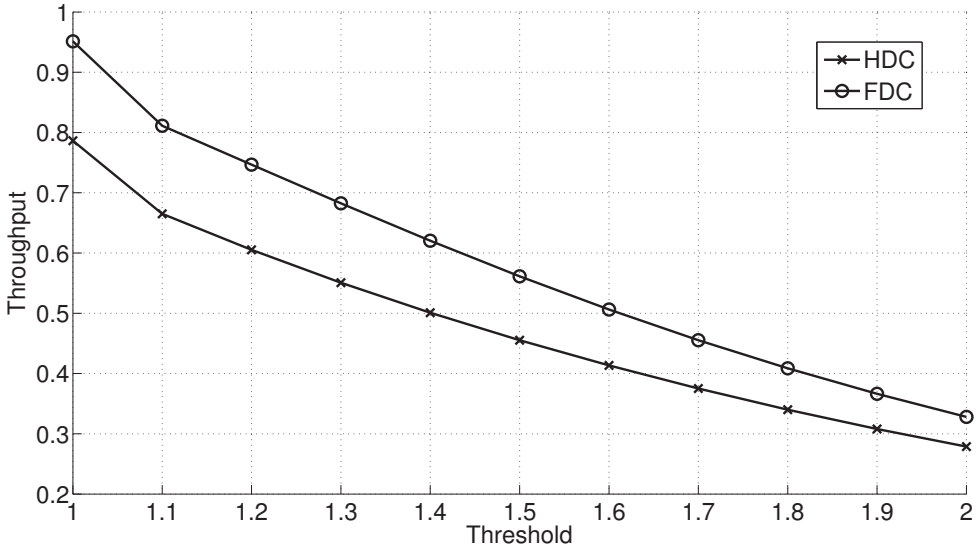

Figure 5.5: Throughput comparison between FDC and HDC with varying threshold β.

5.6 Conclusion

This chapter has included a MAC scheduling algorithm for an uplink full-duplex cooperative network with a full-duplex relay and MIMO nodes. This new algorithm can yield much larger throughput than a previously developed cooperative algorithm based on a half-duplex relay and SISO nodes. We have also compared our algorithm with TDMA and random access.

Chapter 6

Conclusion

In this dissertation, we have provided novel designs for a few fundamental problems of optimizations, estimation, and scheduling in both optical and radio frequency wireless communications. For an IM/DD multi-carrier optical wireless system, a power efficient constellation design procedure is shown in our study, which takes advantage of the compactness of sphere-packing in high dimensional space. Our scheme fully utilized the lighting bias energy to carry information instead of conventional non-information-carried DC-bias to get one extra feasible modulation dimension and highly increase data rate. It can also flexibly constrain peak-to-average power ratio (PAPR) into a desirable range to get better bit-error-rate (BER). A zero-forcing digital pre-equalizer is considered for the first time in optical MSM systems for diffuse/selective fading channel. Further, an optimal bits-to-symbol mapping algorithm in multiple dimensions is provided.

For an IM/DD multi-color visible light communication system, we have provided power efficient constellation design subject to multiple practical lighting constraints such

as the average optical power, illumination color, CRI, LER, and PAPR. For systems having ideal channel, we have shown that with our optimized constellations and labeling, significant power gain is achieved and this gain grows while illumination color becomes more unbalanced. For systems having channel with cross-talks, we propose to employ an SVD based pre-equalizer and redesign the constellations subject to a transformed set of constraints. It is illustrated then that systems employing such method greatly outperform counterparts employing ZF or LMMSE based post-equalizers at the receiver end.

In the third part, a training source allocation scheme was propose to uniquely find the optimal solution that fixes the problem of unbalanced channel estimation error in a two-hop relaying system. Close-form expressions of estimation error for both phases are derived in terms of lengthes of training pilots in both phases. Performance analysis includes plots of the estimation errors of source-to-relay channel against the length of relay training slots, the length of sources training slots, the relay amplification gain, and channel prior information channels accordingly.

In the last part, we considered a transmission scheduling problem for an uplink MIMO relaying network. A MIMO full duplex relay was employed to collect lost packets from transmitting nodes to destination links. A close-form expression of throughput was derived for a point-to-point fast-fading MIMO link, based on which throughput for transmitting nodes and relay are calculated. Then we propose a low complexity searching algorithm, which provides optimized schedules of nodes and relay accesses. Our full duplex scheme is compared with a half duplex counterpart as well as random access and

TDMA access methods, and significant thoughput gains are observed.

Bibliography

[1] J. Armstrong, "OFDM for optical communications," *J. Lightw. Technol.*, vol. 27, no. 3, pp. 189-204, Feb. 2009.

[2] J. R. Barry, "Wireless Infrared Communications," Kluwer Academic Press, Boston, MA, 1994.

[3] B. Bai, Q. He, Z. Xu, and Y. Fan, "The color shift key modulation with non-uniform signaling for visible light communication," IEEE ICCC-WS-OWCC, 37 (2012).

[4] M. Beko and R. Dinis, "Designing good multi-dimensional constellations," *IEEE Wireless Commun. Lett.*, vol. 1, no. 3, pp. 221-224, June 2012.

[5] D. Bertsekas, *"Nonlinear Programming,"* 2nd ed. Belmont, MA, Athena Scientific, 1995.

[6] J.A.C. Bingham, "Multicarrier modulation for data transmission: an idea whose time has come," *IEEE Commun. Mag.*, vol. 28, pp. 5-14, May 1990.

[7] F. Boccardi and G. Caire, "The p-sphere encoder: peak-power reduction by lattice precoding for the MIMO Gaussian broadcast channel," *IEEE Trans. Commun.*, vol. 54, no. 11, pp. 2085-2091, Nov. 2006.

[8] H. Bolcskei, R. U. Nabar, O. Oyman and A J Paulra, "Capacity scaling laws in MIMO relay networks," IEEE Trans. Wireless Comm., pp. 1433-1444, June 2006.

[9] A.D. Broadbent, Color Research and Applications, "A critical review of the development of the CIE1931 RGB color-matching functions," 29, 267 (2004).

[10] J.B. Carruthers and J.M. Kahn, "Multiple-subcarrier modulation for nondirected wireless infrared communication," *IEEE J. Sel. Areas Commun.*, vol. 14, no. 3, pp. 538-546, Apr. 1996.

[11] J.B. Carruthers and J.M. Kahn, "Modeling of nondirected wireless infrared channels," *IEEE Trans. Commun.*, vol. 45, no. 10, Oct. 1997.

[12] C. Chen, P. Wu, H. Lu, Y. Lin, J. Wen, and F. Hu, " Bidirectional phase-modulated hybrid cable television/radio-over-fiber lightwave transport systems," Opt. Lett., **38**, 2345 (2013).

[13] H. Chen and H. Liang, "Combined selective mapping and binary cyclic codes for PAPR reduction in OFDM systems," *IEEE Trans. Wireless Commun.*, vol. 6, no. 10, pp. 3524-3528, Oct. 2007.

[14] J. Chen and C. Li, "Tone reservation using near-optimal peak reduction tone set selection algorithm for PAPR reduction in OFDM systems," *Signal Processing Letters*, IEEE, vol. 17, no. 11, pp. 933-936, Nov. 2010.

[15] CIE (1999), "Colour rendering (TC 1-33 closing remarks)," Publication 135/2, Vienna: CIE Central Bureau, ISBN 3-900734-97-6.

[16] N. Cvijetic and T. Wang, "WiMAX over free-space optics - evaluating OFDM multi-subcarrier modulation in optical wireless channels," *IEEE Sarnoff Symposium*, 27-28 Mar. 2006.

[17] cvx Users' Guide - CVX Research, Inc.

[18] T. E. Darcie, "Subcarrier multiplexing for lightwave networks and video distribution systems," *IEEE J. Select. Areas Commun.*, vol. 8, pp. 1240-1248, Sept. 1990.

[19] R. Drost and B. Sadler, "Constellation design for color-shift keying using billiards algorithms," IEEE Globecom Workshop, 980 (2010).

[20] M. Duarte and A. Sabharwal, "Full-duplex wireless communications using off-the shelf radios: Feasibility and first results," In Proc. Asilomar 2010.

[21] H. Elgala and T. Little, "Reverse polarity optical-OFDM (RPO-OFDM): dimming compatible OFDM for gigabit VLC links," Opt. Express, **21**, 24288 (2013).

[22] S. Gabler and C. Wolff, "A quick and easy approximation to the distribution of a sum of weighted chi-square variables," Statistische Hefte 28, pp. 317-325, 1987.

[23] Q. Gao, J.H. Manton, G. Chen, and Y. Hua, "Power-efficient constellation design for a multi-carrier optical wireless system," *IEEE Milcom 2013*, pp. 1645-1650, Nov. 2013.

[24] F. Gao, T. Cui, and A. Nallanathan, *"On channel estimation and optimal training design for amplify and forward relay network,"* IEEE Trans. Wireless Commun., vol. 7, no. 5, pp. 1907-1916, May 2008.

[25] O. Gonzales, "OFDM over indoor wireless optical channel," *IEE Proc. Optoelectron.*, vol. 152, no. 4, pp. 199-204, Aug. 2005.

[26] F. Gray, "Pulse code communications," U.S. Patent 2 632 058, Mar. 1953.

[27] S. Han and J. Lee, "An overview of peak-to-average power ratio reduction techniques for multicarrier transmission," *IEEE Trans. Wireless Commun.*, vol. 9, no. 2, pp. 523-527, Apr. 2005.

[28] M.Z. Hassan, "Subcarrier intensity modulated wireless optical communications with rectangular QAM," *J. Opt. Commun. Netw.*, vol. 4, no. 6, pp. 522-532, June 2012.

[29] S. Hranilovic and S. Kumar, "All-Optical multihop free-space optical communication systems," *J. of Lightw. Tech.*, vol. 29, no. 18, pp. 2663-2669, Sept. 2009.

[30] Y. Hua, Y. Mei and Y. Chang, "Wireless antennas making wireless communications perform like wireline communications," IEEE Topical Conference on Wireless Communication Technology, pp. 47-73, Honolulu, Hawaii, Oct 15-17, 2003.

[31] Y. Hua, P. Liang, Y. Ma, A. Cirik and Q. Gao, "A method for broadband full-duplex radio", IEEE Signal Processing Letters, Dec 2012.

[32] IEEE 802.15.7 Visible Light Communication Task Group, https://mentor.ieee.org/802.15/documents?is group=0007.

[33] IEEE JSAC Special Issue on Theories and Methods for Advanced Wireless Relays, Part I, Sept 2012 and Part II Aug 2013.

[34] M. Jain, J. I. Choi, T. M. Kim, D. Bharadia, S. Seth, K. Srinivasan, P. Levis, S. Katti, and P. Sinha, "Practical, real-time, full duplex wireless", In Proc. Mobicom 2011.

[35] Y. Jia and A. Vosoughi *"Impact of channel estimation error upon sum-rate in amplify-and-forward two-way relaying systems,"* in Proc. IEEE Int. Workshop Signal Process. Advances in Wireless Commun., pp. 1C5, 2010.

[36] T. Jiang, Y. Yang, and Y. Song, "Exponential companding transform for PAPR reduction in OFDM systems," *IEEE Trans. Broadcasting*, vol. 51, no. 2, pp. 244-248, June 2005.

[37] J. M. Kahn and J.R. Barry, "Wireless infrared communications," *Proc. IEEE*, vol. 85, no. 2, pp. 265-298, Feb. 1997.

[38] J. Karout, E. Agrell, K. Szczerba, and M. Karlsson, "Optimizing constellations for single-subcarrier intensity modulated optical systems," *IEEE Trans. Inf. Theory*, vol. 58, no. 7, pp. 4645-4659, July 2012.

[39] S. M. Kay, *"Fundamentals of Statistical Signal Processing,"* Volume I: Estimation Theory. Prentice Hall PTR, 1993.

[40] J. K. Kim and E. F. Schubert, "Transcending the replacement paradigm of solid-state lighting," Opt. Express, **16**, 21835 (2008).

[41] A. Lalos, A. Rontogiannis, and K. Berteridis, *"Channel estimation techniques in amplify and forward relay networks,"* IEEE SPAWC, pp. 446-450, July 2008.

[42] J. Laneman, D. Tse and G. Wornell, *"Cooperative Diversity in Wireless Networks: Efficient Protocols and Outage Behavior,"* IEEE Trans. Inf. Theory, vol. 50, no. 12, Dec. 2004.

[43] P. Lioliou, M. Viberg, and M. Coldrey, *"Efficient Channel Estimation Techniques for Amplify and Forward Relaying Systems,"* IEEE Trans. Commun., vol. 60, no. 11, pp. 3150-3155, Nov. 2012.

[44] P. Lioliou and M. Viberg, *"Least-squares based channel estimation for MIMO relays,"* in Proc. International ITG Workshop on Smart Antennas, Feb. 2008.

[45] P. Lioliou and M. Viberg, and M. Matthaiou, *"Bayesian Channel Estimation Techniques for AF MIMO Relaying Systems,"* Vehicular Technology Conference (VTC Fall), pp. 1-5, 2011.

[46] A.S. Lioumpas, G.K. Karagiannidis, and S. Arnon, "Adaptive subcarrier PSK intensity modulation in free space optical systems," *IEEE Trans. Commun.*, vol. 59, no. 5 pp. 1368-1377, May 2011.

[47] C. K. Lo, S. Viswanath, and J. Robert W. Heath, "Rate bounds for MIMO relay channels using precoding," in Proc. IEEE Global Telecommun. Conf., pp. 1172-1176, Nov. 2005.

[48] J. Ma, P. Orlik, J. Zhang and G. Y. Li, *"Pilot matrix design for interim channel estimation in two hop MIMO AF relay systems,"* in Proc International Conference on Communications, Dresden, Germany, pp. 1-5, Jun. 2009.

[49] E. Monteiro and S. Hranilovic, "Constellation design for color-shift keying using interior point methods," IEEE OWC-WS, 1224 (2012).

[50] S. H. Muller and J. B. Huber, "OFDM with reduced peak-to-average power ratio by optimum combination of partial transmit sequences," *IEE Electron. Lett.*, vol. 33, pp. 368-369, Feb. 1997.

[51] A. Nosratinia and A. Hedayat, *"Cooperative Communication in Wireless Networks,"* IEEE Communications Magazine, vol 42, no 10, Oct. 2004.

[52] G. Nguyen and S. Kompella, "Optimization of Transmssion Schedules In Capture-Based Wireless Networks," IEEE MILCOM 2008, pp. 1 - 7, 2008.

[53] G. Nguyen and S. Kompella, "Cooperation for Transmission Scheduling in Wireless Networks," IEEE MILCOM 2009, Paper 900539, 2009.

[54] G. Nguyen, J. Wieselthier, S. Kompella, and A. Ephremides, "Transmission Strategies For Single-Destination Wireless Networks," IEEE MILCOM 2011.

[55] J. Pang, G. Shen, D. Wang, L. Jiang, and W. Wang, *"Channel Estimation and Optimal Training Design for Amplify and Forward MIMO Relay Channel under Spatial Fading Correlation,"* Vehicular Technology Conference Fall (VTC 2010-Fall), pp. 1-5, Sep. 2010.

[56] C. S. Patel and G. L. Stuber *"Channel Estimation for Amplify and Forward Relay Based Cooperation Diversity Systems,"* IEEE Trans. Wireless Commun., vol 6, no 6, pp. 2348-2356, June 2007.

[57] W.O. Popoola, "Subcarrier intensity modulated free-space optical communication systems," Ph.D. Thesis, Northumbria University, 2009.

[58] S. Rajagopal, R.D. Roberts, and S. Lim, "IEEE 802.15.7 visible light communication: modulation schemes and dimming support", *IEEE Commun. Mag.*, Mar. 2012.

[59] Y. Rong, A. Khandaker, *"Channel estimation of dual-hop MIMO relay systems using parallel factor analysis,"* 17th Asia-Pacific Conference on Communications, pp. 278-283, Oct. 2011.

[60] F. Schreckenbach, N. Gortz, J. Hagenauer, and G. Bauch, "Optimization of symbol mappings for bit-interleaved coded modulation with iterative decoding," *IEEE Commun. Lett.*, vol. 7, no. 12, Dec. 2003.

[61] A. Sendonaris, E. Erkip, and B. Aazhang, *"User Cooperation Diversity – Part I: System Description,"* IEEE Trans. Wireless Commun., vol. 51, no. 11, Nov. 2003.

[62] S.B. Slimane, "Peak-to-average power ratio reduction of OFDM signals using broadband pulse shaping," *IEEE VTC*, vol.2, pp. 889-893, 2002.

[63] A. Stimson, "Photometry and Radiometry for Engineers," New York: Wiley and Son.

[64] H. Suraweera, G. Karagiannidis, and P. Smith, *"Performance Analysis of the Dual-Hop Asymmetric Fading Channel,"* IEEE Trans. Wireless Commun., vol. 8, no. 6, June 2009.

[65] J. Tan and G. Stuber, "Analysis and design of symbol mappers for iteratively decoded BICM," *IEEE Trans. Wireless Commun.*, vol. 4, no. 2, Mar. 2005.

[66] T. Ohtsuki, "Multiple-subcarrier modulation in optical wireless communications," *IEEE Commun. Mag.*, vol. 41, no. 3, pp. 74-79, Mar. 2003.

[67] S. Teramoto and T. Ohtsuki, "Multiple-subcarrier optical communication systems with subcarrier signal-point sequence," *IEEE Trans. Commun.*, vol. 53, no. 10, pp. 1738-1743, Oct. 2005.

[68] T. Kong and Y. Hua, *"Optimal Design of Source and Relay Pilots for MIMO Relay Channel Estimation,"* IEEE Trans. Signal Process., vol. 59, no. 9, Sep. 2011.

[69] T. Kong and Y. Hua, *"Optimal channel estimation and training design for MIMO relays,"* in Proc. Asilomar Conf. Signals, Syst., Comput., Pacific Grove, CA, pp. 663-667, Nov. 2010.

[70] G. Ungerboeck, "Channel coding with multilevel/phase signals," *IEEE Trans. Inf. Theory*, vol. 28, no. 1, pp. 55-67, Jan. 1982.

[71] G. Ungerboeck, "Trellis-coded modulation with redundant signal sets-Parts I and II," *IEEE Commun. Mag.*, vol. 25, pp. 5-20, Feb. 1987.

[72] J. Vucic and K.-D. Langer, "High-speed visible light communications: State-of-the-art," in OFC/NFOEC, 1 (2012).

[73] Y. Wang and Z. Luo, "Optimized iterative clipping and filtering for PAPR reduction of OFDM signals," *IEEE Trans. Commun.*, vol. 59, no. 1, pp. 33-37, Jan. 2001.

[74] Y. Wang, Y.G. Wang, N. Chi, J. Yu, and H. Shang, "Demonstration of 575-Mb/s downlink and 225-Mb/s uplink bi-directional SCM-WDM visible light communication using RGB LED and phosphor-based LED," Opt. Express, **21**, 1203 (2013).

[75] S. Watson, M. Tan, S. Najda, P. Perlin, M. Leszczynski, G. Targowski, S. Grzanka, and A. E. Kelly, "Visible light communications using a directly modulated 422 nm GaN laser diode," Opt. Lett., **38**, 3792 (2013).

[76] Z. Xu and B.M. Sadler, "Ultraviolet communications: potential and state-of-the-art", *IEEE Commun. Mag.*, Mar. 2012.

[77] R. You and J. Kahn, "Average power reduction techniques for multiple-subcarriers intensity-modulated optical signals," *IEEE Trans. Commun.*, vol. 49, no. 12, pp. 2164-2170, Dec. 2001.

[78] K. Zeger and A. Gersho, "Pseudo-gray coding," *IEEE Trans. Commun.*, vol. 38, pp. 2147-2158, Dec. 1990.

[79] L. Zeng, D. O'Brien, H. Minh, G. Faulkner, K. Lee, D. Jung, Y. Oh, and E. Won, "High data rate multiple input multiple output (MIMO) optical wireless communications using white LED lighting," JSAC, **27**, 1654 (2009).

[80] X, Zhou, A. Lamahewa, P. Sadeghi, and A. Hjoungnes, *"Relaying Energy Allocation in Training-Based Amplify and Forward Relay Communications,"* Communications Theory Workshop (AusCTW), Australian, pp. 1-6, Mar. 2012.

Appendix A

Selected Optimized Constellations

The optimized constellations $\Theta_{E,16}^{0,2}$, $\Theta_{P,16}^{0,2}$, $\Theta_{E,16}^{1,2}$, and $\Theta_{P,16}^{1,2}$ are listed with a given order $(0000, 0001, \ldots, 1111)$ by applying the BSA at SNR=10dB.

$\Theta_{E,16}^{0,2} = \{(1.4514, 0.0527, 0.6814, 0.3327, 0.0282), (0.7202, 0.5695, 0.1722, 0.3244, 0.2160),$
$(1.2032, 0.2489, 0.3290, -0.2405, 0.7819), (1.1484, -0.2025, -0.0656, 0.6490, 0.4580),$
$(1.4097, 0.6370, 0.1505, -0.1936, -0.2851), (1.1380, 0.1383, -0.0538, 0.6275, -0.4886),$
$(1.4055, 0.3465, -0.5197, 0.0022, 0.3691), (0.7123, 0.3648, -0.5046, -0.1093, -0.3425),$
$(0.7042, 0.0167, 0.6471, -0.3300, 0.0151), (0.7097, -0.6024, 0.1988, 0.2763, -0.2043),$
$(1.4127, -0.6016, 0.1626, -0.1893, 0.3320), (0.7121, -0.3645, -0.5056, -0.1100, 0.3416),$
$(1.1716, -0.1970, 0.2791, -0.2796, -0.7582), (0.0173, 0, 0, 0, 0), (1.1215, 0, -0.1417,$
$-0.7808, -0.0007), (1.4179, -0.3368, -0.5555, -0.0263, -0.3595)\}$

$$\Theta_{P,16}^{0,2} = \{(1.4976, 0.3817, 0.6085, 0.1446, -0.3005), (1.5015, -0.3913, 0.5752, 0.1322, 0.3329), (1.0434, -0.0129, 0.1305, -0.7170, -0.1426), (1.5320, -0.6861, -0.1680, -0.2493, -0.1301), (1.4980, 0.7078, -0.1088, -0.3211, 0.1024), (2.1578, 0.0221, 0.0177, 0.0027, -0.0026), (0.7029, 0.3826, 0.5762, -0.1057, 0.2517), (1.1242, 0.0122, -0.1249, -0.1455, 0.6901), (1.1508, -0.0242, -0.1371, 0.0674, -0.6917), (1.1764, -0.0020, 0.0725, 0.7514, 0.0062), (0.7595, -0.5048, 0.5416, -0.0235, -0.3083), (0.7537, -0.6670, -0.2388, 0.2658, 0.2217), (0.7410, 0.6899, -0.1923, 0.2692, -0.1642), (1.5241, 0.1483, -0.7023, 0.2567, 0.1128), (0.0112, 0, 0, 0, 0), (0.6930, 0.0131, -0.6804, -0.2681, -0.0102)\}$$

$$\Theta_{E,16}^{1,2} = \{(1.6562, -0.4895, 0.2213, 0.5880, 0.2367), (1.0887, -0.2969, 0.7102, 0, 0), (0.8165, 0, 0, -0.0286, -0.5766), (0, 0, 0, 0, 0), (1.3608, 0, 0, 0.0477, 0.9611), (1.0887, 0.6551, 0.4043, 0, 0), (1.6614, 0.1615, 0.5024, 0.0238, -0.6466), (1.6614, -0.5471, -0.2474, 0.5094, 0.1762), (1.0887, -0.7294, -0.2462, 0, 0), (1.6562, -0.4895, 0.2213, -0.5616, 0.2938), (1.0887, 0.1292, -0.7589, 0, 0), (1.3608, 0, 0, 0.8084, -0.5219), (0.8165, 0, 0, -0.4851, 0.3131), (0.8165, 0, 0, 0.5137, 0.2635), (1.6114, 0.5471, -0.2474, -0.4894, 0.2258), (1.3608, 0, 0, -0.8562, -0.4392)\}$$

$$\Theta_{P,16}^{1,2} = \{(1.6293, 0, 0, -0.9651, -0.6292), (0.8165, 0, 0, 0.4443, 0. - 0.3687),$$

$$(0.8165, 0, 0, 0.0971, 0.5691), (1.6614, 0.3886, 0.3517, 0.6243, -0.1700),$$

$$(1.0887, 0.7255, 0.2574, 0, 0), (1.0887, -0.0927, 0.7642, 0, 0), (1.0887,$$

$$- 0.3240, -0.6983, 0, 0), (0, 0, 0, 0, 0), (1.6293, 0, 0, -0.9651, -0.6292),$$

$$(1.3608, 0, 0, 0.1639, -0.9482), (1.6614, 0.3886, 0.3571, -0.0548, -0.6447),$$

$$(0.8165, 0, 0, -0.5414, -0.2004), (1.0887, -0.7403, 0.2109, 0, 0), (1.4808,$$

$$0.5793, -0.8722, 0, 0), (1.3608, 0, 0, 0.7392, 0.6161), (1.3608, 0, 0, 0.9031, 0.3321)\}$$

Appendix B

Proof of Proposition 1

The transmitted signal $s_i(t)$, $i \in [1, N_c]$, can be written as

$$s_i(t) = \eta[m_i(t) + b_i(t)] \qquad t \in [0, T_s] \tag{B.1}$$

where $m_i(t)$ is an electrical domain waveform before biasing, $b_i(t) = c_{i,0}\Pi(\frac{t}{T_s})$ is the DC-bias. For notation simplicity, we replace $s_i(t)$ and $b_i(t)$ by $s(t)$ and $b(t) = c_0\Pi(\frac{t}{T_s})$. $s(t)$ goes through a frequency selective fading channel defined as in (2.14), where $\max_i(\tau_i) \ll T_s$ such that $\Pi(\frac{t-\tau_i}{T_s})$ can be approximated by $\Pi(\frac{t}{T_s})$, the receiver-side signal $y(t)$ can be written as

$$\begin{aligned} y(t) &= \gamma\eta[m(t) + b(t)] * h(t) \\ &= \sum_i \beta_i m(t - \tau_i) + c_0 \sum_i \beta_i b(t - \tau_i) \end{aligned} \tag{B.2}$$

where $\gamma\eta = 1$ is assumed thus the above equation holds. Using basis defined in equation (5.22)$-$(2.8) and with some manipulations, we have

$$\begin{aligned}\sum_i \beta_i m(t-\tau_i) &\approx \sum_{k=1}^{K}\Big[c_k^c \sum_i \beta_i \cos(2\pi f_k(t-\tau_i)) \\ &\quad + c_k^s \sum_i \beta_i \sin(2\pi f_k(t-\tau_i))\Big]\Pi(\frac{t}{T_s}) \\ &= \sum_{k=1}^{K}\Big[c_k^c \mathrm{Re}\big(\sum_i \beta_i e^{-j2\pi f_k\tau_i}\cdot e^{j2\pi f_k t}\big) \\ &\quad + c_k^s \mathrm{Im}\big(\sum_i \beta_i e^{-j2\pi f_k\tau_i}\cdot e^{j2\pi f_k t}\big)\Big]\Pi(\frac{t}{T_s}) \end{aligned} \tag{B.3}$$

where c_k^c and c_k^s are the real and imaginary part coefficients modulating the k-th basis function. Define $z_k = \sum_i \beta_i e^{-k2\pi f_k\tau_i}$, thus the equation on the bottom of page holds:

In order to compensate the selective fading channel effect, we input c_k^c and c_k^s into the corresponding pre-equalizer which guarantees

$$\begin{cases} \hat{c_k^c}\mathrm{Re}(z_k) + \hat{c_k^s}\mathrm{Im}(z_k) = c_k^c \\ \hat{c_k^s}\mathrm{Re}(z_k) - \hat{c_k^c}\mathrm{Im}(z_k) = c_k^s \end{cases} \tag{B.4}$$

Therefore

$$\begin{bmatrix} \mathrm{Re}(z_k) & \mathrm{Im}(z_k) \\ -\mathrm{Im}(z_k) & \mathrm{Re}(z_k) \end{bmatrix} \begin{bmatrix} \hat{c_k^c} \\ \hat{c_k^s} \end{bmatrix} = \begin{bmatrix} c_k^c \\ c_k^s \end{bmatrix} \tag{B.5}$$

$$\begin{bmatrix} \hat{c_k^c} \\ \hat{c_k^s} \end{bmatrix} = \frac{1}{|z_k|^2} \begin{bmatrix} \mathrm{Re}(z_k) & -\mathrm{Im}(z_k) \\ \mathrm{Im}(z_k) & \mathrm{Re}(z_k) \end{bmatrix} \begin{bmatrix} c_j^c \\ c_j^s \end{bmatrix} \triangleq \mathbf{P}_k \begin{bmatrix} c_j^c \\ c_j^s \end{bmatrix} \tag{B.6}$$

Thus we obtain the pre-equalizers $\mathbf{P}_k$ (k=[1,K]) for each subcarrier. For the biasing part, similarly

$$\sum_i \beta_i b(t-\tau_i) \approx c_0(\sum_i \beta_i)\Pi(\frac{t}{T_s}) \tag{B.7}$$

therefore, the corresponding pre-equalizer $p_0 = 1/\sum_i \beta_i$.

Remark: The above analysis is based on pulse shape defined by (2.8). When β is small, the proposition holds approximately when pulse shape given by (2.9) is used. There are other ways of choosing the pulse-shaping functions, e.g., the cyclic shifted squared root of raised cosine (SRRC) pulse-shaping function suggested in [62]. However, since the complex exponentials are the only eigenfunctions of linear time invariant (LTI) system and use of SRRC will distort the basis, Proposition 1 no longer holds. One might need to design a joint pre-equalizer $\tilde{\mathbf{P}}$ of size $(2K+1) \times (2K+1)$ with non-zero non block-diagonal elements to compensate for both the selective fading channel and change of basis instead of the block diagonal $\mathbf{P}$ suggested in Proposition 1. This is out of the scope of the paper and will be discussed in our future work.